The impact of bio-irrigation on the isotopic signature of benthic inorganic nitrogen fluxes

May 15, 2013

MSc thesis: Jurjen Rooze

Supervisors:
Prof. dr. C. Meile
Prof. dr. C. P. Slomp

Table of Contents

1. Introduction

Sediments play an important role in the cycling of elements in oceans. Roughly a quarter of the organic matter (OM) produced in sunlit waters is exported to the ocean floor (Sarmiento and Gruber, 2006), where it can be either permanently removed from the oceans through burial or it can be recycled to CO_2 and nutrients and exported back to the overlying water. Predicting the fate of OM entering sediments requires understanding of the processes that take place within sediments. The sum of all sedimentary processes, may they be biological, chemical, or physical in nature, that are involved in the initial modification of sedimenting material is termed *early diagenesis* (Berner, 1980). Basically it refers to all the processes that determine the properties of the top ~20 cm of sediments (Sarmiento and Gruber, 2006).

1.1 Diagenetic processes

Transport of solutes in pore water can be controlled by advection or diffusion. Advective flow is caused by pressure gradients in sediments, which for example can be the result of currents acting on rippled surfaces of sediments or the motion of waves. To which extent advection controls the transport regime is dependent on forcing mechanisms and the permeability of the porous medium. Advection is especially important in permeable sandy sediments in coastal areas (Huettel, 1990). When there are no pressure gradients or permeability is low, transport of solutes is governed by diffusion.

The OM raining onto sediments contains energy that can be released through reduction-oxidation (redox) reactions in which one or more electrons are transferred between electron-acceptors and donors. The most important electron donor is reduced organic matter, which gets decomposed into dissolved inorganic carbon (DIC), dissolved inorganic nitrogen (DIN), and dissolved inorganic phosphorus (DIP).

Microbes have evolved to use the energy released during these reactions for their own energy metabolism. Their enzymes catalyze the redox reactions and their cell biology determines which intermediates are produced during the degradation process. Hence, to a large extent the chemistry in sediments is regulated by biology (Jørgensen, 2000). In sediments several electron acceptors are present that can be used by microbes to oxidize the OM. The Gibbs free energy ΔG released during reactions is the energy that can be used to perform work:

$$\Delta G = \Delta G^{\circ} + RT \ln \frac{\prod_i (product)^{ni}}{\prod_j (reactant)^{nj}} \qquad (1.1)$$

where ΔG^o is the standard free energy change for a reaction, R is the gas constant, T is the absolute temperature (K), n_i and n_j refer to the stoichiometry of the reaction, and the brackets denote activity.

Pore water profiles of sediments show generally that oxidants are consumed in order of decreasing energy production (Froelich *et al.*, 1979). Thus in the top of sediments aerobic organisms outcompete their anaerobic counterparts, since oxic

respiration yields the most free energy under standard conditions (Table 1.1). Deeper in sediments, where oxygen concentrations are depleted, the reduction of other electron acceptors, such as nitrate and manganese oxide, become the energetically most feasible way to oxidize organic matter. This vertical distribution of electron acceptors leads to the redox stratification found in sediments: in the top of sediments conditions are oxidizing, while with increasing depth conditions become more reducing.

Table 1.1. Standard free energy changes (ΔG^o at pH 7) for respiration pathways of organic matter remineralization in nature, with H_2 and acetate as electron donors. Calculation conditions: 25 ^oC and unit activity for all reactants and products (Canfield *et al.*, 2005).

Reaction	kJ per reaction ΔG^o (H_2)	ΔG^o (acetate)
Oxic respiration		
$O_2 + 2\ H_2 \rightarrow 2\ H_2O$	-456	
$O_2 + ½\ C_2H_3O_2^- \rightarrow HCO_3^- + ½\ H^+$		-402
Denitrification		
$4/5\ H^+ + 4/5\ NO_3^- + 2\ H_2 \rightarrow 2/5\ N_2 + 12/5\ H_2O$	-460	
$4/5\ NO_3^- + 3/5\ H^+ + ½\ C_2H_3O_2^- \rightarrow 2/5\ N_2 + HCO_3^- + 2\ H_2O$		-359
Mn reduction (pyrolusite)		
$4\ H^+ + 2\ MnO_2 + 2\ H_2 \rightarrow 2\ Mn^{2+} + 4\ H_2O$	-440	
$7/2\ H^+ + 2\ MnO_2 + ½\ C_2H_3O_2^- \rightarrow 2\ Mn^{2+} + HCO_3^- + 2\ H_2O$		-385
Fe reduction		
$8\ H^+ + 4\ FeOOH + 2\ H_2 \rightarrow 4\ Fe^{2+} + 8\ H_2O$	-296	
$15/2\ H^+ + 4\ FeOOH + ½\ C_2H_3O_2^- \rightarrow HCO_3^- + 4\ Fe^{2+} + 6\ H_2O$		-241
Sulfate reduction		
$H^+ + ½\ SO_4^{2-} + 2\ H_2 \rightarrow 2\ H_2O + ½\ H_2S$	-98.8	
$½\ H^+ + ½\ SO_4^{2-} + ½\ C_2H_3O_2^- \rightarrow ½\ H_2S + HCO_3^-$		-43.8
Methanogenesis		
$½\ H^+ + ½\ HCO_3^- + 2\ H_2 \rightarrow CH_4 + 3/2\ H_2O$	-74.8	
$½\ H_2O + ½\ C_2H_3O_2^- \rightarrow CH_4 + ½\ HCO_3^-$		-19.9

Bioturbation and bio-irrigation

Aquatic sediments are subjected to many forms of *bioturbation*, which refers in a broad sense to any biological activity that mixes sediments. Thus this includes for instance the reworking of sediments by sea cucumbers, rooting plants, and microbes (Meysman *et al.*, 2006b). Organisms that cause bioturbation are often considered to be *ecosystem engineers*, since they strongly affect other organisms by changing the environment.

Lugworms are considered to have a large impact on the cycling of nutrients in sediments (Norkko *et al.*, 2012). They are deposit feeders that swallow sediment in order to take up nutrients stored in soils. Lugworms generate advective flows in the burrows in order to have an oxygen supply and to flush out metabolites. This

results in the mixing of anoxic pore-water with oxygen rich water from overlying water column. The oxygen enrichment of pore waters by biological processes may exceed that of physical processes (Archer and Devol, 1992). Since the supply of oxygen changes the redox conditions in sediments, a broad range of biogeochemical reactions are affected. For instance, this process would enhance nitrification while it inhibits denitrification.

Sediment pore waters can exchange with the overlying water, and the extent to which macrofaunal activity enhances solute exchange (*i.e.* the magnitude of bioirrigation) is dependent on chemical, physical, and biological factors. The reactivity and solubility of the solute is important, as pore water constituents produced in the sediment that form solids by reacting with oxygen, sulfide, or carbonates become immobile (Meile *et al.*, 2005). The permeability of the sediment is important, since in clays solute transport is controlled by diffusion, while in sandy sediments advective irrigation is more important (Meysman *et al.*, 2006a). Different worm species have distinct pumping rates and create burrows with a specific geometry. For instance, *Arenicola marina* create J-shaped burrows, while *Schizocardium* species make U-shaped burrows. This leads to different water flow patterns and spatial chemical distributions in the upper sediment (Furukawa *et al.*, 2001; Meile *et al.,* 2003), which enhance the heterogeneity of sediments.

1.2 Nitrogen cycling in the ocean

Nitrogen is an essential element for all life on earth, since it is a constituent of proteins, RNA, and DNA. In oceans, DIN is introduced in the food web though the uptake by phytoplankton and bacteria. As a result DIN concentrations in the euphotic zones of oceans are often low, limiting growth of phytoplankton communities and thus primary production (Ryther and Dunstan, 1971). Inventories of bioavailable nitrogen in oceans are almost exclusively regulated by biological processes (Fennel *et al.*, 2009). Here we will briefly discuss the nitrogen cycle, which interrelates biological processes with the various chemical forms of nitrogen found in nature (Figure 1.1).

Nitrogen fixing organisms can take up dinitrogen dissolved in seawater. These are prokaryotes that possess the enzyme nitrogenase. Breaking the bonds in nitrogen gas is highly energy demanding. However, in waters that receive high amounts of incident solar radiation these microbes have an advantage, since they are less dependent on the availability of dissolved nitrogen (Nedwell and Aziz, 1980). Nitrogen fixation is the main source of nitrogen in oceans (Gruber and Galloway, 2008).

Ammonification refers to the mineralization of organic nitrogen into ammonium. The reaction pathway is dependent on the composition of the nitrogenous source; for instance small organic molecules could undergo simple deamination reactions to produce ammonium, while organic nitrogen that consists of large polymers first has to undergo a series of complex metabolic steps that break up the organic matter into soluble monomers (Herbert, 1999). In general, ammonification of detritus entering sediments is a rapid process after which the produced ammonium is recycled back to the overlying water. This results in an

average turnover time of nitrogen that is short compared to typical oceanic time scales (Jensen *et al.*, 1990).

Nitrification, the process in which ammonium is oxidized to nitrate, consists of two steps. In the first step, ammonium is oxidized to nitrite by ammonium oxidizing bacteria and ammonium oxidizing archaea. In the second step nitrite is oxidized to nitrate by bacteria from the genus *Nitrobacter* (Hagopian and Riley, 1998). Nitrifying organisms include autotrophic and heterotrophic species that are all dependent on oxygen (Ward, 2008).

Respiratory denitrification is a process in which nitrate is used as a terminal electron acceptor for the oxidation of organic matter (Devol, 2008). The ability to denitrify is widespread amongst different taxonomical groups of bacteria. The process occurs under suboxic conditions, namely in oxygen minimum zones of the oceans and in anaerobic parts of sediments. Denitrification involves a chain of reactions in which nitrite, nitric oxide, and nitrous oxide are produced as intermediates that leave the microbial cell and hence can accumulate in the environment (Betlach and Tiedje, 1981; Codispoti *et al.*, 1992). However, nitric oxide concentrations are usually below detection limits since it is highly reactive.

$$NO_3 \rightarrow NO_2 \rightarrow NO \rightarrow N_2O \rightarrow N_2$$

Every step in the chain is catalyzed by different enzyme systems, named nitrate reductase, nitrite reductase, nitric oxide reductase, and nitrous oxide reductase. The production of nitrate by nitrification often fuels denitrification and the combined process is called *coupled nitrification-denitrification*. Denitrification and nitrification also share nitrite and nitrous oxide as intermediates. In addition, both processes can be coupled to anaerobic ammonium oxidation (see next paragraph), since that reaction is dependent upon the supply of nitrite.

Anaerobic ammonium oxidation (anammox) is the process in which nitrite reacts with ammonium to form dinitrogen gas:

$$NH_4 + NO_2 \rightarrow N_2 + 2\ H_2O$$

This reaction was first observed in a waste water treatment tank (Graaf *et al.*, 1990) and in 1999 the bacteria that mediate the reaction were identified (Strous *et al.*, 1999). Since then a few more species of anammox bacteria have been identified of which *Scalindua* is the only marine genus. This genus has been found in nature, for instance in the Black Sea (Kuypers *et al.*; 2003), the Arabian Sea (Woebken *et al.*, 2008), and in oxygen minimum zones of the Pacific Ocean (Galan *et al.*, 2009, 2012). All species possess an organelle, called anammoxosome, in which the reaction is believed to occur. The cell membrane of anammoxosomes feature unique lipids named ladderanes, that contain two or more fused cyclobutane rings (Sinninghe Damste *et al.*, 2002), which act as biomarkers for anammox. ^{15}N compound labeling experiments have been used to measure anammox reaction rates (Dalsgaard *et al.*, 2005), and it seems to be a widespread process in coastal sediments (Rysgaard *et al.*, 2004; Schmid *et al.,* 2007) and estuarine environments (Nicholls and Trimmer, 2009).

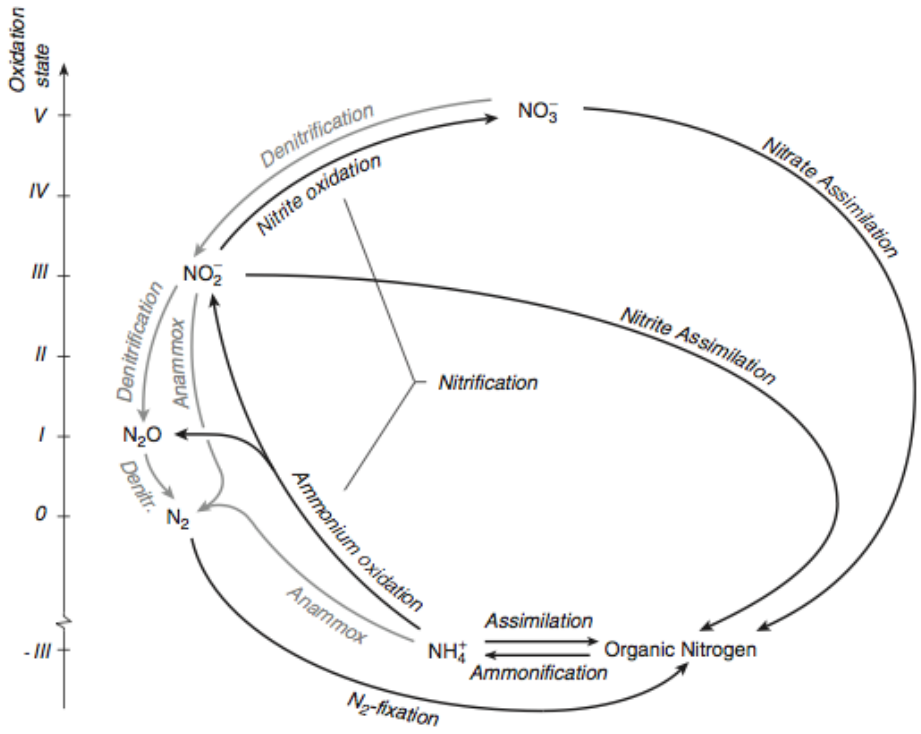

Figure 1.1. The nitrogen cycle depicting the important processes and chemical forms involved in the biogeochemical cycling of nitrogen. The various chemical forms are plotted versus their oxidation state. The processes in grey generally occur under anoxic condition. (Gruber, 2008)

Nitrogen budgets

Here the nitrogen budgets refer to combined or fixed nitrogen, *i.e.* nitrogen atoms that are bonded to at least one other type of atom. The reason is that dissolved N_2 is inert and N_2 concentrations are relatively unimportant to the nitrogen cycle. Hence, oceanic nitrogen is nitrogen that is *bioavailable* (*i.e.* fixed in organic matter or in mineralized form), while fixed nitrogen that reacts to N_2 will be considered as lost from the oceans throughout the text.

The magnitude of sink and sources of oceanic nitrogen are not well constrained yet. Estimates of these fluxes differ widely (Table 1.2) and uncertanties may be larger than 50%. One of the main problems is the great imbalance between sinks and sources, which are unlikely to be real. This is because N sinks exceeding sources by 10-100 Tg N yr^{-1}, with a pool size on the order of 500,000 Tg N, would lead to a consumption of oceanic N over timescales of 5,000 to 50,000 years, which is inconsistent with the geologic record in the Holocene (Altabet, 2007).

Table 1.2. Present-day (ca. 1990) global marine nitrogen budgets estimates by Codispoti *et al.* (2001), Galloway *et al.* (2004), and Gruber (2004). Table adopted from Gruber, 2008.

Process	Codispoti *et al.*	Galloway *et al.*	Gruber
		Sources (Tg N yr^{-1})	
Pelagic N_2 fixation	117	106	120 +/- 50
Benthic N_2 fixation	15	15	15 +/- 10
River input (DON)	34	18	35 +/- 10
River input (PON)	42	30	45 +/- 10
Atmospheric deposition	86	33	50 +/- 20
Total Sources	294	202	263 +/- 55
		Sinks (Tg N yr^{-1})	
Organic N export	1		1
Benthic N_2 production	300	206	180 +/- 50
Water column N_2 production	150	116	65 +/- 20
Sediment burial	25	16	25 +/- 10
N_2O loss to atmosphere	6	4	4 +/- 2
Total sinks	482	342	275 +/- 55

The largest source of nitrogen in the oceans is nitrogen fixation. Recently Großkopf *et al.* (2012) reported much higher global fixation rates of 177 Tg N yr^{-1} based on a new measuring method (Mohr *et al.*, 2010) and argued that older methods may have underestimated fixation rates by more than 50%. The inputs from terrestrial run-off and atmospheric deposition may have significantly increased in recent times (Duce *et al.*, 2008). Estimates of the pre-industrial magnitude of both these fluxes have been estimated to be around 25 Tg N yr^{-1} (Brandes and Devol, 2002). However, the use of nitrogenous fertilizers in agriculture may have increased the riverine nitrogen input with 50 Tg N per year, while the combustion of fossil fuels may have lead to an increased atmospheric input of 40 Tg N per year (Gruber and Galloway, 2008).

N_2 production constitutes the main loss of oceanic nitrogen. To which extent anammox or denitrification account for these losses is not well constrained. Most N_2 production takes place in anoxic parts of sediments and is internally fuelled by coupled ammonification-nitrification. According to Codispoti (2001), up to 70% of global denitrification occurs in continental shelf sediments. Sedimentary denitrification rates are largely dependent upon the *in situ* production of nitrate through nitrification (Middelburg *et al.*, 1996). Estimates of global rates of water column denitrification widely differ, but are generally considered to be much lower than sedimentary denitrification (Table 1.2). Estimated burial fluxes have been relatively small and hence it is assumed that most nitrogen that enters sediments is either remineralized and recycled back to the overlying water or denitrified and permanently lost from the oceans.

As will be discussed in the next chapter, the isotopic signature of nitrate has been used to establish a quantitative view of the oceanic N cycle. Hence, below a brief overview of the key factors of isotope fractionation is given. Aside from isotopic signatures, global N fluxes can also be constrained by the abundance of N relative to P. Biological activity both in the water column and the sediment tightly

couple the cycling of many elements, in particular carbon – life's backbone – and the key nutrients nitrogen and phosphorous. This is reflected in the Redfield stoichiometry (Redfield *et al.*, 1963), the molar ratio of C, N, and P found in plankton that is on average 106:16:1. This ratio is remarkably similar in different ocean regions. Primary production and degradation of planktonic biomass thus adds or removes N and P from the water-column in this proportion and variability of N:P ratios in distinct oceanic regions are caused by biochemical processes that add or remove N and P with a N:P stoichiometry different than 16:1. This is formalized in the concept of the tracer N^*, which is defined as (Gruber and Sarmiento, 2002):

$$N^* = NO_3 - 16PO_4 + 2.9 \text{ µmol kg}^{-1} \quad (1.2)$$

where the offset is chosen so that the global average N^* is roughly 0. Processes that remove or add OM with a N:P ratio of 16:1, such as photosynthesis and remineralization, have no impact on N^*, while other processes such as DNF and N_2 fixation do change N^*. NO_3 and PO_4 concentrations can be queried from databases in order to calculate N^* in distinct oceanic regions. Negative N^* indicate that N is scarce relative to P, which may be found in areas with high DNF rates, while positive values indicate that P is scarce relative to N, for instance in regions with much nitrogen fixation. Thus N^* is a biogeochemical tracer, which can be used to constrain N and P budgets (Gruber, 2004).

1.3 Isotope geochemistry

Here equations are derived to describe microbially-mediated isotopic reactions with different reaction dynamics and occurring within closed and open systems.

Kinetic isotope fractionation

The isotopic signature of benthic exchange fluxes, such as that of ^{15}N and ^{14}N, can be linked to biogeochemical processes occurring within the sediment. The concept is based on the discrimination of microbial enzymes against heavier isotopes, which results in different reaction rates for light and heavy isotopes. Consequently, over time reactants will be enriched in heavy isotopes and the products will consist of more light isotopes.

The isotopic fractionation factor for a reaction is defined as:

$$\alpha = \frac{dP'/dP}{S'/S} \quad (1.3)$$

where dP' and dP are the instantaneous products of the isotope substrates S' and S. Rearranging equation 1.3 and multiplying it with dP/dt yields:

$$\frac{dP'}{dt} = \frac{dP}{dt}\frac{S'}{S}\alpha \quad (1.4)$$

Equation 3 shows that the evolution of the isotopic composition of products does not only depend on reaction rates, but also on the substrate composition (Bender, 1990). Following this concept, the isotopic signature of benthic nitrate fluxes provides an extra constraint on coupled nitrification-denitrification, since kinetic fractionation by nitrification decreases the $^{15}N/^{14}N$ ratio in nitrate, while denitrification increases that ratio.

The isotopic signature of biochemical processes is dependent upon reaction dynamics. For first-order kinetics:

$$S \overset{k}{\rightarrow} P, \qquad S' \overset{k'}{\rightarrow} P', \tag{1.5}$$

this leads to:

$$\frac{dP}{dt} = kS, \ \frac{dP'}{dt} = k'S' \tag{1.6}$$

Combining equation 1.4 and 1.6 yields:

$$\alpha = \frac{k'}{k} = const. \tag{1.7}$$

This relationship can be used to obtain analytical solutions for S(t), S'(t), P(t), and P'(t) (Mariotti *et al.*, 1981). The drawback of first-order kinetics is that it may poorly reflect the role of enzymes that catalyze reactions. Since these enzymes have limited amounts of binding sites for substrates, reaction rates are dependent on the enzyme availability. The Michaelis-Menten model adopts the following reaction scheme:

$$S + E \overset{k_1/k_2}{\longleftrightarrow} C \overset{k3}{\rightarrow} P, \quad S' + E \overset{k'1/k'2}{\longleftrightarrow} C' \overset{k'3}{\longrightarrow} P, \tag{1.8}$$

where E is the enzyme concentration and C is the complex formed when the substrate binds to the enzyme. This implies that the mass conversation law for E is:

$$E_0 = E(t) + C(t) + C'(t), \tag{1.9}$$

where E_0 is the initial enzyme concentration. The system can be simplified by assuming that the complex concentrations do not change over time, *i.e.* $dC/dt = 0$ and $dC'/dt = 0$. This so called quasi steady-state assumption yields the following solutions (Haldane, 1930; Laidler, 1955; Maggi and Riley, 2009):

$$\frac{dP}{dt} \approx k_3 \frac{E_0 S}{S + K\left(1 + \frac{S'}{K'}\right)} \approx -\frac{dS}{dt}, \ \frac{dP'}{dt} \approx k'_3 \frac{E_0 S'}{S' + K'\left(1 + \frac{S}{K}\right)} \approx -\frac{dS'}{dt}, \tag{1.10}$$

$$\alpha = \frac{dP'}{dP} / \frac{S'}{S} \approx \frac{k'_3 K}{k_3 K'} \tag{1.11}$$

with $K = (k_2 + k_3) / k_1$ *and* $K' = (k'_2 + k'_3) / k'_1$. The Michaelis-Menten model assumes the enzyme concentration to be constant over time, while this concentration can change over time. The coupled Michaelis-Menten-Monod framework assumes that the total enzyme concentration is dependent on the biomass concentration B:

$$zB(t) = E(t) + C(t) + C'(t) \tag{1.12}$$

where z is the proportionality constant and the amount of enzyme per microorganism is assumed constant. According to Monod kinetics (Monod, 1949), the biomass is correlated to the yield of products and the death rate β:

$$\frac{dB}{dt} = Y\left(\frac{dP}{dt} + \frac{dP'}{dt}\right) - \beta B, \tag{1.13}$$

where Y is the biomass yield coefficient. When the quasi steady-state assumption for the complex concentrations is used, then this leads to the following solutions (Maggi and Riley, 2009):

$$\frac{dP}{dt} \approx k_3 \frac{zBS}{S + K\left(1 + \frac{S'}{K'}\right)} \approx -\frac{dS}{dt}, \ \frac{dP'}{dt} \approx k'_3 \frac{zBS'}{S' + K'\left(1 + \frac{S}{K}\right)} \approx -\frac{dS'}{dt} \tag{1.14}$$

$$\frac{dB}{dt} = \frac{k_3 YzBS}{S + K\left(1 + \frac{S'}{K'}\right)} + \frac{k'_3 S'YzB}{S' + K'\left(1 + \frac{S}{K}\right)} - \beta B \tag{1.15}$$

Equation 1.11 also holds for Monod kinetics. The coupled Michaelis-Menten-Monod framework can be improved by releasing the quasi-steady assumption, since experimental studies have indicated that the concentration of enzyme complexes may increase over time and lead to distinct fractionation patterns (Maggi and Riley,

2009). However, in that scenario there are no analytical solutions for *P'(t)*, *P(t)*, *S'(t)*, and *S(t)*, which means that all mass conversation laws and kinetic equations must be included in the model. Also α is then time-dependent:

$$\frac{dP}{dt} = k_3 C, \quad \frac{dP\prime}{dt} = k'_3 C', \tag{1.16}$$

$$\alpha = \frac{dP\prime}{dP} / \frac{dS\prime}{dS} = \frac{k\prime_3 C\prime S}{k_3 C S\prime} = \frac{k'_3 R_C(t)}{k_3 R_S(t)}, \tag{1.17}$$

where $R_C = C'(t)/C(t)$ and $R_S = S'(t)/S(t)$ (see Maggi and Riley 2009 for a derivation).

Instead of α, more often the epsilon notation is used to represent the isotope effect: $\varepsilon = (\alpha - 1)*1000$. In this text ε_{Nit} and ε_{DNF} denote the degree of fractionation during nitrification and denitrification, respectively.

Closed and open systems

The difference between closed and open systems is that the first type can only exchange heat and momentum with its surroundings, whereas the latter one can exchange matter in addition. Natural systems are typically not fully open systems nor fully closed systems (Kendall and Caldwell, 1998). On the hand oceans resemble open systems, because they can exchange matter with the atmosphere and land. On the other hand, through slow mixing and ventilation oceans have a spatially heterogeneous chemical composition. This can lead to local accumulation and depletion of chemical species, which is typical for closed systems.

The way the isotopic composition of substrates and products evolve over time is dependent on whether a fractionation process occurs within a closed or an open system. When the substrate pool is closed, the isotope effect of kinetic fractionation will decrease over time as the substrates become enriched in heavy isotopes, which leads to heavier products. Ultimately when all substrate has been consumed the products will have the same isotopic composition as the initial substrate pool, which means there has been no overall isotope effect. In contrast, chemical reactions in open systems can have a stable isotopic signal if there is enough supply of fresh substrate.

The evolution of the isotopic fractionation for open and closed systems is derived below, following Mariotti *et al.* (1981). Commonly, simplified equations are used, because these are more intuitive and allow one to do the calculations by hand. Going over the derivation of these formulas helps to see which assumptions are being made and what the effects are on the accuracy of the results. Throughout this section no assumptions are imposed regarding reaction dynamics, except that the fractionation factor α is assumed to be time-independent.

Closed Systems

Equation 1.3 can be reorganized to:

$$\int_{t0}^{t} \frac{dP\prime}{S\prime} = \alpha \int_{t0}^{t} \frac{dP}{S} \tag{1.18}$$

Using *dP = -dS* yields:

$$\int_{t0}^{t} \frac{dS\prime}{S\prime} = \alpha \int_{t0}^{t} \frac{dS}{S} \tag{1.19}$$

$$\ln \frac{S\prime}{S\prime_0} = \alpha \ln \frac{S}{S_0} = \ln \left(\frac{S}{S_0}\right)^{\alpha} \tag{1.20}$$

$$\frac{S\prime}{S\prime_0} = \left(\frac{S}{S_0}\right)^{\alpha} \tag{1.21}$$

Then both sides are divided by S/S_0:

$$\frac{S'/S}{S\prime_0/S_0} = \left(\frac{S}{S_0}\right)^{\alpha-1} \tag{1.22}$$

If $R_s = S'/S$, then:

$$\frac{R_S}{R_{S,0}} = \left(\frac{S}{S_0}\right)^{\alpha-1} \tag{1.23}$$

The fraction f is the substrate present at t=t relative to t=0:

$$f = \frac{S_t + S\prime_t}{S_0 + S\prime_0} \approx \frac{S_t}{S_0} \tag{1.24}$$

where the simplification seems to be appropriate for nitrogen isotopes, since ^{15}N only accounts for 0.366% of atmospheric nitrogen. This leads to the Rayleigh equation:

$$R_s \approx R_{s,0} f_t^{\alpha-1} \tag{1.25}$$

which shows that in a closed system, the isotopic composition at any time can be derived if the initial isotopic composition and the amount of substrate that has reacted are known.

Isotopic composition is usually determined with a mass spectrometer, which measures the isotopic ratio of the sample relative to the isotopic ratio of an internal standard. From this method stems the δ notation that has become the conventional way to report isotopic ratios.

$$\delta = \left(\frac{R_{sample}}{R_{standard}} - 1\right) 1000 \tag{1.26}$$

Combining equations 1.25 and 1.26 gives:

$$(\alpha - 1) \ln f \approx \ln \frac{10^{-3}\delta_s + 1}{10^{-3}\delta_{s,0} + 1} \tag{1.27}$$

Then the enrichment factor can be introduced:

$$\varepsilon \approx 10^3 \frac{\ln\left(\frac{10^{-3}\delta_S + 1}{10^{-3}\delta_{S,0} + 1}\right)}{\ln f} \tag{1.28}$$

The last equation is simplified by using the next assumptions: $\ln(u + 1) \approx u$, when u is small relative to 1 and $\ln\left(\frac{u+1}{v+1}\right) \approx u - v$, when both u and v are small relative to 1. This yields:

$$\varepsilon \approx \frac{\delta_s - \delta_{s,0}}{\ln f} \tag{1.29}$$

According to Mariotti (1981), the last equation only holds when $|\varepsilon| < 20‰$ and for $\delta_{s,0}$ values not too different from zero. This relationship is often used to determine ε in incubation experiments.

Next a simple expression for the mass balance of isotopes is derived that relates the isotopic composition of the product and substrate with the initial isotopic composition of the substrate.

$$\frac{S\prime_0}{S_0} = \frac{S'}{S_0} + \frac{S'_0 - S'}{S_0} \tag{1.30}$$

$$= \frac{S'}{S_0} + \frac{S_0 - S}{S_0} * \frac{S'_0 - S'}{S_0 - S} \tag{1.31}$$

$$= \frac{S}{S_0}\frac{S\prime}{S} + \left(1 - \frac{S}{S_0}\right)\frac{P\prime}{P} \tag{1.32}$$

Combining the last equation with equation 1.24 yields:

$$\frac{S\prime_0}{S_0} \approx f\frac{S\prime}{S} + (1-f)\frac{P\prime}{P} \tag{1.33}$$

This gives the expression for the mass balance:

$$\delta_{s,0} \approx f\delta_s + (1-f)\delta_p \tag{1.34}$$

Reorganizing the last equation and combining it with equation 1.29 yields:

$$\delta_p \approx -\frac{(\varepsilon \ln f + \delta_{s,0})f - \delta_{s,0}}{1-f} \tag{1.35}$$

$$\approx -\varepsilon\frac{f\ln f}{1-f} - \frac{\delta_{s,0}(-1+f)}{1-f} \tag{1.36}$$

$$\approx -\varepsilon\frac{f\ln f}{1-f} + \delta_{s,0} \tag{1.37}$$

The expression $\frac{f\ln f}{1-f}$ tends towards -1 when f tends to 1. Thus, the following equation holds for the initial product.

$$\delta_p(0+dt) \approx \delta_{s,0} + \varepsilon \tag{1.38}$$

Since the last equation is based on equation 1.29, the equation only works with small $|\varepsilon|$ and $\delta_{s,0}$.

Open Systems

The instantaneous product refers to products in open systems that are immediately removed from the system after their formation. This applies for example to nitrogenous gases that are produced through benthic denitrification and then bubble out of the sediment.

Below the definition of the fractionation factor is given, where the subscript 'pi' denotes the instantaneous product formed in an infinitesimally small time-step.

$$\alpha = \frac{R_{pi}}{R_s} = \frac{\delta_{pi}+1000}{\delta_s+1000} \tag{1.39}$$

$$\alpha\delta_s + 1000\alpha = \delta_{pi} + 1000 \tag{1.40}$$

This gives:

$$\delta_s\left(1+\frac{\varepsilon}{1000}\right) + 1000\left(1+\frac{\varepsilon}{1000}\right) = \delta_{pi} + 1000 \tag{1.41}$$

$$\delta_s\left(1+\frac{\varepsilon}{1000}\right) + \varepsilon = \delta_{pi} \tag{1.42}$$

Hence, since ε is usually small relative to 1000, the equation can be simplified:

$$\varepsilon \approx \delta_{pi} - \delta_s \tag{1.43}$$

Research objectives

A high degree of isotope fractionation is inherent to denitrification. However, studies have indicated that it is not expressed in sediments due to complete consumption of the nitrate pool. Yet as long as there is an efflux of NO_3 from the sediment, fractionation may occur even if the sediment acts as a net nitrate sink. Our hypothesis is that active pumping by the lugworm *Arenicola marina* may lead to short-circuiting of NO_3, *i.e.* that a part of the NO_3 in the fluid injected into the sediment is not denitrified and can escape the sediment, which then would be enriched in ^{15}N due to fractionation during benthic DNF.

The research questions were:

1. What is the sensitivity of the mean isotopic composition of fixed oceanic nitrogen to the degree of fractionation during benthic N_2 production?
2. Does bio-irrigation, *i.e.* burrow flushing by *Arenicola marina*, enhance N isotopic fractionation in sediments?
3. How do different environmental settings affect the degree of N isotope fractionation during benthic N_2 production?

2. The oceanic $\delta^{15}N$ as constraint on marine nitrogen budgets

Analysis of sedimentary $\delta^{15}N$ records has shown that the isotopic composition of oceanic nitrogen has been stable in the last 3,000 years (Altabet, 2007), which implies that before industrialization began the total masses of ^{14}N and ^{15}N in the oceans were constant. This requires that of both ^{14}N and ^{15}N the in- and out-fluxes must have balanced each other and hence that the nitrogen inventories were in steady-state.

The dominant sources and sinks of oceanic nitrogen feature distinct isotopic imprints, which contribute to the mean $\delta^{15}N$ value of dissolved oceanic nitrogen. Nitrogen fixation introduces organic nitrogen that is slightly enriched in ^{14}N, with a $\delta^{15}N$ of -1 ± 1‰ (Minagawa and Wada, 1986; Carpenter *et al.*, 1997). N_2 production in the water-column of oxygen minimum zones has a large isotope effect of -25 ± 5‰ (Brandes *et al.*, 1998; Altabet *et al.*, 1999; Voss *et al.*, 2001). Isotopic fractionation during sedimentary N_2 production is generally thought to be negligible. Even though sediments are (semi-)open systems with exchange across the sediment-water interface and burial, they are typically considered efficient sinks of nitrate, which limits the effect of fractionation. However, to date there are only relatively few field studies that directly corroborate this argument (Brandes & Devol, 1997; Brandes & Devol, 2002; Lehmann *et al.,* 2004). The impact of the other sources and sinks on the oceanic $\delta^{15}N$ are most likely small, either due to their isotopic composition being similar to that of oceanic NO_3 or the size of their fluxes (Brandes & Devol, 2002).

The oceanic $\delta^{15}N$ has been used to approximate the ratio between nitrogen fixation flux F_{nf}, sedimentary N_2 production flux F_{sd}, and water-column N_2 production flux F_{wd} (Brandes & Devol, 2002; Deutsch *et al.*, 2004; Altabet, 2007; Sigman *et al.*, 2009). This is based on the reasoning shown below. From the steady-state assumption follows:

$$^{15}F_{nf} = {}^{15}F_{sd} + {}^{15}F_{wd}, \tag{2.1}$$

where ^{15}F denotes ^{15}N fluxes. Then these terms are substituted by:

$$R_{air}\alpha_{nf}F_{nf} \approx R_{oc}(\alpha_{sd}F_{sd} + \alpha_{wd}F_{wd}), \tag{2.2}$$

where R_{air} and R_{oc} are respectively the $^{15}N/^{14}N$ ratios of air and oceanic nitrogen, and α_{nf}, α_{sd}, and α_{wd} are the fractionation factors of nitrogen fixation, sedimentary nitrogen production, and water-column nitrogen production, while F denote total fluxes ($F = {}^{15}F + {}^{14}F$). The fraction of water-column N_2 production is defined as:

$$f_d = \frac{F_{wd}}{F_{wd}+F_{sd}} \tag{2.3}$$

Since the consensus is that $\alpha_{sd} = 1$, one obtains:

$$R_{air}\alpha_{nf} \approx R_{oc}\big((1 - f_d) + \alpha_{wd}f_d\big) \tag{2.4}$$

$$f_d \approx \frac{\frac{R_{air}\alpha_{nf}}{R_{oc}}-1}{\alpha_{wd}-1} \tag{2.5}$$

This yields a very rough estimate that approximately 25% of the total oceanic N_2 production occurs in the water-column and 75% in sediments, which does not match with estimates from nitrogen budgets (see Introduction, Table 1.2). The estimate calculated above may underestimate the degree of isotopic fractionation inherent to sedimentary N_2 production, since even if α_{sd} only differs slightly from

one this may have a large impact on the oceanic $\delta^{15}N$ given the magnitude of the sink.

In order to examine the role of sedimentary N fractionation we constructed a simple model that estimates the steady-state $\delta^{15}N$ of oceanic fixed nitrogen based on the magnitude of source and sink fluxes and on their inherent isotopic signals. The goal was to test widely differing parameterizations in order to examine to which processes the oceanic $\delta^{15}N$ is most sensitive and to cover an appropriate scope of each parameter in regard of the uncertainty of its actual value.

2.1 Conceptual Model

The conceptual model (Figure 2.1) of the preindustrial oceanic nitrogen budget is simplified to two state variables, namely ^{15}N and ^{14}N. Both variables represent the total moles of combined nitrogen. Here we assume that the nitrate and DON pools form the total nitrogen pool, because these are by far the most abundant nitrogen species. The sources and sinks are considered to be fluxes that add or remove a constant amount of nitrogen per year.

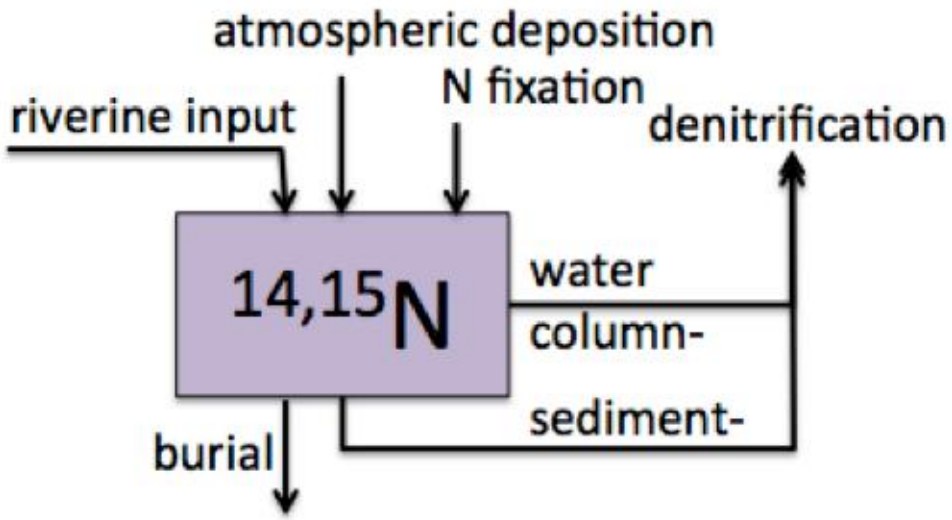

Figure 2.1. Conceptual model of the preindustrial sources and sinks of combined nitrogen in the oceans. The state variables ^{14}N and ^{15}N are the total moles of ^{14}N and ^{15}N in nitrate and DON in the oceans.

Nitrogen fixation F_{nf}, atmospheric deposition F_{ad}, and riverine inputs F_{riv} are considered to be the dominant sources, while sedimentary N_2 production F_{sd}, water-column N_2 production F_{wd}, and burial of organic matter F_{bur} account for the sinks. The magnitude of these fluxes are not well constrained and hence the model was setup to run multiple simulations to cover a broad range of conditions (Table 2.1). In order to be at steady-state, for each simulation the total N_2 production rate was set to a value so that it balanced the sources and sinks. The ratio between sedimentary N_2 production and water-column N_2 production was varied.

For the analysis sets with different values and ranges for the parameters were used. The baseline uses very wide ranges for especially the F_{sd}/F_{wd} ratios, degree of fractionation during water-column DNF, and nitrogen fixation rate F_{nf}.

Two other sets were used with magnitudes and variabilities of N sources and sinks based on Eugster and Gruber (2012) and Gruber and Sarmiento (1997), while for the isotope effect of water-column DNF a narrower range was employed.

Table 2.1. The parameter sets used in for sensitivity analysis. The total N_2 production rate was adjusted to balance the sources.

	Baseline		**Eugster & Gruber (2012)**		**Gruber & Sarmiento (1997)**	
	Flux *Tg N yr^{-1}*	*Isotope effect (‰)*	*Flux* *Tg N yr^{-1}*	*Isotope effect (‰)*	*Flux* *Tg N yr^{-1}*	*Isotope effect (‰)*
F_{wd}		ε=0 to -25		-10 to -20		-10 to -20
F_{sd}		ε=0 to -10		0 to -9		0 to -9
F_{bur} *	-15 to -35	δ^{15}N=6	14	δ^{15}N=6	14	δ^{15}N=6
F_{ad} *	20 to 30	δ^{15}N=-5	14	δ^{15}N=-5	10 to 20	δ^{15}N=-5
F_{riv} *	20 to 30	δ^{15}N=4	14	δ^{15}N=4	27 to 55	δ^{15}N=4
F_{nf} **	100 to 250	ε=-1	94 to 175	ε=-1	84 to 166	ε=-1
F_{sd}/F_{wd}	1 to 8		1 to 4			
$NO_{3,t=0}$ (Tg) ***	580,000	δ^{15}N=5				
$DON_{t=0}$ (Tg) ***	77,000	δ^{15}N=1.5				
$NO_{3,t=0}$ NO_3 + DON		δ^{15}N=4.6				

*Brandes and Devol (2002): F_{bur} = 25 Tg N yr^{-1}, δ^{15}N = 6‰; F_{ad} = 25 Tg N yr^{-1}; δ^{15}N = -4‰; F_{riv} = 25 Tg N yr^{-1}, δ^{15}N of 4‰. **Großkopf T. *et al.* (2012): F_{nf} = 177 Tg N yr^{-1}. ***Based on Gruber (2008). See text for references δ^{15}N of F_{nf}.

2.2 Quantitative model

Each source or sink is given as a total nitrogen flux F (Table 2.1) that is divided into a ^{14}N flux ^{14}F and a ^{15}N flux ^{15}F:

$$F = {}^{14}F + {}^{15}F \tag{2.6}$$

J' and J have the units mole per time, while the total fluxes in Table 2.1 are given in mass per time. Since the goal is to calculate the $^{15}N/^{14}N$ molar ratios, it is unnecessary to convert grams into moles.

The δ^{15}N of the fluxes associated with riverine inputs, atmospheric deposition, and burial can be measured. This value can be converted into the $^{15}N/^{14}N$ ratio R_n:

$$R_N = \left(\frac{{}^{15}\partial N}{1000} + 1\right) R_{air} \tag{2.7}$$

The $^{15}N/^{14}N$ ratio is converted into the fraction f of ^{15}N in total flux J_{tot}:

$$f = \frac{{}^{15}N}{{}^{14}N + {}^{15}N} = \frac{R_N}{1 + R_N} \tag{2.8}$$

Then the fluxes of ^{15}N and ^{14}N can be obtained by:

$${}^{15}F = fF \tag{2.9}$$

$${}^{14}F = F - {}^{15}F \tag{2.10}$$

The isotopic signals of the biochemical reactions are described by enrichment factors, since the isotope effects due to kinetic fractionation is dependent on the isotopic composition of their substrates. In this model the simplification is made that the isotopic composition of the substrate for water-column N_2 production, and

sedimentary N_2 production is identical to that of the total oceanic nitrogen inventories. The substrate of nitrogen fixation is atmospheric nitrogen. In order to to calculate the fluxes ^{15}F and ^{14}F, the enrichment factor is converted into an isotopic fractionation factor:

$$\alpha = 10^{-3}\varepsilon + 1 \tag{2.11}$$

From the definition of the isotopic fractionation factor follows:

$$^{15}F = \alpha \frac{S\prime}{S} {}^{14}F \tag{2.12}$$

Then:

$$F = {}^{14}F\left(1 + \alpha\frac{S'}{S}\right) \tag{2.13}$$

can be reorganized to:

$$^{14}F = \frac{F}{\left(\alpha\frac{S'}{S}+1\right)} \tag{2.14}$$

The mass balances are:

$$\frac{d^{14}N}{dt} = {}^{14}F_{wd} + {}^{14}F_{sd} + {}^{14}F_{bur} + {}^{14}F_{ad} + {}^{14}F_{riv} + {}^{14}F_{nf} \tag{2.15}$$

$$\frac{d^{15}N}{dt} = {}^{15}F_{wd} + {}^{15}F_{sd} + {}^{15}F_{bur} + {}^{15}F_{ad} + {}^{15}F_{riv} + {}^{15}F_{nf} \tag{2.16}$$

Using the initial conditions given in Table 2.1, the evolution of the isotopic composition of oceanic nitrogen can be calculated (Figure 2.2).

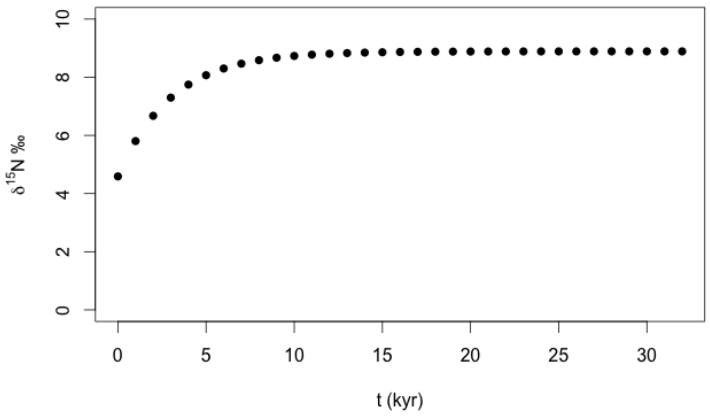

Figure 2.2. The evolution of the isotopic composition of oceanic combined nitrogen for a random set of parameters.

Analytical solution

Deriving an analytical solution of the steady-state $\delta^{15}N$ is useful to verify the correctness of the numerical model. When the $\delta^{15}N$ of oceanic nitrogen is in steady-state, then:

$$\sum F_{sources} = \sum F_{sinks} \quad (2.17)$$
$$\sum {}^{14}F_{sources} = \sum {}^{14}F_{sinks} \quad (2.18)$$
$$\sum {}^{15}F_{sources} = \sum {}^{15}F_{sinks} \quad (2.19)$$

Here the ^{15}N fluxes are used to calculate the $\delta^{15}N$ of oceanic nitrogen. The mass balance is:

$${}^{15}F_{ad} + {}^{15}F_{nf} + {}^{15}F_{riv} = {}^{15}F_{sd} + {}^{15}F_{wd} + {}^{15}F_{bur} \quad (2.20)$$

The following equation has all the terms that are in the model dependent on the oceanic $^{15}N/^{14}N$ ratio on the right side and the others on the left side:

$${}^{15}F_{ad} + {}^{15}F_{nf} + {}^{15}F_{riv} - {}^{15}F_{bur} = {}^{15}F_{sd} + {}^{15}F_{wd} \quad (2.21)$$

The fluxes of atmospheric deposition, riverine inputs, and burial are assumed to have a constant $\delta^{15}N$ over time. The ^{15}N fluxes of these processes can be obtained by:

$$R_x = (\delta^{15}N * 10^{-3} + 1)R_{air} \quad (2.22)$$
$$f_x = \frac{{}^{15}N}{{}^{15}N + {}^{14}N} = \frac{R_x}{1+R_x} \quad (2.23)$$
$${}^{15}F_x = f_x F_x \quad (2.24)$$

The ^{15}F of nitrogen fixation is dependent upon the fractionation factor:

$$\alpha_{nf} = \frac{dP'/dP}{S'/S} = \frac{{}^{15}F_{nf}/{}^{14}F_{nf}}{S'/S} \quad (2.25)$$

This can be reorganized to:

$${}^{15}F_{nf} = \alpha_{nf}\frac{S'}{S}{}^{14}F_{nf} = \alpha_{nf}\frac{S'}{S}\left(F_{nf} - {}^{15}F_{nf}\right) \quad (2.26)$$

For nitrogen fixation the substrate is N_2 in air, hence $S'/S = R_{air}$. The last equation can be solved for $^{15}F_{nf}$:

$${}^{15}F_{nf} = \frac{R_{air}\alpha_{nf}F_{nf}}{R_{air}\alpha_{nf}+1} \quad (2.27)$$

The substrate of N_2 production is oceanic nitrogen, which means that $S'/S = R_{oc}$. Hence one can obtain for water-column N_2 production and sedimentary N_2 production:

$${}^{15}F_{wd} + {}^{15}F_{sd} = \frac{R_{oc}\alpha_{wd}F_{wd}}{R_{oc}\alpha_{wd}+1} + \frac{R_{oc}\alpha_{sd}F_{sd}}{R_{oc}\alpha_{sd}+1} \quad (2.28)$$

Introducing C, to substitute all the terms on the left side of equation 2.21:

$$C = \frac{R_{oc}\alpha_{wd}F_{wd}}{R_{oc}\alpha_{wd}+1} + \frac{R_{oc}\alpha_{sd}F_{sd}}{R_{oc}\alpha_{sd}+1} \quad (2.29)$$

This equation can be solved for R_{oc}

$$R_{oc} = \frac{-\sqrt{(Cs+Cz-S-Z)^2-4C(Csz-sZ-Sz)}-Cs-Cz+S+Z}{2(Csz-sZ-Sz)} \quad (2.30)$$

where $S = \alpha_{wd}F_{wd}$, $s = \alpha_{wd}$, $Z = \alpha_{sd}F_{sd}$, and $z = \alpha_{sd}$.

2.3 Results

The broad ranges used in the baseline for the different parameters led to large differences between minimum and maximum $\delta^{15}N$ values (Figure 2.3). The median values were closest to the $\delta^{15}N$ of oceanic nitrogen when the enrichment factor of sedimentary N_2 production ε_{N2} was ~ -5‰. The results also indicated that there are relatively few conditions under which the consensus value of ε_{N2} (0‰) would lead to realistic results.

In order to zoom in on realistic results, cumulative distribution functions (CDF) were calculated for $\delta^{15}N$ values in the range of 4–6‰ (Figures 2.4, 2.5, 2.6). It shows that in the baseline most results are obtained for ε_{N2} values between -3 to -8‰. The slope of the CDF curves of the other parameter are much more linear than that of ε_{N2} (e.g. Figures 2.5 and 2.6), which indicates that the $\delta^{15}N$ of oceanic nitrogen is most sensitive to ε_{N2}. Results of simulations with parameter sets derived from Eugster and Gruber (2012) and Gruber and Sarmiento (1997) showed similar trends and indicated that ε_{N2} may fall in a range of 0 to -6‰.

The number of simulations of parameters sets (Table 2.1) leading to realistic $\delta^{15}N$ were plotted as a function of clustered variables (Figures 2.7 and 2.8). Outcomes of the baseline parameter set showed strong correlation between ε_{N2} and ε_{wd}, *i.e.* that more fractionation during benthic DNF is possible, with decreasing ε_{wd} values (Figure 2.7). These results also indicated that ε_{N2} less negative than -3 lead to a relatively small number of realistic simulations. Results of the parameter set of Eugster and Gruber (2012) showed the same correlation between ε_{N2} and ε_{wd} (Figure 2.8a). These results had generally less negative ε_{N2} values, mainly in a range of 0 to -6‰. ε_{N2} values were more negative with decreasing F_{sd}:F_{wd} ratio (Figure 2.8b).

2.4 Discussion

Brandes and Devol (2002) were the first to publish a one-box steady-state model of oceanic nitrogen isotopes. Their most important finding was that the oceanic $\delta^{15}N$ was controlled by the ratio of water-column N_2 production over sedimentary N_2 production and that this ratio was approximately 1:4. In stark contrast, our results show that the oceanic $\delta^{15}N$ is far less sensitive to this ratio, but that fractionation during sedimentary and water-column N_2 production are more important parameters (Figures 2.4 – 2.6). The discrepancy might be caused by the wider range of isotopic signals for sedimentary N_2 production covered in our simulation. Results of the baseline indicate that most realistic results are obtained of ε_{N2} values in the range of -8 to -3‰, which barely overlaps with the range of -1.5 ± 2‰ chosen by Brandes and Devol (2002). Likewise, Brandes and Devol (2002) use for water-column N_2 production ε_{wd} values of -25 ± 3‰, whereas we find that based on CDF of combined parameters, ε_{wd} should be most likely less negative than -19‰. As already pointed out by Deutsch *et al.* (2004), the homogeneous one-box model does not take into account that water-column N_2 production occurs in oxygen minimum zones, where the nitrate is locally enriched in ^{15}N compared to the ocean mean $^{15}N/^{14}N$. This local enrichment leads to higher rates of $^{15}N^{14}N$ production, which means that on global scales the expression of isotope fractionation during water-column N_2 production is lower. Thus a homogenous one-box model should have lower ε_{wd} values to account for the difference between the local substrate composition in areas where N_2 production occurs and the global mean $^{15}N/^{14}N$ ratio. This is in agreement with our results, but not with the parameterization chosen by Brandes and Devol (2002), who overestimate the impact of water-column N_2 production on the oceanic $\delta^{15}N$.

The advantage of using mass balances for both ^{14}N and ^{15}N to obtain mean $\delta^{15}N$ values, rather than approximating it directly from the $\delta^{15}N$ of the various fluxes, is that it is also accurate when the isotopes are not distributed homogeneously throughout the oceans, which also holds true for equation 2.30. Other models need special parameterization to account for mixing of water parcels with different isotopic composition (Altabet *et al.*, 2007). For instance, when a water parcel, wherein nitrate concentrations are low and the mean $\delta^{15}N$ is high through denitrification, mixes with a water parcel that has a normal composition, the $\delta^{15}N$ of the resultant water parcel will be biased towards the water parcel with the higher nitrate concentrations. Therefore, Thunell *et al.* (2004) even argued that water-column N_2 production may be unimportant for the mean oceanic $\delta^{15}N$ due to the depleted nitrate concentrations found in oxygen minimum zones.

These considerations indicate that parameterizations sets where ε_{wd} is far less negative than values actually measured in OMZ's are not necessarily unrealistic. Based on the CDF plot of ε_{N2} (Figure 2.4a), this means that the global average value of ε_{N2} may lie anywhere in the range of -3 to -8‰.

Comparison outcomes of different parameter sets

The trends observed between the parameter sets were similar, but the baseline simulation yielded relatively more realistic $\delta^{15}N$ values with more negative ε_{N2} values compared to the parameter sets based on Eugster and Gruber (2012) and Gruber and Sarmiento (1997). This is caused primarily by the wider range of F_{sd}/F_{wd} ratios used in the baseline simulations. Higher F_{sd}/F_{wd} values allow more fractionation during benthic DNF as the effect of fractionation during water-column DNF given its smaller magnitude is decreased. Nitrogen budgets generally estimate that on a global scale benthic N_2 production rates are 2 to 3 times larger than water-column N_2 production rates (Table 1.2). This suggests that the range of F_{sd}/F_{wd} values from 1 to 8 employed in the parameter set of the baseline is less realistic than the range from 1 to 4 used in the other two parameter sets (Table 2.1). Therefore, ε_{N2} falls most likely within a range of 0 to -6‰ (Figure 2.4b,c).

Comparison of predicted ε_{N2} values with literature

Brandes and Devol (1997) hypothesized that isotopic fractionation of nitrogen in sediments might be important for the $^{15}N/^{14}N$ ratio in the overlying water. They conducted an incubation experiment with estuarine sediment and measured the isotopic composition of N_2 and NO_3 in the overlying water over time. Since both the $\delta^{15}N$-N_2 and the $\delta^{15}N$-NO_3 remained constant, they concluded that no significant degree of fractionation occurred within the sediment. A later incubation experiment of continental margin sediment indicated that sedimentary denitrification had enrichment factors between 0 and -3‰ based on the isotopic composition of nitrate in the overlying water (Brandes and Devol, 2002).

Lehmann *et al.* (2004) investigated whether fractionation during sedimentary N_2 production could be important in continental shelf sediments, where bioturbation plays an important role and thus N fractionation is less likely to be limited by diffusion. They found that all nitrate produced through nitrification was consumed by denitrification. During incubation experiments the isotopic signal

of nitrate fluxes remained stable, which was explained by a balancing effect of coupled nitrification-denitrification: *i.e.* that nitrification produced nitrate enriched in ^{14}N, but that this was countered by isotopic fractionation during denitrification. The ammonium fluxing out of the sediment was enriched in ^{15}N due to fractionation during nitrification. Lehmann *et al.* (2004) suggested the possibility that this would ultimately affect the $\delta^{15}N$ of the oceanic nitrate pool, since most ammonium is oxidized to nitrate in the overlying water. In their experiment they did not measure the isotopic composition of produced N_2, but if NH_4 became heavier and NO_3 did not change, this should mean that N_2 was enriched in ^{14}N, which may support our predicted global mean negative ε_{N2} values.

Lehmann *et al.* (2007) measured $^{15}N/^{14}N$ ratios of pore water nitrate over depth of sediments collected in shallow parts of the Bering Sea. Deeper in the sediment nitrate was enriched in ^{15}N, but this was poorly communicated to the overlying water. The isotopic composition of pore water NH_4 was not measured, but model results indicated that NH_4 fluxes out of the sediment should have been enriched in ^{15}N. This led to an estimate of -4‰ for fractionation during benthic DNF, while the isotopic composition of the NO_3 efflux was similar to NO_3 in the overlying water. Granger *et al.* (2011) estimated, based on mass balances, that N_2 produced in sediment of the Bering Sea shelf should have been enriched for -6 and -8‰ compared to DIN in the overlying water.

Alkhatib *et al.* (2012) were the first to actually measure the $\delta^{15}N$ of reduced dissolved N in pore water for the calculations of ε_{N2}. Their results from estuarine and near coastal sediments indicated that N_2 should have been enriched for -4.6 ± 2‰.

Conclusion

The model results indicate that the mean oceanic $\delta^{15}N$ is most sensitive to ε_{N2} and second-most sensitive to ε_{wd}, which differs from previous studies that indicate that the ratio between the total fluxes of sedimentary and water-column N_2 production is most important. The global average ε_{N2} has most likely a value between 0 and -6‰.

In the baseline, a wide range of ε_{wd} values between -19 to -5‰ could lead to the most realistic simulations of the mean oceanic $\delta^{15}N$, which indicates that this parameter is not well-constrained by the model. The $^{15}N/^{14}N$ ratios measured in oxygen minimum zones cannot be compared to the global mean ε_{wd}, due to locally elevated $\delta^{15}N$ values of substrate and regarding the uncertain effects of mixing of water parcels from these zones with other oceanic waters.

In the short literature review, enrichment factors for benthic DNF can be found that match well with the model results. These studies generally show that the isotopic composition of nitrate does not change much during incubations, due to the opposite isotope effects of nitrification and denitrification on nitrate. However, partial nitrification leads to ammonium fluxing out of the sediment that is enriched in ^{15}N, leading to a higher mean oceanic $\delta^{15}N$. Initial studies by Brandes and Devol (1997 & 2002) may have overlooked the contribution of ammonium enriched in ^{15}N to the total oceanic nitrogen pool, thereby underestimating the impact of sedimentary N isotope fractionation on the composition of the overlying water.

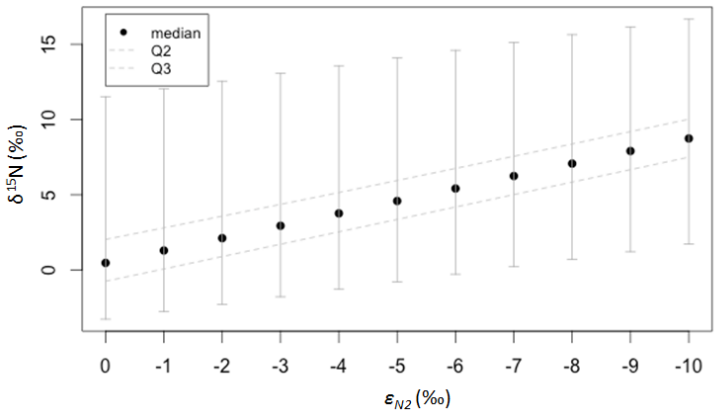

Figure 2.3. $\delta^{15}N$ values as function of ε_{N2} obtained by simulations with baseline ranges of parameters (Table 2.1) The bars show the maximum and minimum values, Q2 and Q3 are the second and third quartiles, the circles represent medians.

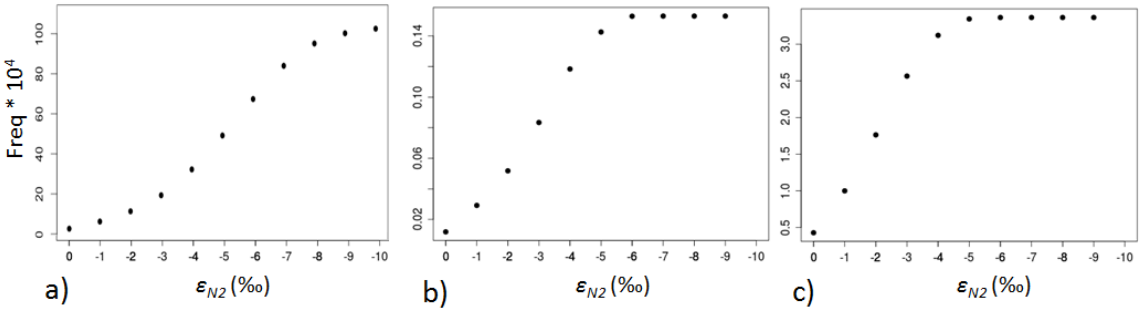

Figure 2.4. Cumulative distribution function of ε_{N2} for steady-state $\delta^{15}N$ solutions in the range of 4-6‰ based on parameter sets of a) the baseline, b) Eugster and Gruber (2012), and c) Gruber and Sarmiento (1997) (Table 2.1).

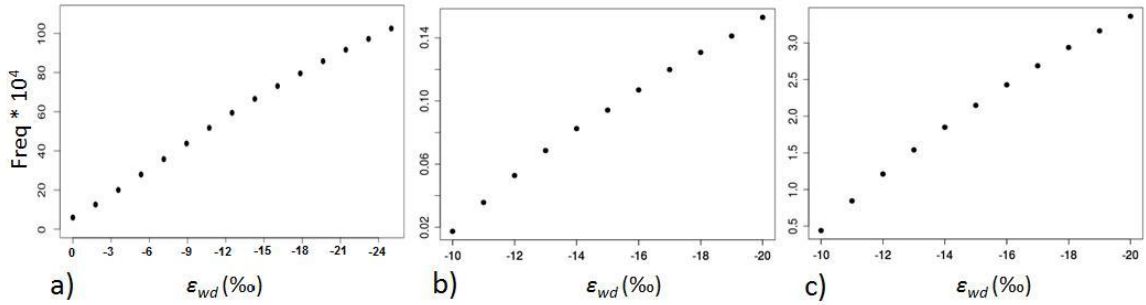

Figure 2.5. Cumulative distribution function of ε_{wd} for steady-state $\delta^{15}N$ solutions in the range of 4-6‰ based on parameter sets of a) the baseline, b) Eugster and Gruber (2012), and c) Gruber and Sarmiento (1997) (Table 2.1).

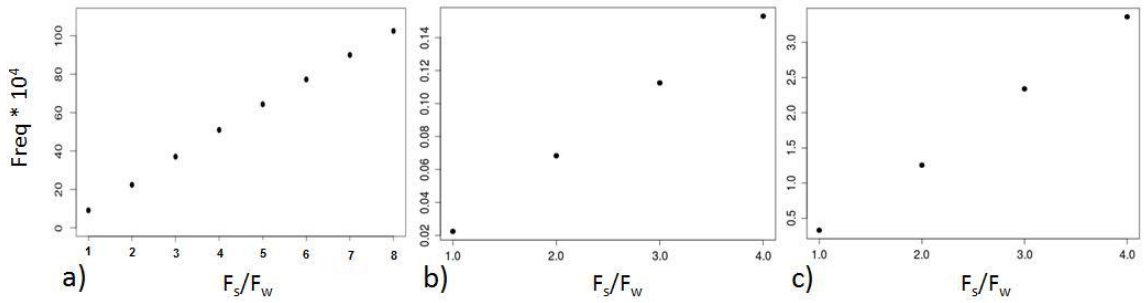

Figure 2.6. Cumulative distribution function of F_s/F_w for steady-state $\delta^{15}N$ solutions in the range of 4-6‰ based on parameter sets of a) the baseline, b) Eugster and Gruber (2012), and c) Gruber and Sarmiento (1997) (Table 2.1).

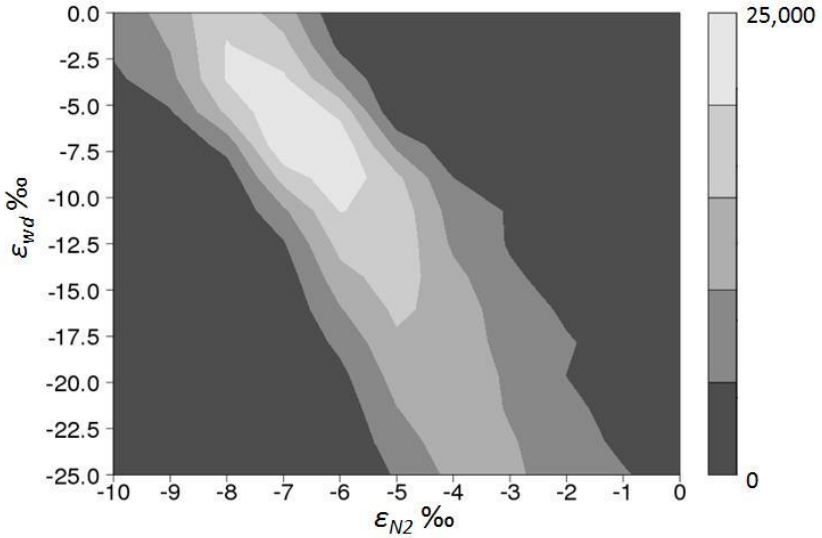

Figure 2.7. Number of simulations with the parameter set of the baseline leading to realistic results ($\delta^{15}N$ values between 4-6‰) as function of ε_{N2} and ε_{wd} on the vertical and horizontal axis, respectively.

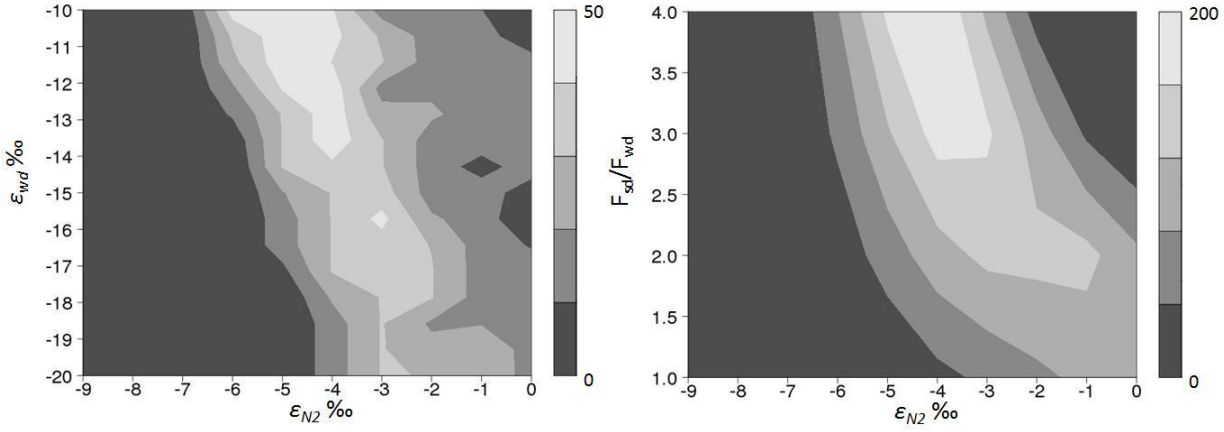

Figure 2.8. Number of simulations with the parameter set of Eugster and Gruber (2012) (Table 2.1) leading to realistic results ($\delta^{15}N$ values between 4-6‰) as function of a) ε_{N2} and ε_{wd}, b) F_{sd}/F_{wd} and ε_{N2}.

3. The effects of bio-irrigation on benthic N isotopic fractionation

In the first chapter it was shown that it is highly likely that sedimentary N_2 production causes fractionation and that this may have a large impact on the isotopic composition of oceanic nitrate. However, empirical data on benthic N fractionation are scarce and not unambiguous (see literature review, chapter 1). Here we use reaction-transport models to spatially resolve reaction rates and transport fluxes, and to identify conditions that promote isotopic fractionation in benthic environments.

Generally it is assumed that benthic N_2 production causes little to no N fractionation due to complete consumption of NO_3, so that enzymatic discrimination against $^{15}NO_3$ cannot be expressed (Brandes and Devol, 1997; Lehmann *et al.*, 2004). However, as long there is an efflux of NO_3 from the sediment, fractionation may occur even if the sediment acts as a *net* nitrate sink. For example, in coastal environments, where NO_3 transport is typically governed by advection or bioirrigation (Meile and Van Cappellen, 2005), advective flow through sand ripples or pumping by tube-dwelling organisms can bring NO_3 into the sediment that partially gets denitrified – and undergo fractionation – before a fraction escapes back into the overlying water. In addition to such short-circuiting of NO_3, *i.e.* the fast exchange of NO_3 between the sediment and the overlying water, the pumping of oxic water into deeper anoxic parts of sediments also changes redox conditions, which affects the rates of various remineralization pathways and the coupling between nitrification and denitrification (Na *et al.*, 2008; Kristensen *et al.*, 2011). How these factors alter the isotope signatures is poorly constrained.

The main goal in this chapter is to determine with a reactive transport model to what extent burrow ventilation can cause fractionation of N isotopes during sediment N cycling, and whether this is likely to have a significant impact on the mean oceanic $\delta^{15}N$. As a case study, the surroundings of a single idealized burrow are modeled. The model simulations are meant to reflect characteristics of predominant pumping macrofauna such as the lugworm *Arenicola sp.*, deposit feeders that create J-shape burrows in order to digest OM stored in sands (Volkenborn *et al*., 2007). In intertidal sand flats of the eastern North Sea, where on average 20 to 40 adult *A. marina* live per square meter, these worms are considered to be the dominant sediment reworkers (Flach and Beukema, 1994). The feeding pockets of adults are typically positioned at 20 to 40 cm depths in the sediment. With piston-like tail-to-head movements, the worms pump water across the SWI into the burrow in order to obtain oxygen for respiration and to remove toxic metabolites. The injection of fluid at the feeding pocket into the sediment leads to an advection-dominated flow regime and spatial heterogeneity in the environment near the burrow (Meysman *et al.*, 2006a). The work here expands on one-dimensional models, which have been used so far for the benthic N isotope studies (Lehmann *et al.*, 2007; Prokopenko *et al*, 2011), as they cannot capture the dynamics under these circumstances adequately.

3.1 Model description

The model simulates biochemical processes in sediment near a single burrow with emphasis on fractionation during nitrogen cycling (Figure 3.1). It accounts for the activity of a juvenile *Arenicola marina* or adult *A. pacifica*, with a feeding pocket located at 15 cm depth in the sediment. Dissolved species in the overlying water including O_2, dissolved organic matter (DOM), NO_3, and SO_4 are injected at the feeding pocket into the sediment. The concentration of these species in the injected water are the same as in the overlying water, with the exception of the oxygen concentration that is 60% lower due to respiration by the lugworm. Sediment DOM is replenished through the degradation of POM to DOM, DOM diffusing into the sediment, and via the feeding pocket. Oxidation of DOM in the model, occurs through reduction of O_2, NO_3, $Fe(OH)_3$, and SO_4. The model includes the recycling of $Fe(OH)_3$ and SO_4, through re-oxidation of Fe and HS. When DOM is remineralized, organic N is converted into NH_4 through ammonification. The NH_4 either migrates out of the sediment or it can be re-oxidized to NO_3 through nitrification. The size of the NO_3 pool is dependent on nitrification, denitrification, and fluxes across the SWI. In the model N fractionation through nitrification and denitrification is accounted for, whereas the NH_4 produced *in situ* is assumed to have the same isotopic composition as POM and DOM in the overlying water. Hence, the NH_4 pool only can get heavier through nitrification, while NO_3 can get lighter through nitrification, and heavier through denitrification. Therefore, the isotopic composition of N_2 produced through denitrification is dependent on fractionation during nitrification and denitrification, and the magnitude of these fluxes. A detailed summary of the reactions included in the model is given in Table 3.1.

3.2 Implementation

The model uses a 2D domain with axial symmetry to represent the physical 3D environment (Figure 3.2a). The feeding pocket was located at 15 cm below the SWI. Above the feeding pocket the feeding funnel is located, characterized by a 10 times higher permeability than the rest of the sediment (Meysman *et al.*, 2006a). The distance between the SWI and the bottom of the domain was set to 20 cm, and a domain radius of 10 cm was chosen, reflecting a density of 32 organisms/m^2 (Flach and Beukema, 1994). To discretize the model domain a triangular mesh was used, with element sizes between 60 μm and 10 mm. The mesh was finest near the feeding funnel and SWI in order to calculate sharp concentration gradients accurately (Figure 3.2b).

The distribution of dissolved species was described by the following mass balance equation:

$$\frac{\delta C_i}{\delta t} = \nabla(D_i \nabla C_i) - \nabla(\boldsymbol{v} C_i) + R, \qquad (3.1)$$

where D_i is the diffusion coefficient, C_i the concentration, $\boldsymbol{v}$ the velocity vector, and R the net reaction rate.

Transport processes

The molecular and ionic diffusion coefficients D^{mol} were calculated following Boudreau (1997) as a function of temperature (10 °C) and salinity (35). To correct for tortuosity in the porous medium the relationship of Boudreau (1996) was used:

$$D_i = \frac{D_i^{mol}}{(1-2\ \ln\phi)}, \quad (3.2)$$

where ϕ denotes the porosity. The second term accounts for advection, which is driven by pumping of the lugworm. Following Meysman *et al.* (2006a), first a flow model was run that calculated the pore water velocity field $\boldsymbol{v}$. The "Free and Porous Media Flow" package from Comsol 4.3 was used for this purpose, which uses the Darcy-Brinkman equation (Le Bars and Worster, 2006):

$$\frac{\rho}{\phi}\frac{\delta \boldsymbol{v}}{\delta t} = \nabla\left[-pI + \frac{\eta}{\phi}(\nabla\boldsymbol{v} + (\nabla\boldsymbol{v})^T) - \frac{2\eta}{3\phi}(\nabla\boldsymbol{v})I\right] - \left(\frac{\eta}{k} + \beta|\boldsymbol{v}| + O\right)\boldsymbol{v} + F, \quad (3.3)$$

$$\rho\nabla\boldsymbol{v} = O, \quad (3.4)$$

where ρ is the density of seawater, p the pressure, φ the porosity, $\boldsymbol{v}$ the velocity vector, I the interfacial viscous stress exchange, η the dynamic viscosity of seawater, k the permeability of porous medium, β the viscous force proportional to the square of the fluid velocity, F is force term which accounts for other forces that act on the volume such as gravity, and O accounts for the sources and sinks of seawater, *i.e.* the pumping of seawater into the sediment.

Boundary conditions: The right side and bottom were specified as no flow boundaries and the top of the model as an open boundary. The left border is the symmetry axis, where the net velocity of pore water is 0. At the injection pocket water was pumped into the sediment at a rate of 1.6 ml min^{-1} (Volkenborn *et al.*, 2007). The area below the SWI and the bottom of the model was specified as the porous matrix.

Reaction network

All reactions accounted for in the model are listed in Table 3.1. Their parameterization reflects a coastal environment at a water-depth of approximately 100 m. The concentrations of solids, *i.e.* POM and $Fe(OH)_3$, were imposed to the model and constant during simulations in order to reduce computation time. The $Fe(OH)_3$ profile was obtained by implementing the 1D model (Appendix A) described in Thullner *et al.* (2009), which used a flux of 12.1 µmol cm^{-2} y^{-1} at the top and a no gradient condition at the bottom of the model domain. For the POM profile an analytical solutions was used, whereby the POM flux at the top of sediment was determined with the following equation:

$$J_{POM} = 1800 * 10^{(-0.5086-0.000389*zw)}, \quad (3.5)$$

where *zw* is the seafloor depth in meters. The following equation described the POM profile:

$$a = \frac{u-\sqrt{u^2+4*k_{POM}*D_b}}{2*D_b}, \quad (3.6)$$

$$A = \frac{-J_{POM}}{D_b*a+u}, \quad (3.7)$$

$$POM = A * e^{az}, \quad (3.8)$$

where u is the sedimentation rate, which was set to 0.398 cm y^{-1} (Middelburg *et al.*, 1997), D_b the bioturbation coefficient set to 27.5 cm^2 y^{-1} (Middelburg *et al.*, 1997),

and k_{POM} the degradation rate of POM (Table 3.2). Rate constants (Table 3.2) for Fe oxidation, HS oxidation, and FeS precipitation were taken from Van Cappellen and Wang (1995). The various mineralization reactions of DOM with different electron acceptors use a first-order rate law with respect to DOM. The turnover time of DOM in sediments can be used to calculate k as shown in the following formula:

$$\tau = \frac{DOM}{R_{DOM}} = \frac{1}{k}, \quad (3.9)$$

where τ is the turnover time, R_{DOM} the reaction rate of DOM, and k the reaction rate coefficient of DOM. The value for k used in the model corresponds to a turnover time of 14 hours, which typifies highly reactive DOM (Alperin *et al.,* 1994).

Boundary conditions: For dissolved species, fixed concentrations in the water above the sediment were used as upper boundary conditions. Following Van Cappellen and Wang (1995) and Thullner *et al.* (2009), the SO_4 concentration was set to 28 mM, while the concentrations of NH_4, Fe^{2+}, and HS were set to zero (Table 3.3). The bottom-water concentration of DOM used in the model was based on Lonborg and Sondergaard (2009), who determined bioavailable DOC concentrations in shallow water (23 m) near the Danish coast. The imposed NO_3 and O_2 concentrations were based on empirical data from the World Ocean Atlas 2009 (Garcia *et al*, 2010a,b). From the 5-Minute Global Relief Data Collection bathymetry database (http://www.ngdc.noaa.gov), locations were selected where the seafloor is between 90 and 110 m depth (Figure 3.3) and NO_3 and O_2 concentrations nearest to the SWI were taken (Appendix C). Figure 3.4 shows higher O_2 concentrations at higher latitudes, caused by increased solubility at lower temperatures. Also a strong decrease of NO_3 concentrations from the northern regions towards the tropics is apparent. Simulations for two scenarios were run. The first one represented a sediment at higher latitudes, with an O_2 concentration of 340 µM (7 mL/L) and a NO_3 concentration of 25 µM. The second scenario represented sediments in the tropics, with an oxygen concentration of 190 µM (4 mL/L) and a NO_3 concentration of 5 µM. Throughout the text we will refer with 'baseline' to simulations that reflect the conditions at higher or lower latitudes with all the standard parameters (Tables 3.2 and 3.3) and a burrowing depth of 15 cm.

The composition of the water injected at the feeding pocket had a different composition than the water above the sediment (Table 3.3). The O_2 concentration was 40% of that in the overlying water due to uptake by the lugworm for respiration. The assumption was made that feeding by the lugworm on POM had no effect on the DOC concentrations in the water.

Definitions

Throughout the text, net fluxes will be distinguished from fluxes in and out the sediment. All fluxes account for flow across the SWI and the feeding pocket. Q values of species j are defined as:

$$Q_j = \frac{F_{j,out}}{F_{j,in} + Rj_{,prod}}, \quad (3.10)$$

where $F_{j,out}$ is the flux out, $F_{j,in}$ the flux in, and $R_{j,prod}$ the *in situ* production rate of species j. Hence, Q values indicate how much of a solute is flushed out relative to its

total sources. $R_{j,prod}$ for NH_4 and NO_3 reflect organic matter mineralization and nitrification rates, respectively.

Three definitions for enrichment factors are used to quantify benthic N fractionation. The first relates the isotopic composition of the produced N_2 gas to the mean oceanic isotopic composition of NO_3:

$$\varepsilon_{N2} = \left(\frac{\left({}^{15}N/{}^{14}N\right)_{gas}}{\left({}^{15}NO_3/{}^{14}NO_3\right)_{ocean}} - 1 \right) * 1000. \quad (3.11)$$

The second one compares the isotopic composition of the produces nitrogen gasses to the composition of nitrate in the sediment:

$$\varepsilon_{sed} = \left(\frac{\left({}^{15}N/{}^{14}N\right)_{gas}}{\left({}^{15}NO_3/{}^{14}NO_3\right)_{sediment}} - 1 \right) * 1000, \quad (3.12)$$

where NO_3 denote concentrations in the sediment. The third one is defined as:

$$\varepsilon_{flux} = \left(\frac{(F_{15NH4}+F_{15NO3}+F_{DO15N})/(F_{NH4}+F_{NO3}+F_{DON})}{\left({}^{15}N/{}^{14}N\right)_{gas}} - 1 \right) * 1000, \quad (3.13)$$

where F_{15NH4}, F_{15NO3}, F_{DO15N}, F_{NH4}, F_{NO3},*and* F_{DON} represent the heavy and light net sediment uptake fluxes of nitrate, ammonia, and *in situ* produced DON, respectively.

3.3 Results

Nitrogen cycling: Simulations were run to steady-state for sediments at 100 m water-depth, with bottom-water conditions typical for sediments at higher latitudes and lower latitudes (Figure 3.4). Most O_2 in the sediment is localized in a plume around the feeding pocket, where aerobic degradation of DOM and nitrification take place. Here the NO_3 concentrations build up and migrate towards the DNF zone, which encapsulates the aerobic zone. The simulations with a burrowing depth of 15 cm have Q_{NO3} values of ~25% (Table 3.4), which indicates that roughly 75% of the NO_3 from the aerobic zone is denitrified. Compared to the lower latitudes more benthic DNF takes place at higher latitudes, which is caused by higher nitrification rates and NO_3 influxes. Higher O_2 concentrations in the bottom-water led to higher remineralization rates, which may be caused directly by higher oxic respiration rates and indirectly through oxidation of DOM through the reduction of electron acceptors formed through re-oxidation of NH_4, Fe and HS. In the anoxic zone DOM degradation takes place through reduction of $Fe(OH)_3$ and SO_4. There NH_4 can accumulate, since no O_2 available for nitrification.

In the simulations with a burrow-depth of 5 cm instead of 15 cm, the NO_3 plumes at the feeding pocket are smaller (Figure 3.6). There is more short-circuiting of NO_3, *i.e.* more NO_3 that is injected at the feeding pocket escapes DNF and is flushed back to the overlying water. The simulations with shallower burrowing depths also show lower nitrification rates and higher NH_4 effluxes.

Isotope signatures: For the simulations at both latitudes, ε_{N2} values are negative (Table 3.5), which indicates that N_2 produced *in situ* is significantly enriched in ^{14}N compared to NO_3 in the overlying water. The simulations with fractionation turned off during either nitrification or DNF, show that ε_{N2} values are most sensitive to fractionation during nitrification. Since ε_{sed} values are negative, the *in situ* produced N_2 gas is lighter than the average NO_3 in the sediment, which reflects fractionation

during DNF. However, this fractionation leads to heavier NO_3 in the sediment, which limits the expression of the isotope effect of DNF on the N_2 production. When fractionation during both DNF and nitrification are turned off, ε_{N2} values are still negative, due to the DNF of *in situ* produced NO_3 that has the same isotopic composition as DOM, which is lighter than NO_3 in the overlying water (Table 3.5).

In the baseline simulations NH_4 fluxes from the sediment to the overlying water carry the isotopic signal of benthic nitrification and are enriched in ^{15}N compared to DOM, while the outward NO_3 fluxes have essentially the same isotopic composition as NO_3 in the overlying water. The same holds true for simulations with a burrowing depth of 5 cm, since here the NO_3 fluxes out of the sediment are even lighter than NO_3 in the overlying water. The isotopic composition of outward NH_4 fluxes also have a greater impact on the mean oceanic $\delta^{15}N$, because their magnitude is larger than the fluxes of NO_3 (Table 3.4).

Sensitivity analysis: The sensitivity of the N isotope effect of DNF were evaluated by changing the mineralization and nitrification rate coefficients, by using different NH_4 concentrations in the injected water, and by decreasing the pumping velocity in the baseline simulation at higher latitudes (Table 3.6). Increasing the NH_4 concentration in the fluid injected at the feeding pocket and enhancing the ammonification rate by using a higher DOM degradation constant lead to more negative ε_{N2} values. Hence, the degree of fractionation during benthic DNF seems to be sensitive to the size of the NH_4 pool available for nitrification. A higher nitrification rate leads to less fractionation, which indicates that NH_4 concentrations may become depleted in the nitrification zone, while NH_4 concentrations in the anoxic zone are substantial given the large flux of NH_4 out of the sediment. Lower pumping velocities lead to significantly lower DNF and nitrification rates and lower fluxes of NH_4 out of the sediment. The results show a trend of an increasing degree of fractionation during benthic DNF with decreasing bio-irrigation rates. Comparing simulations with and without bio-irrigation (first and last column in Table 3.6), and artificially suppressing fractionation during nitrification and denitrification, showed that fractionation during DNF had a larger and nitrification a smaller impact on ε_{N2} values in the absence of bio-irrigation compared to the baseline simulation.

3.4 Discussion

The simulations indicate that benthic DNF can cause fractionation and that coupled nitrification-denitrification plays an important role. The outcomes for benthic N fractionation strongly depend on how the model captures N dynamics in the sediment. Therefore, the model output shall be compared to literature first and thereafter the fractionation patterns shall be discussed.

N dynamics: Most nitrification takes place near the feeding pocket (Figures 3.4 and 3.5), where also NO_3 from the overlying water is injected. Assuming that NO_3 from these two sources is mixed homogenously before being denitrified, the contribution of coupled nitrification-denitrification would be equal to the percentage of NO_3 that cannot escape the sediment, which is roughly 75% (100% - Q_{NO3}).

The areal rates of DNF and nitrification given by the model at both high and low latitudes (Table 3.4) fall in the broad range of values found in literature (Table 3.7). The simulations show relatively high ammonium efflux-ratios Q_{NH4} compared to results of Lehmann *et al.* (2004), who reported ratios in the range of 6 – 66%. In that study nitrification rates were determined in the range of 0.8 to 2.0 mmol N m^{-2} d^{-1}, which exceed our model outcomes and lead to less NH_4 fluxing out of the sediment. However, higher ammonium efflux-ratios may be typical for sediments inhabited by lugworms. Na *et al*. (2008) measured during incubation experiments with *A. marina,* high effluxes of NH_4 (4.7 mmol m^{-2} d^{-1}) and inferred from mass balances that nitrification should account for 0.6 – 0.8 mmol N m^{-2} d^{-1}, which is similar to our model outcomes of the higher latitudes and corresponds to a Q_{NH4} of ~90%. In their experiment they determined a much higher DNF rate of 4.7 mmol N m^{-2} d^{-1}, which requires a very high flux of NO_3 into the sediment (3.9 mmol N m^{-2} d^{-1}). They were unable to reproduce these experiment results with a model, which in fact yielded a DNF flux of 1.3 mmol N m^{-2} d^{-1} similar to our model.

Fractionation patterns: Fractionation during nitrification provides a light source of NO_3 for DNF, which then leads to the production of light N_2. A high nitrification rate in the sediment may lead to less fractionation during this process, when this leads to strong depletion of NH_4 concentration in nitrification zones. However, when nitrification rates are low, while DNF rates are high, then even if a high degree of fractionation occurs during nitrification, the impact on the isotopic composition of the *in situ* produced N_2 gas is limited. A simple box model was created to illustrate the importance of the magnitude of nitrification as a source for DNF (Figure 3.7). It represents sediment where the NO_3 pool is formed through fluxes from the overlying water F_{NO3} and *in situ* produced NO_3, F_{Nit}. Based on the baseline simulation at higher latitudes, F_{NO3} was set to the influx of NO_3 at the feeding pocket with the same isotopic composition as NO_3 in the overlying water, while F_{Nit} was varied from 0 to roughly twice the simulated nitrification rate and had the same isotopic composition as NO_3 produced *in situ*. The following equations were used as rate laws for DNF:

$$F_{DNF} = k * {}^{14}NO_3, \tag{3.14}$$

$$F'_{DNF} = \alpha_{DNF} * k * {}^{15}NO_3, \tag{3.15}$$

where F and F' denote fluxes of ^{14}N and ^{15}N, respectively. Assuming steady-state, the size of the NO_3 pools were calculated as follows:

$${}^{14}NO_3 = \frac{F_{Nit}+F_{NO3}}{k}, \tag{3.16}$$

$${}^{15}NO_3 = \frac{F'_{Nit}+F'_{NO3}}{k*\alpha_{DNF}}. \tag{3.17}$$

Fractionation during DNF changes the pool sizes of $^{14}NO_3$ and $^{15}NO_3$, but does not lead to the production of lighter N_2 as the isotope effect of DNF cannot be expressed, since no NO_3 fluxes out of the sediment. Therefore, when the nitrification rate is 0, the isotopic composition of produced N_2 gas is equal to that of NO_3 in the overlying-water and hence ε_{N2} is 0 (Figure 3.8). When the influx of NO_3 produced *in situ* increases, the produced N_2 becomes lighter and then ε_{N2} decreases.

Higher NH_4 concentrations in the injection water lead to the production of lighter N_2, because the injected NH_4 increases the nitrification rate, while it also increases the NH_4 pool available for nitrification. However, the amount of NH_4 injected at the feeding pocket of *A. marina* is poorly constrained. An estimate can be based on literature: Reize and Schöttler (1989) determined that *A. marina* excrete 100 µmol NH_4 per gram dry weight in 72 h. The dry weight of one *A. marina* lugworm is roughly 0.5 gram (Riisgard *et al.*, 1996), while the pumping rate is 1.6 ml min^{-1}. This allows the calculation of the NH_4 concentration in the injected water, which yields 8 µM NH_4. One could also argue that uptake of O_2 is coupled to organic matter uptake and the associated release of NH_4. For example, the baseline simulation of higher latitudes uses a ~200 µM lower concentration of O_2 in the injected water than in the overlying water, in order to account for oxygen uptake by the lugworm. Assuming Redfield stoichiometry, this corresponds to the production of 23 µM NH_4, which is similar to the higher NH_4 concentration used during the sensitivity analysis (Table 3.6). Given the high sensitivity of ε_{N2} values to this parameter, irrigation might enhance fractionation during benthic DNF in sediments under waters with higher NH_4 concentrations. A higher DOM degradation rate constant increased the remineralization rate including the O_2 uptake for respiration, which leads to a lower nitrification rate and higher NH_4 production. Therefore, a higher degree of fractionation could occur during nitrification, which led to slightly more negative ε_{N2} values.

A higher nitrification rate coefficient led to less fractionation during the sensitivity analysis. This may be due to complete consumption of NH_4 at sites in the sediment were nitrification takes place. This parameter has a rather large impact on the degree of fractionation, but is not well constrained. The value of k_{Nit} used in the baseline of $0.63 * 10^7$ μM^{-1} y^{-1} is rather low, while the value in the sensitivity analysis of $2.50 * 10^7$ μM^{-1} y^{-1} rather high, compared to k_{Nit} values found in literature, which range from $0.5 * 10^7$ to $2.9 * 10^7$ μM^{-1} y^{-1} (Berg *et al.*, 2003; Soetaert *et al,.* 1996; Wang and Van Cappellen, 1996). The discrepancies found in literature may be explained by different concentrations of nitrifiers or inhibitors, such as sulfur (Joye and Hollibaugh, 1995), at distinct locations. Temperature and salinity are generally considered less important variables for nitrification rates in marine sediments, because microbial nitrifying communites can adapt to these parameters that are rather stabile. Nitrification potentials in warmer and colder regions are therefore similar (Ward, 2008).

Fractionation during DNF occurs to some extent in all simulations. Generally, lower DNF rates lead to more fractionation, due to partial consumption of the NO_3 pool. Shallower burrowing depths leads to more short-circuiting of NO_3, corresponding to larger fractionation due to incomplete consumption of the substrate pool. From the simulations with a burrowing depth of 5 cm at higher latitudes it became apparent that this leads indeed to a flux of heavier NO_3 out of the sediment. The extent of short-circuiting should be limited for sediments inhabited by adult *A. marina*, since their feeding pockets are located relatively deep in the sediment.

The model outcomes indicate that lower pumping rates lead to a higher degree of benthic N fractionation, contrary to the expected enhanced fractionation.

Less bio-irrigation leads to a significant decrease of DNF rates (Table 3.6), which allows more fractionation during this process as a smaller fraction of the NO_3 pool is consumed. Less bio-irrigation led to a higher *in situ* DOC remineralization rate, which can only be caused by less DOC being flushed out of the sediment. The impact of nitrification on ε_{N2} values decreased, while it is unlikely that the degree of fractionation during nitrification decreased, since a lower nitrification rate and higher ammonification rate lead to the consumption of a smaller fraction of the NH_4 pool. This was verified by calculating the $\delta^{15}N$ of NO_3 produced *in situ*, yielding -24.7‰ in the simulation without bioirrigation and -11.4‰ in the baseline simulation. Therefore it most likely that the impact of nitrification on ε_{N2} values is lower due to decreased coupled nitrification-DNF. In the baseline simulation, NO_3 produced in the oxic zone is pumped towards the DNF zone, which enhances this coupling. In the model without bio-irrigation the nitrification zone is placed above the DNF zone, which allows NO_3 produced *in situ* to diffuse the overlying water. The fact that simulations with and without bio-irrigation show fractionation may seem to suggest a strong degree of N fractionation in most sediments. However, simulations without bio-irrigation may be unrealistic, since the parameterization was adjusted for sediments with bio-irrigation. For instance, the high mineralization rates may be unjustified, which lead to very high NH_4 effluxes compared to literature (e.g. Lehmann *et al.*, 2004).

Given that DOM has a $\delta^{15}N$ of 1.5‰, while oceanic NO_3 has one average a $\delta^{15}N$ of 5‰, DNF of NO_3 produced through coupled ammonification-nitrification should always lead to negative ε_{N2} values. Since *in situ* produced NO_3 is an important source for benthic DNF ε_{N2} should be negative even if no fractionation during nitrification and DNF would occur.

Conclusion

The simulations indicated in general that a significant degree of fractionation may occur within sediments. The model outcomes do not support the hypothesis that sediments inhabited by *Arenicola marina* enhances fractionation, since their burrows are too deep to allow a significant degree of short-circuiting of NO_3. Yet the simulations with a burrowing depth of 5 cm show that active pumping by lugworms may lead to short-circuiting (Figure 3.6) and increased fractionation. Therefore, it is more likely that instead of *A. marina* other tube-dwelling organisms, which burrow less deep into the sediment, enhance N fractionation.

The simulations without bio-irrigation showed more fractionation compared to the baseline simulation. This was caused by decreased DNF rates, which allow more fractionation during this process. Since the parameterization of these simulations without bio-irrigation were adjusted to simulations with bio-irrigation, the outcomes may be unrealistic. More effort should be put in understanding why we found also fractionation in *non*-bioturbated sediments, while other model studies have indicated that benthic DNF causes little fractionation (Lehmann *et al.*, 2007; Prokopenko *et al.*, 2011).

The extent of coupled nitrification-denitrification is higher in bio-irrigated sediments, which as fractionation during nitrification provides a light source of NO_3 for DNF, may be the locations exhibiting most fractionation. Also model outcomes

indicated that DNF rates are higher in bioturbated sediments, which means that any fractionation during this process will have a larger impact on the mean oceanic $\delta^{15}N$.

Table 3.1. Reaction pathways, stoichiometries, and rate laws implemented in the model.

POM degradation:

$(CH_2O)_x(NH_3)_{y(s)} \rightarrow (CH_2O)_x(NH_3)_{y(aq)}$

$$R_{POM} = k_{POM} * POM$$

Primary redox reactions (DOM respiration):

Oxic respiration

$(CH_2O)_x(NH_3)_{y(aq)} + x\ O_2 \rightarrow x\ CO_2 + y\ NH_3 + x\ H_2O$

$$R_{O2} = k * DOM \frac{O_2}{O_2 + K_{m,O2}}$$

Denitrification

$(CH_2O)_x(NH_3)_{y(aq)} + 0.8x\ NO_3^- \rightarrow 0.4x\ N_2 + 0.2x\ CO_2 + 0.6x\ H_2O + y\ NH_3 + 0.8x\ HCO_3^-$

$$R_{Den} = (k * DOM - R_{O2}) \frac{{NO_3}^-}{{NO_3}^- + K_{m,NO3}}$$

$$R_{Den,15NO3} = \alpha_{Den}(k * DOM - R_{O2}) \frac{{}^{15}{NO_3}^-}{{NO_3}^- + K_{m,NO3}}$$

Iron oxide reduction

$(CH_2O)_x(NH_3)_{y(aq)} + 7x\ CO_2 + 4x\ Fe(OH)_3 \rightarrow 4x\ Fe^{2+} + y\ NH_3 + 8x\ HCO_3^- + 3x\ H_2O$

$$R_{Fe(OH)3} = \left(k * DOM - R_{O2} - R_{Den} - R_{Den,15NO3}\right) \frac{Fe(OH)_3}{Fe(OH)_3 + K_{m,Fe(OH)3}}$$

Sulfate reduction

$(CH_2O)_x(NH_3)_{y(aq)} + 0.5x\ SO_4^{2-} \rightarrow 0.5x\ H_2S + 0.5y\ NH_3 + x\ HCO_3^-$

$$R_{SO4} = \left(k * DOM - R_{O2} - R_{Den} - R_{Den,15NO3} - R_{Fe(OH)3}\right) \frac{{SO_4}^{2-}}{{SO_4}^{2-} + K_{m,SO4}}$$

Secondary redox reactions (reoxidation):

Nitrification

$NH_4^+ + 2\ O_2 \rightarrow NO_3^- + 2\ H^+ + H_2O$

$$R_{Nit} = k_{Nit} * O_2 * {NH_4}^+$$

$$R_{Nit,15NH4} = \alpha_{Nit} * k_{Nit} * O_2 * {}^{15}{NH_4}^+$$

Sulfide oxidation

$HS^- + 2\ O_2 \rightarrow SO_4^{2-} + H^+$

$$R_{HS,Ox} = k_{HS} * HS^- * O_2$$

Iron oxidation

$Fe^{2+} + ¼\ O_2 + 2\ HCO_3^- + ½\ H_2O \rightarrow Fe(OH)_3 + 2\ CO_2$

$$R_{Fe,Ox} = k_{Fe} * Fe^{2+} * O_2$$

Dissolution reaction:

Iron sulfide dissolution

$FeS + H^+ \rightarrow Fe^{2+} + HS^-$

$$R_{FeS} = k_{FeS}\left(\frac{Fe^{2+} * HS^-}{K_{FeS} * H^+} - 1\right)$$

Table 3.2. Model parameters

Parameter	Value	Description
k_{POM}	0.221 y^{-1}	Rate coefficient for POM degradation[1]
k	1.73 d^{-1}	Rate coefficient for DOM degradation[2]
$K_{m,O2}$	8 µmol dm^3	Half-sat. constant of oxic resp.[1]
$K_{m,NO3}$	10 µmol dm^{-3}	Half-sat. constant of DNF[1]
$K_{m,Fe(OH)3}$	12.5 µmol cm^{-3}	Half-sat. constant of Fe(III) reduction[1]
$K_{m,SO4}$	1000 µmol dm^{-3}	Half-sat. constant of SO_4 reduction[1]
k_{Nit}	0.63 * 10^7 dm^3 mol^{-1} y^{-1}	Rate coefficient for NH_4^+ oxidation[4]
k_{HS}	7.06 * 10^8 dm^3 mol^{-1} y^{-1}	Rate coefficient for HS^- oxidation[1]
k_{Fe}	2.35 * 10^9 dm^3 mol^{-1} y^{-1}	Rate coefficient for Fe^{2+} oxidation[1]
pK_{FeS}	2.95	Equilibrium constant for FeS formation[1]
$\delta^{15}NO_3$	5 ‰	Isotope composition of NO_3[5]
$\delta^{15}N_{Org}$	1.5 ‰	Isotope composition of OM[5]
α_{Den}	0.980	Fractionation factor for DNF[6]
α_{Nit}	0.975	Fractionation factor for nitrification[6,7]
φ	0.85	Porosity
O	1.6 ml min^{-1}	Pumping rate[8]

[1]Thullner *et al.*, 2009. [2]See text. [3]Value fitted. [4]Cook *et al.* 2006. [5]Gruber, 2008. [6]Prokopenko *et al.*, 2011. [7]Casciotti and Buchwald, 2012. [8]Volkenborn *et al.*, 2010.

Table 3.3 Boundary conditions and composition of bottom-water and injected water

Upper boundary conditions	Value
F_{POM} (µmol cm^{-2} y^{-1})[a]	510
F_{FeOH3} (µmol cm^{-2} y^{-1})[b]	12.1
DOC (µM)[c]	50
SO_4 (mM)[b]	28
NH_4[b]	0
O_2 (µM)[d]	HL: 340, LL: 190
NO_3 (µM)[d]	HL: 25, LL: 5
Concentrations in injected water	
O_2 (µM)[d]	HL: 136, LL: 76
NH_4(µM)[d]	13
DOC(µM)[c]	50

[a]Middelburg *et al.* (1997), [b]Van Cappellen and Wang (1995), [c]Lonborg and Sondergaard (2009), [d]See text. HL and LL denote *resp.* higher and lower latitudes.

Table 3.4. Areal reaction rates and benthic fluxes of sediment at 100 m depth at high and low latitudes

	Low latitudes		**High latitudes**	
Burrowing depth	15 cm	5 cm	15 cm	5 cm
Denitrification (mmol N m^{-2} d^{-1})	0.39	0.24	1.46	0.85
Nitrification (mmol N m^{-2} d^{-1})	0.21	0.15	0.55	0.39
Remineralization (mmol N m^{-2} d^{-1})	1.42	1.49	1.67	1.68
NO3 net flux (mmol N m^{-2} d^{-1})*	-0.18	-0.09	-0.91	-0.46
NO3 flux out (mmol N m^{-2} d^{-1})	0.11	0.17	0.54	0.79
NH4 net flux (mmol N m^{-2} d^{-1})	1.21	1.34	1.12	1.29
NH4 flux out (mmol N m^{-2} d^{-1})	1.50	1.63	1.58	1.75
Q_{NO3} (%)	22	41	27	48
Q_{NH4} (%)	88	92	74	82

*Negative and positive values denote fluxes in and out of the sediment, respectively.

Table 3.5. Isotopic signatures of benthic fluxes for sediment at 100 m water-depth.

	Low latitudes		High latitudes	
Burrowing depth	15 cm	5 cm	15 cm	5 cm
$\delta^{15}N$ of NO_3 flux out (‰)	4.8	2.0	4.7	3.6
$\delta^{15}N$ of NH_4 flux out (‰)	5.6	5.0	7.6	6.8
ε_{N2} (‰)	-11.3	-12.8	-6.3	-8.5
ε_{sed} (‰)	-10.1	-10.5	-7.6	-8.9
ε_{flux} (‰)	5.2	9.5	1.1	7.2
ε_{N2} when $\varepsilon_{den} = 0$ (‰)	-10.5		-5.7	
ε_{sed} when $\varepsilon_{nit} = 0$ (‰)	-2.5		-2.0	
ε_{flux} when $\varepsilon_{den} = 0$ and $\varepsilon_{nit} = 0$ (‰)	-1.8		-1.3	

Table 3.6. Results sensitivity analysis of the baseline simulation at higher latitudes.

	Baseline $C_{NH4,inj}$ 13 µM	$C_{NH4,inj}$ 0	$C_{NH4,inj}$ 25 µM	k_{Nit} * 4	k * 10	O * 0.1	O * 0
Denitrification (mmol N m^{-2} d^{-1})	1.46	1.16	1.70	1.67	1.43	0.36	0.30
Nitrification (mmol N m^{-2} d^{-1})	0.55	0.25	0.79	0.84	0.47	0.10	0.14
Remineralization (mmol N m^{-2} d^{-1})	1.68	1.68	1.68	1.68	2.02	1.64	1.77
NH_4 flux out (mmol N m^{-2} d^{-1})	1.50	1.43	1.76	1.30	2.01	1.55	1.61
ε_{N2} (‰)	-6.3	-4.2	-8.0	-4.0	-7.1	-6.8	-7.8
ε_{N2} when ε_{den} = 0 (‰)	-5.7						-2.8
ε_{sed} when ε_{nit} = 0 (‰)	-2.0						-5.6
ε_{flux} when ε_{den} = 0 and ε_{nit} = 0 (‰)	-1.3						-0.4

$C_{NH4,inj}$ is the NH_4 concentration in the injected water, k_{Nit} and k are rate coefficients of resp. nitrification and DOM degradation, O is the pumping rate. See Tables 3.4 and 3.5 for comparison with the baseline.

Table 3.7. Compilation of data on sedimentary nitrification and DNF rates in natural environments.

Location (water-depth)	Site description	Nitrification (mmol N m^{-2} d^{-1})	Denitrification (mmol N m^{-2} d^{-1})
Tasman Bay & Beatrix Bay, New Zealand (~30 m)[1]	Shallow coastal, muddy sand, musselfarming	0.05 - 0.10	0.19 – 0.36
Santa Monica Bay, USA (<67 m)[2]	Shallow coastal sediment	0.78 – 2.02	1.15 – 2.47
North Sea (<200 m)[3]	Shallow continental shelf, fine sand	0.23 – 0.30	0.24 – 0.32
Svalbard, Norway (115 – 330 m)[4]	Arctic coastal, silty and cohesive sediment	0.02 – 0.07	0.16 – 0.63
St. Lawrence Estuary, Canada (300 – 400 m)[5]	Coastal, hypoxic bottom-water	0.31	0.27
NE Pacific, Washington, USA (630 m)[6]	Continental margin	1.9	3.2
Sagami Bay, Japan (1450 m)[7]	Continental margin	0.22	0.72
NE Atlantic Ocean (4800 m)[8]	Abyssal plain	0.059	0.0051

References: [1]Christensen *et al.* (2002), [2]Lehmann *et al.* (2004), [3]Lohse *et al.* (1996), [4]Glud *et al.* (2004), [5]Crowe *et al.* (2011), [6]Devol (1991), [7]Glud *et al.* (2009), [8]Brunnegard *et al.* (2004).

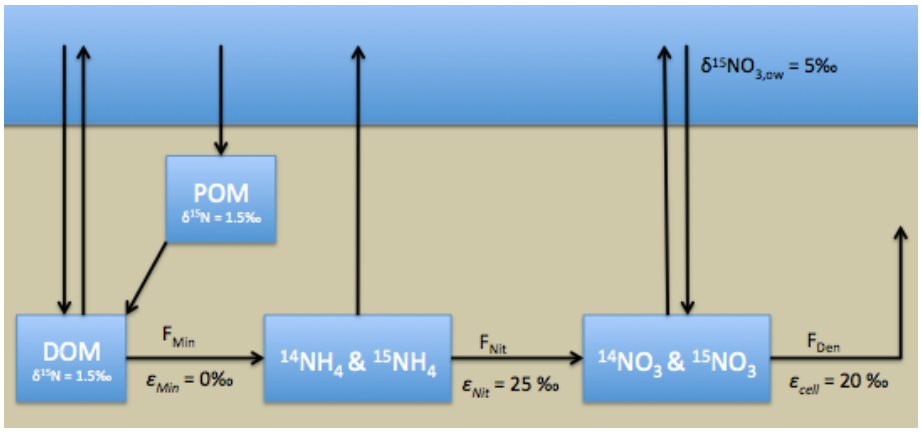

Figure 3.1. Nitrogen cycling in sediment. F_{min} denotes the mineralization of DOM, F_{Nit} represents the nitrification rate, and F_{Den} the denitrification rate. The enrichment factors $\varepsilon_{Min,}$ $\varepsilon_{Nit,}$ and ε_{cell} denote the inherent N isotope effect at cell level for mineralization, nitrification, and denitrification, respectively.

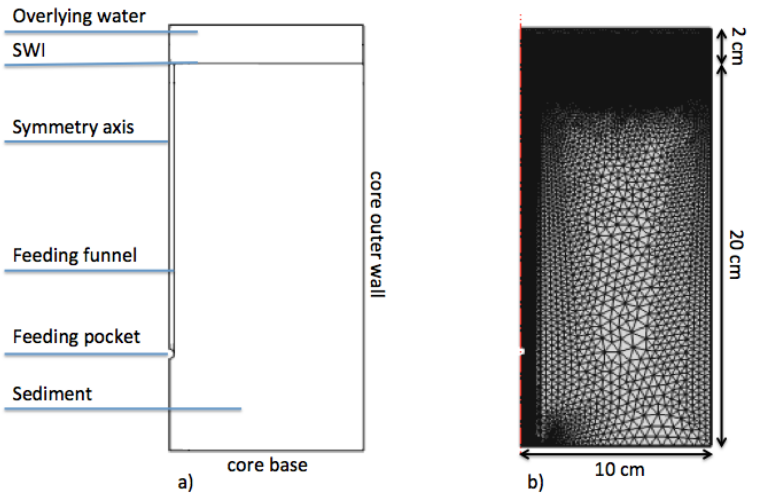

Figure 3.2. The model domain's geometry (a) and fine mesh (b). The left border is the symmetry axis of the cylinder.

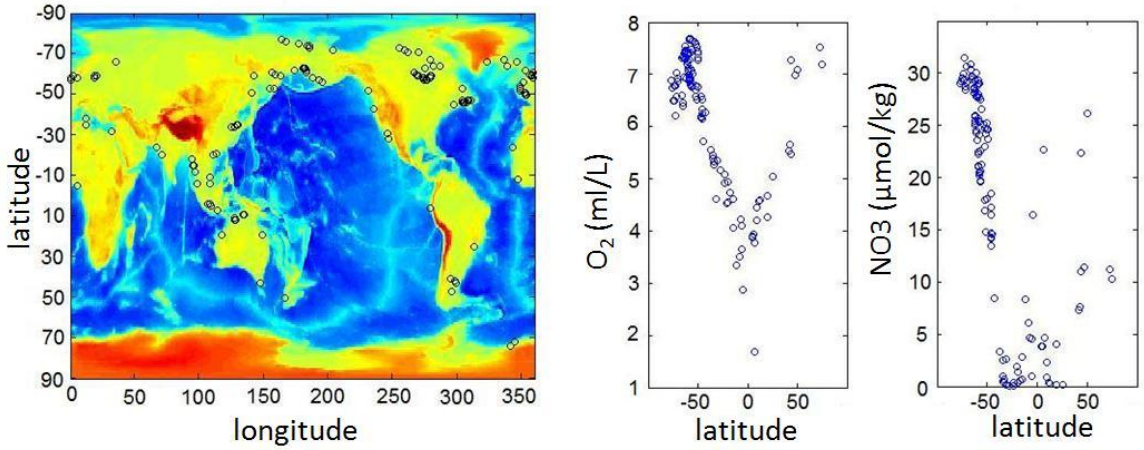

Figure 3.3. Sample locations near sediments at 90 to 110 m water-depth and the respective oxygen and nitrate concentrations at these locations.

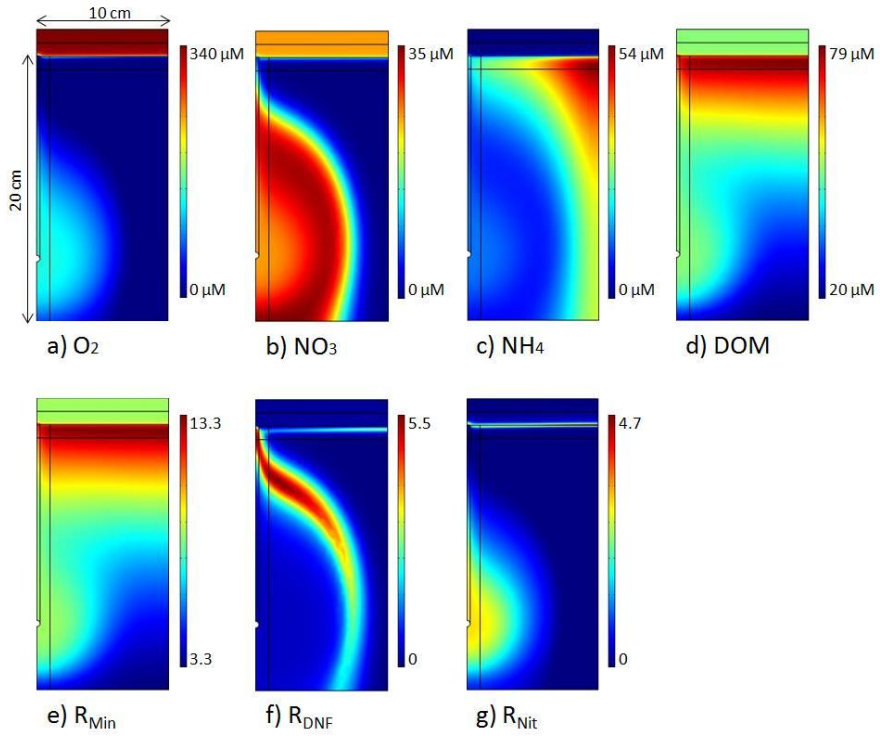

Figure 3.4. Steady-state concentration and reaction fields from simulation of bioturbated sediment at higher latitudes. Feeding pocket of lugworm is located at 15 cm depth, rates of mineralization R_{Min}, denitrification R_{DNF}, and nitrification R_{Nit} are in µmol cm^{-3} d^{-1}.

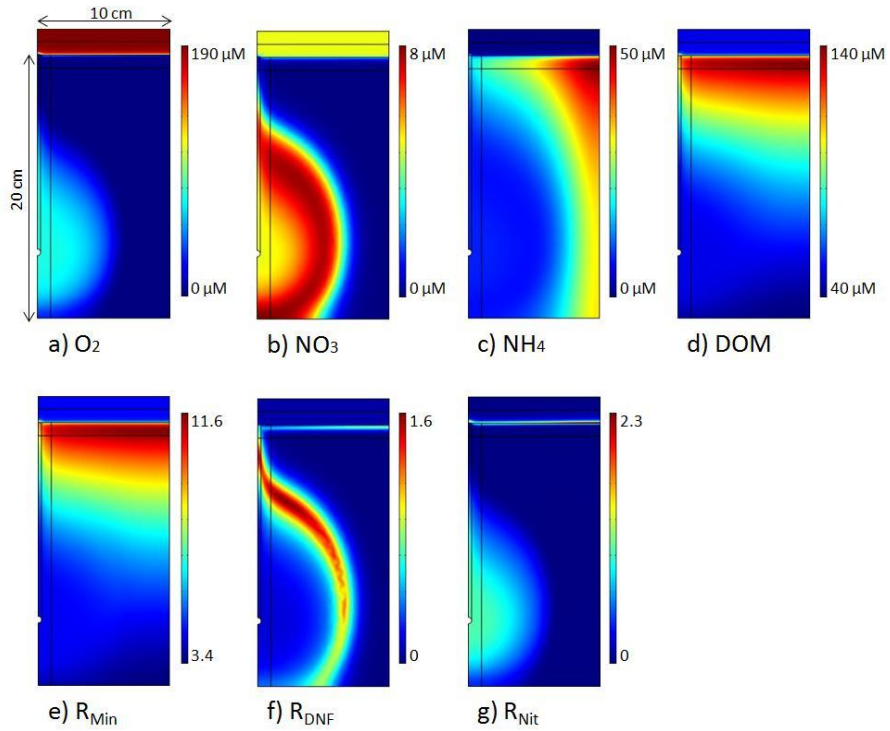

Figure 3.5. At lower latitudes; simulated steady-state concentrations and reaction rates in a bioturbated sediment at 100 m water-depth. Rates of mineralization R_{Min}, denitrification R_{DNF}, and nitrification R_{Nit} are in µmol cm^{-3} d^{-1}.

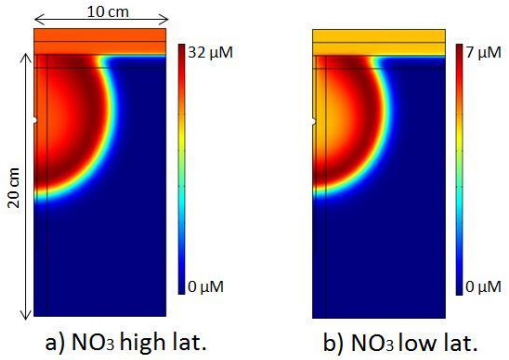

Figure 3.6. Nitrate concentration fields surrounding 5 cm deep burrows in sediment at (a) higher and (b) lower latitudes.

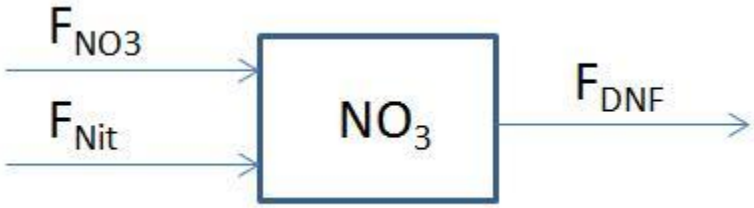

Figure 3.7. One-box model to illustrate the importance of magnitude of source for isotopic composition of produced N_2 gas. F_{DNF}, F_{Nit}, and F_{NO3} denote the areal DNF rate, nitrification rate, and influx of NO_3, respectively.

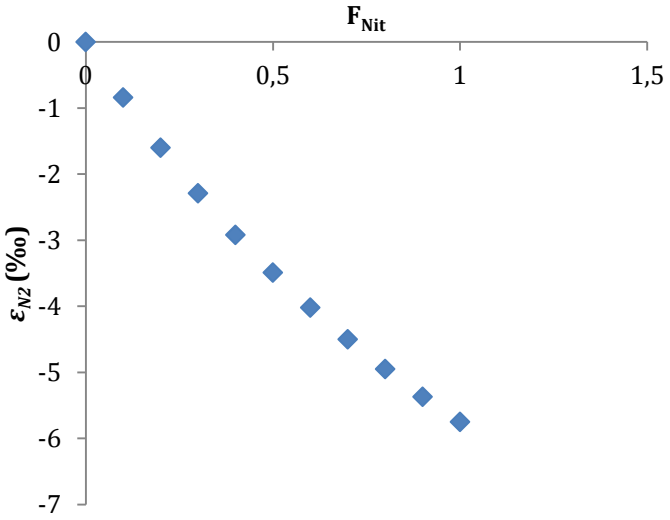

Figure 3.8. Effects of changing the nitrification rate on the isotopic composition of produced N_2 gas. F_{Nit} denotes the nitrification rate in mmol N m^{-2} d^{-1} and has a $\delta^{15}N$ of -11.4‰.

4. Patterns in sediment N fractionation

Benthic N dynamics are controlled to a large extent by mineralization of OM and therefore also by the rain rate of labile POM, which in turn is dependent on primary productivity in surface waters and the degradation of the settling OM. The latter aspect is highlighted by the study of Middelburg *et al.* (1997), which found a statistically significant correlation between water-depth and the areal benthic mineralization rate. The equations worked out by these authors were later used by Thullner *et al.* (2009) to setup reaction-transport models for different water-depths.

Here we follow their approach and consider water-depth as the master variable for diagenetic processes in marine sediments, in order to setup simulations of distinct natural benthic environments with consistent parameterizations. The main goal is to identify (i) patterns in N fractionation and (ii) conditions with likely substantial sedimentary N fractionation, which may be useful for follow-up experimental research. Additionally, this potentially allows scaling up of model outcomes to a global scale, by integrating the results of N isotope fractionation at different water-depths over the corresponding seafloor surface area. This may help to gain a better understanding of the relative importance of fractionation during benthic DNF on the mean oceanic $\delta^{15}N$.

4.1 Methods

The same model was used as in the previous chapter, but with parameter values adjusted for water-depth (Table 4.1). The NO_3 and O_2 bottom-water concentrations were determined with the same method as in Chapter 3, using the World Ocean Atlas 2009. At greater water-depths bottom-water concentrations were rather similar at higher and lower latitudes, which made running simulations with different bottom-water concentrations unnecessary. Since DOM concentrations are poorly constrained, DOM bottom water concentrations were set to 50 µM for all water-depths. NH_4 concentrations in the injected water were slightly lower at greater water depths reflecting reduced sediment metabolism. Following Thullner *et al.* (2009) k_{Nit} values at 2000 and 3500 m water-depths were set to 2/3 of that at 100 m.

Scaling up: Areal denitrification rates at various depths were obtained by using the formula given by Bohlen *et al*. (2012):

$$F_{DNF} = F_{tot,POC}\left[a + b * c^{(O_2 - NO_3)_{bw}}\right], \quad (4.1)$$

where F_{DNF} is the areal net loss of DIN, $F_{tot,POC}$ the areal total rain rate of POC, O_2 and NO_3 are concentrations in µM, and a, b, and c are fitted parameters with values of a= 0.060, b = 0.19, and c = 0.99, respectively. The total rain rate of POC $F_{tot,POC}$ includes a refractory fraction of POC F_{bur} that will be buried, and a labile POC part that corresponds to the F_{POM} used in the 3D model. Hence:

$$F_{tot,POC} = F_{bur} + F_{POM}. \quad (4.2)$$

F_{POM} was obtained by the relationship of Middelburg *et al.* (1997), while Bohlen *et al.* (2012) determined this parameter with a more sophisticated method based on primary production data. Equation 4.2 can be solved using the empirical relationship also given by Bohlen *et al*. (2012):

$$F_{bur} = 0.14 * {F_{tot,POC}}^{1.11}; \quad \text{for water-depths < 2000 m,} \tag{4.3}$$

$$F_{bur} = 0.014 * {F_{tot,POC}}^{1.05}; \quad \text{for water-depths > 2000 m.} \tag{4.4}$$

Bottom-water concentrations were obtained for use in Eq. 4.1 from the World Ocean Atlas (Garcia *et al*, 2010a,b). The 5-Minute Global Relief Data Collection bathymetry database (http://www.ngdc.noaa.gov) was queried to integrate areal DNF rates over the corresponding seafloor surface (see Appendix D). Then these outcomes were combined with the ε_{N2} values computed in the RTM model, to calculate a global, areal weighted average estimate of ε_{N2}.

4.2 Results

Different burrowing depths and distinct bottom-water conditions at lower and higher latitudes had a large impact on DNF rates, which fell in a broad range (Figure 4.1), while at greater water-depth DNF rates were more constant. In general DNF rates computed were high compared to typical measured values (Lehmann *et al.*, 2004), and decreased with water-depth. Sediment nitrification rates were more variable in shallow than in deep water, while no strong trend with increasing water-depth was apparent (Figure 4.1). DOC mineralization rates decreased with increasing water-depth and were less sensitive to different O_2 and NO_3 bottom-water concentrations and the burrowing depth. Since mineralization rates decreased with water-depth, while nitrification rates did not, the ammonia efflux-ratios Q_{NH4} decreased with depth (Tables 4.2 and 4.3). Q_{NO3} values increased with water-depth, due to decreasing DNF rates.

The overall fractionation during benthic DNF increased with water-depth as ε_{N2} values became more negative, which indicates that lighter N_2 was produced (Figure 4.1). This was caused by increased fractionation during DNF, given the more negative ε_{sed} values (Table 4.2), which relate the isotopic composition of the produced N_2 gas to NO_3 in the sediment. Simulations with fractionation during DNF turned off showed less negative ε_{N2} with increasing depth, indicating that less fractionation during nitrification occurred.

At 100 m water-depth ε_{N2} where more negative at lower than at higher latitudes, while this was the opposite at 500 m depth. A shallower burrowing depth led to higher Q_{NH4} and Q_{NO3} values at all water-depths, while DNF rates decreased, which was more pronounced at smaller water-depths (Tables 4.2, 4.3). Shallower burrowing led at 100 and 500 m water-depth to more negative ε_{N2} values, while at greater water-depths ε_{N2} values became less negative.

Turning bio-irrigation off (Table 4.4) led - compared to the baseline simulations (Table 4.2) - to lower areal DNF and nitrification rates, while DOC mineralization rates were significantly higher at 100 and 500 m water-depth, but slightly lower at 2000 and 3500 m water-depth. The ε_{N2} values were similar at 100 and 500 m water-depth (Tables 4.2, 4.4), but at greater depths the degree of fractionation was significantly less without bio-irrigation. The ε_{sed} values fell all in a range between -12.0 and -14.2 ‰.

To estimate a global average fractionation factor, the simulation at different water-depths were weighted by seafloor surface and by the extent of DNF. Rather than relying on the results of our small-scale high-resolution models, DNF rates

were estimated as a function of water-depth using POM fluxes by Middelburg *et al.* (1997), combined with Eqns. 4.1 – 4.4, which resulted in 267 Tg N y^{-1}. The predominance of shallow water DNF then led to a ε_{N2} of -10.4 ‰ (Table 4.5).

4.3 Discussion

The O_2 and NO_3 bottom-water concentrations for sediments at shallower water-depth are more dependent on the latitudinal positioning than at greater depth. These parameter have a great impact on DNF rates, which depend on NO_3 concentrations in the sediment and thus on nitrification rates, which in turn depend on O_2 availability and sediment NO_3 uptake. Since these parameters vary per site more at shallow water-depth, so do DNF rates. DNF rates tend to decrease with increasing depth due to lower mineralization rates, which leads to lower substrate availability for DNF. This is caused due to a lower rain rate of POM, which leads to lower DOC *in situ* production rates, and higher O_2 concentrations in sediments, which consumes DOC faster than DNF. The latter aspect is highlighted by enhanced NO_3 efflux ratios (Table 4.2). Nitrification rates may be less sensitive to changes in the POM rain rate, since the effects of higher O_2 availability and lower NH_4 concentrations (lower Q_{NH4}) cancel each other out.

In the simulations at 100 m and 500 m water-depth, fractionation during nitrification is more important than fractionation during DNF, while in the simulations at 2000 m and 3500 m fractionation during DNF is more important. These observations correspond to opposite trends of Q_{NO3} and Q_{NH4} values with increasing depth, which are a measure to which extent the substrate pools for DNF and nitrification, respectively, are consumed. DNF rates are significantly lower in sediments at greater water-depths, while nitrification rates (Figure 4.1) and NO_3 concentration in the overlying water (Table 4.1) remain relatively constant. Therefore a smaller fraction of the benthic NO_3 pool is consumed, which allows more expression of the isotope effect inherent to DNF. Relatively constant nitrification rates and lower *in situ* NH_4 productions with increasing water-depth lead to a relatively high degree of consumption of the NH_4 pool and thus less expression of the isotope effect inherent to nitrification.

The NO_3 concentration in the overlying water were very distinct between higher and lower latitudes at 100 m water-depth, while they were equal at 500 m water-depth. Since fractionation occurred mainly during nitrification at these depth, ε_{N2} values were much more negative at lower latitudes in the 100 m simulation, since *in situ* produced light NO_3 was the main source for DNF. At 500 m water-depth nitrification was quantitatively a smaller source for DNF at lower latitudes than at latitudes, due to lower O_2 concentrations, while the influx of NO_3 was the same. Hence, at 500 m ε_{N2} values are more negative at higher than at lower latitudes. Shallower burrows lead to higher Q_{NO3} and Q_{NH4} values. At 100 m and 500 m depth this leads to more negative ε_{N2} due to more fractionation during both nitrification and DNF. At greater water-depth the degree of fractionation became less. This is caused by decreased coupled nitrification-denitrification, which leads to more light NO_3 escaping the sediment.

Scaling up: Bohlen *et al.* (2012) estimated that sediments removed 198 Tg fixed N per year, which is significantly lower than the outcome of our estimate of 267 Tg N y^{-1}. The most important difference between their and our method is that they used a more sophisticated method to estimate POC rain rates to the sediments, which for instance also accounted for seasonality, while the POC rate used here was only based on seafloor depth. However, it is the relative contribution of DNF as a function of water-depth that governs the value of ε_{N2}. Therefore, even though 79% of the seafloor is located at more than 2750 m depth, the impact of these on the global average ε_{N2} is limited as the integrated DNF rates are highest in sediments at shallower water-depth.

The value of -10.4 ‰ (Table 4.5) is more negative than the likely range of sediment DNF fractionation suggested using a simple box-model of a steady-state N cycle in Chapter 2. However, it shows that fractionation in bio-irrigated sediments may have a large effect on the isotopic composition of fixed N in the water-column.

In the RTM models the burrowing activity of the lugworm is assumed to be the same at all depths, while it is likely that less lugworms live at greater depths, due to lower availability of food as rain rates of POM are lower. Therefore, simulated transport processes and thus also the N dynamics are most likely untypical for greater depths. Even though bio-irrigation is important in coastal sediments, other processes such as advective flow through sand ripples (Boudreau *et al.*, 2001) are likely important, but not reflected in the model outcomes. N dynamics are likely distinct in different types of environments, e.g. sandy or muddy sediments, so that the estimated global average ε_{N2} must be considered a very crude estimate, biased towards sediments inhabited by lugworms. The models also do not account for anammox, which has a different isotopic imprint. For instance, anammox consumes preferentially light NH_4, leading to heavier NH_4, which may limit the isotope effect of nitrification on NO_3 in the sediment.

Conclusion

DNF rates vary more between sites in shallow water environments due to more distinct O_2 and NO_3 concentrations in bottom-water. With increasing water-depth there was a trend of decreasing DNF rates. DOC remineralization rates decrease with increasing water-depth, while no strong trend for nitrification was observed.

At shallower water-depth fractionation during nitrification is most important, which is caused by a smaller partial consumption of the NH_4 due to higher *in situ* NH_4 production rates. In these simulations a significant part of the NO_3 was consumed by DNF, which led to less fractionation during this process. At greater water-depths NH_4 production decreases, while O_2 concentrations are higher. This leads to lower Q_{NH4} values and less fractionation during nitrification. At these depths DNF rates decrease, while sources of NO_3 remain rather constant, which allows more fractionation during DNF. Shallower burrows lead to more fractionation at lower water-depths, due to higher effluxes of NH_4 and NO_3. At 2000 and 3500 m depth the degree of fractionation decreased due to a lower degree of coupling between nitrification and DNF.

Since on a global scale most DNF takes place in shallower water, the average oceanic $\delta^{15}N$ is most sensitive to the degree of fractionation in these sediments.

Integrating DNF rates over the entire ocean floor yielded a mean oceanic ε_{N2} of -10.4 ‰. However, this is a crude estimate as only sediments inhabited by lugworms were considered, which neglects the effects of other transport regimes in sediments where pore water flow is not driven by bio-irrigation.

Table 4.1. Model parameters and boundary conditions for model setups of sediment at different water-depths.

	100 m	500 m	2000 m	3500 m
O_2 bw (µM)[a]	HL: 340, LL: 190	HL: 240, LL: 140	240	170
NO_3 bw (µM)[a]	HL: 25, LL: 5	HL: 30, LL: 30	35	35
DOM bw (µM)[a]	50	50	50	50
NH_4 inj (µM)[a]	13	13	8	8
F_{POM} (µmol cm^{-2} y^{-1})[b]	510	357	93	24.3
$F_{Fe(OH)3}$ (µmol cm^{-2} y^{-1})[c]	12.1	5.62	0.32	0.02
Φ[c]	0.85	0.80	0.80	0.80
k_{POM} (y^{-1})[d]	0.221	0.174	0.072	0.030
k (y^{-1})[a]	6.3	6.3	3.2	3.2
k_{Nit} (dm^3 mol^{-1} y^{-1})[a]	$0.63 * 10^7$	$0.63 * 10^7$	$0.42 * 10^7$	$0.42 * 10^7$
k_{HS} (dm^3 mol^{-1} y^{-1})[c]	$7.0 * 10^8$	$3.0 * 10^8$	$3.0 * 10^8$	$3.0 * 10^8$
k_{Fe} (dm^3 mol^{-1} y^{-1})[c]	$2.4 * 10^9$	$1.0 * 10^9$	$1.0 * 10^9$	$1.0 * 10^9$
$K_{m,O2}$ (µM)[c]	8	8	8	8
$K_{m,NO3}$ (µM)[c]	10	10	10	10
$K_{m,Fe(OH)3}$ (µmol cm^{-3})[c]	12.5	12.5	12.5	12.5
$K_{m,SO4}$ (µM)[c]	1000	2000	2000	2000

Abbreviations: 'bw' denotes bottom-water, 'inj' denotes injected water. HL and LL indicate higher and lower latitudes, respectively. References: [a]see text, [b]Middelburg *et al.* (1997), [c]Van Cappellen and Wang (1995), [d]Boudreau (1997).

Table 4.2. Overview results of simulations of sediments at different water-depths with burrows at 15 cm depth.

Water-depth	100 m LL	100 m HL	500 m LL	500 m HL	2000 m	3500 m
F_{DNF}	0.39	1.46	1.25	1.41	0.51	0.34
F_{Nit}	0.21	0.55	0.15	0.36	0.40	0.30
F_{Min}	1.42	1.67	0.93	0.94	0.36	0.23
F_{NO3}	-0.18	-0.91	-1.10	-1.05	-0.11	-0.04
F_{NH4}	1.21	1.12	0.78	0.58	-0.05	-0.06
Q_{NO3} (%)	22	27	34	32	71	78
Q_{NH4} (%)	88	74	89	74	37	43
ε_{N2} (‰)	-11.3	-6.3	-3.6	-5.8	-18.9	-20.1
ε_{sed} (‰)	-10.1	-7.6	-11.2	-9.3	-19.0	-20.1
ε_{flux}(‰)	5.2	1.1	0.3	0.0	-0.4	-0.5
ε_{N2}, ε_{den} = 0 (‰)	-10.5	-5.7	-2.8	-4.8	-3.1	-2.7
ε_{N2}, ε_{nit} = 0 (‰)	-2.5	-2.0	-1.2	-1.8	-16.6	-17.9
ε_{N2}, ε_{den} & ε_{nit} = 0 (‰)	-1.8	-1.3	-0.5	-0.9	-0.8	-0.5

Areal net fluxes *F* are in mmol N m^{-2} d^{-1}. LL and HL denote low and high latitudes, while subscript 'DNF' denotes denitrification, 'Nit' nitrification, and 'Min' mineralization. See previous chapter for meaning of ε and Q values.

Table 4.3. Overview results of simulations of sediments at different water-depths with burrows at 5 cm depth.

Water-depth	100 m LL	100 m HL	500 m LL	500 m HL	2000 m	3500 m
F_{DNF}	0.24	0.85	0,85	0,77	0,50	0,30
F_{Nit}	0.15	0.39	0,12	0,24	0,25	0,20
F_{Min}	1.49	1.68	0,92	0,94	0,32	0,19
F_{NO3}	-0.09	-0.46	-0,72	-0,54	-0,25	-0,10
F_{NH4}	1.34	1.29	0,81	0,68	0,07	-0,01
Q_{NO3} (%)	41	48	50	39	71	81
Q_{NH4} (%)	92	82	92	82	59	58
ε_{N2} (‰)	-12.8	-8.5	-6,4	-7,8	-10.4	-16,3
ε_{sed} (‰)	-10.5	-8.9	-11,6	-10,5	-13.5	-20,8
ε_{flux}(‰)	9.5	7.2	1,2	0,9	-0,2	-0,1

Areal net fluxes *F* are in mmol N m^{-2} d^{-1}. LL and HL denote low and high latitudes, while subscript 'DNF' denotes denitrification, 'Nit' nitrification, and 'Min' mineralization. See previous chapter for meaning of ε and Q values.

Table 4.4. Model outcomes for simulations without bio-irrigation.

	100 m LL	100 m HL	500 m LL	500 m HL	2000 m	3500 m
F_{DNF}	0.08	0.30	0.29	0.27	0.17	0.10
F_{Nit}	0.05	0.14	0.03	0.07	0.10	0.07
F_{Min}	1.77	1.77	1.03	1.03	0.30	0.11
ε_{N2} (‰)	-9.7	-8.0	-6.7	-7.1	-9.0	-9.54
ε_{sed} (‰)	-14.1	-12.0	-13.1	-12.2	-12.2	-14.2

Areal net fluxes *F* are in mmol N m^{-2} d^{-1}. LL and HL denote low and high latitudes, while subscript 'DNF' denotes denitrification, 'Nit' nitrification, and 'Min' mineralization. See previous chapter for meaning of ε values.

Table 4.5. Benthic DNF rates and N fractionation at global scale.

Depth interval (m)	DNF rate (mmol N m^{-2} d^{-1})	Surface (10^6 km^2)	DNF rate (Tg N y^{-1})	DNF (%)	DNF rate (Tg ^{14}N y^{-1})	DNF rate (Tg ^{15}N y^{-1})	ε_{N2}* (‰)
0-300	0.93	25.9	123.2	46.2	122.8	0.5	-8.8
300 - 1250	0.80	18.1	73.7	27.6	73.4	0.3	-4.7
1250 - 2750	0.25	32.3	41.7	15.6	41.5	0.2	-18.9
> 2750	0.02	285.8	27.9	10.5	27.8	0.1	-20.1
Total		362.1	266.5		265.5	1.0	-10.4

DNF rates are based on equations 4.1 - 4.4. *For ε_{N2} values, the average was taken out of the simulations for lower and higher latitudes (Table 4.2).

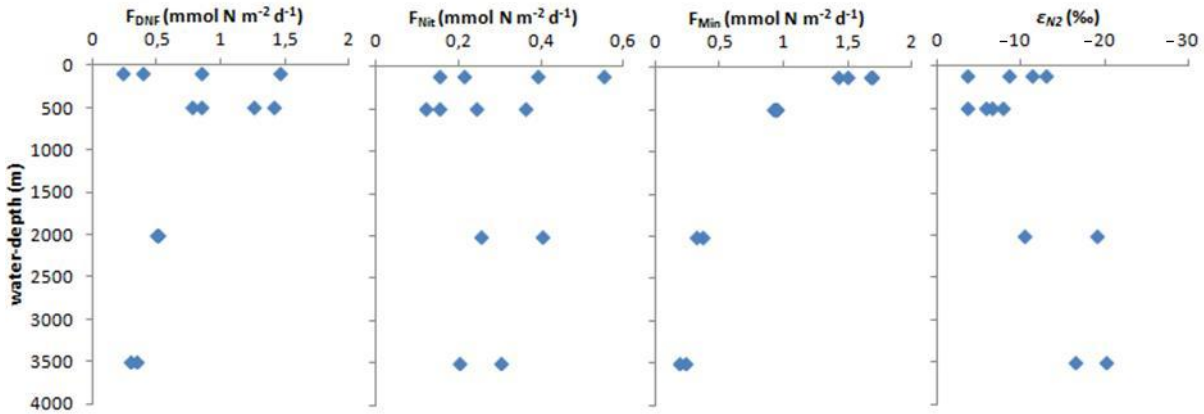

Figure 4.1. Areal rates of DNF, nitrification, mineralization, and ε_{N2} values at different water-depths based on results at higher and lower latitudes and with burrows at 5 and 15 cm depth.

Summary

Even though a high degree of fractionation is inherent to denitrification, studies (Brandes and Devol, 1997; Brandes and Devol, 2002) have indicated that this is not expressed in sediments due to complete consumption of the NO_3 pool. Yet as long as there is an efflux of NO_3 from the sediment, fractionation may occur even if the sediment acts as a net NO_3 sink. We hypothesized that active pumping by *Arenicola marina* would allow short-circuiting of NO_3, *i.e.* that NO_3 in the fluid injected into sediment via the feeding pocket of the lugworm, would only be partially denitrified *in situ*, allowing a fraction to escape the sediment, which then would be enriched in ^{15}N and contribute to a higher mean oceanic $\delta^{15}N$.

Sedimentary $\delta^{15}N$ records have indicated that the isotopic composition of fixed N has been stable in the past 3000 year (Altabet, 2007), which may indicate that in pre-industrial times oceanic ^{14}N and ^{15}N were in steady-state. In Chapter 2, a one-box model was setup to constrain the mean oceanic ε_{N2}, which relates the isotopic composition of N_2 produced in sediments to that of NO_3 (*i.e.* its average water-column signature) in the ocean. Simulations for a wide range of magnitudes and isotope effects of various processes that either remove or add fixed N to the ocean were run with the total N inventory assumed to be at steady-state. Simulations that led to mean oceanic $\delta^{15}N$ values close to the observed value of 5‰ had ε_{N2} values between -1 and -7‰. Results also indicated that the oceanic $\delta^{15}N$ was most sensitive to the degree of fractionation during benthic DNF.

In Chapter 3, sediment N fractionation was constrained with a mechanistic early diagenetic process study. The effects of burrowing by *A. marina* on the isotopic signature of benthic fluxes were quantified with a high resolution reactive transport model, which simulated N dynamics with emphasis on fractionation in a benthic, physical 3D environment. Fractionation during nitrification and hence coupled nitrification-denitrification was crucial for the isotopic composition of *in situ* produced N_2 gas as this provided a source of light substrate for DNF. The effect of fractionation during DNF on ε_{N2} values was rather small for a 15 cm deep burrow as only limited short-circuiting of NO_3 took place, which led to heavier NO_3 in the sediment. Lowering the pumping rate led to an even higher degree of fractionation during benthic DNF, mainly due to decreased, NO_3-limited DNF rates and thus more fractionation during this process. Hence, the simulation outcomes did not support our initial hypothesis. A shallower burrowing depth of 5 cm led to short-circuiting of NO_3 and more fractionation. Therefore, organisms that burrow less deep might enhance fractionation to greater extent than *A. marina*, as the feeding pockets of these lugworms are usually positioned at a depth greater than 15 cm.

In Chapter 4, simulations for distinct benthic environments were carried out to provide first order estimates of the fractionation during sedimentary N_2 production and its potential imprint on water-column isotopic signatures. The degree of fractionation during benthic DNF in shallower waters was mostly dependent on fractionation during nitrification and the degree of coupled nitrification-denitrification. At greater depths

DNF rates decreased, which allowed more fractionation during this process due to a relatively larger NO_3 pool as nitrification rates and bottom-water NO_3 concentrations remained more constant. On a global scale most DNF occurs in coastal sediments, which means that the weighted mean ε_{N2} is largely reflecting the degree of fractionation in these sediments.

References

Alkhatib M., Lehmann M. F., and Del Giorgio P. O. (2012) The nitrogen isotope effect of benthic remineralization-nitrification-denitrification in an estuarine environment. *Biogeosciences* **9**, 1633-1646.

Alperin M. J., Albert D. B., and Martens S. C. (1994) Seasonal variations in production and consumption rates of dissolved organic carbon in an organic-rich coastal sediment. *Geochim. Cosmochim. Acta* **58**, 4909-4930.

Altabet M. A. (2007) Constraints on oceanic N balance/imbalance from sedimentary ^{15}N records. *Biogeosciences* **4**, 75-86.

Altabet M. A., Pilskaln C., Thunell R., Pride C., Sigman D., Chavez F., and Francois R. (1999) The nitrogen isotope biogeochemistry of sinking particles from the margin of the eastern North Pacific. *Deep-Sea Res. 1* **46**, 655–679.

Archer D. and Devol A. H. (1992) Benthic oxygen fluxes on the Washington shelf and slope: A comparison of in situ microelectrode and chamber flux measurements. *Limnol. Oceanogr.* **37**, 614-629.

Bender M. L. (1990). The $\delta^{18}O$ of dissolved O2 in seawater: a unique tracer of circulation and respiration in the deep sea. *J. Geophys. Res.* **95**, 22243–22252.

Berg P., Rysgaard S., and Thamdrup B. (2003) Dynamic modeling of early diagenesis and nutrient cycling. A case study in an Arctic marine sediment. *Am. J. Sci.* **303**, 905-955.

Berner R. A. (1980) *Early diagenesis: a theoretical approach.* Princeton University Press, Princeton.

Betlach M. and Tiedje J. M. (1981) Kinetic explanation for accumulation of nitrite, nitric oxide and nitrous oxide during bacterial denitrification. *Appl. Environ. Microbiol.* **42**, 1074-1084.

Bohlen L., Dale A. W., and Wallman K. (2012) Simple transfer functions for calculating benthic fixed nitrogen losses and C:N:P regeneration ratios in global biogeochemical models. *Glob. Biogeochem. Cycles*, **26**, BG3029.

Boudreau B. P. (1996) The diffusive tortuosity of fine-grained unlithified sediments. *Geochim. Cosmochim. Acta* **60**, 3139-3142.

Boudreau B. P. (1997) *Diagenetic models and their implementation.* 1st ed. Springer-Verlag.

Boudreau B. P. *et al.* (2001) Permeable marine sediments: overturning an old paradigm. *EOS* **82**, 133–136.

Brandes J. A. and Devol A. H. (1997) Isotopic fractionation of oxygen and nitrogen in coastal marine sediments. *Geochim. Cosmochim. Acta* **61**, 1793-1801.

Brandes J. A. and Devol A. H. (2002) A global marine-fixed nitrogen isotopic budget: Implications for Holocene nitrogen cycling. *Global Biochem. Cycles* **16**, 1120.

Brandes J. A., Devol A. H., Yoshinari T., Jayakumar D. A., and Naqvi S. W. A. (1998) Isotopic composition of nitrate in the central Arabian Sea and eastern tropical North Pacific: a tracer for mixing and nitrogen cycles. *Limnol. Oceanogr.* **43**(7), 1680–1689.

Brunnegard J., Grandel S., Stahl H., Tengberg H., and Hall P. O. J. (2004) Nitrogen cycling in deep-sea sediments of the Porcupine Abyssal Plain, NE Atlantic. *Prog. Oceanogr.* **63**, 159-181.

Canfield D. E., Thamdrup B., and Kristensen E. (2005), *Aquatic Geomicrobiology*, 640 pp., Elsevier Academic Press, San Diego.

Carpenter E., Harvey H., Fry B., and Capone D. (1997) Biogeochemical tracers of the marine cyanobacterium Trichodesmium. *Deep-Sea Res. 1* **44**(1), 27–38.

Casciotti K. L. and Buchwald C. (2012) Insights on the marine microbial nitrogen cycle from isotopic approaches to nitrification. *Front. Microbiol.* **3**, 356.

Christensen P. B., Glud R. N., Dalsgaard T., and Gillespie P. (2003) Impact of longline mussel farming on oxygen and nitrogen dynamics and biological communities of coastal sediments. *Aquaculture* **218**, 567-588.

Codispoti L. A., Brandes J. A., Christensen J. P., Devol A. H., Naqvi S. W. A., Paerl H. W., and Yoshinari T. (2001) The ocean fixed nitrogen and nitrous oxide budgets: Moving targets as we enter the anthropocene? *Sci. Mar.* **65**, 85-105.

Codispoti L. A., Elkins J., Yoshinari T., Friederich G. E., Sakamoto C. M., Packard T. T. (1992) *Nitrous oxide cycling in upwelling regions underlain by low oxygen waters.* In: Oceanography of the Indian Ocean. Oxford & IBH Publishing, New Dehli, pp. 271-284.
Cook P. L. M., Wenzholfer F., Rysgaard S., Galaktionov O. S., Meysman F. J. R., Eyre B. D., Cornwell J., Huettel M. and Glud R. N. (2006) Quantification of denitrification in permeable sediments: insights from a two-dimensional simulation analysis and experimental data. *Limnol. Oceanogr.: Methods* **4**, 294–307.
Crowe S. A., Canfield D. E., Mucci A., Sundby A., and Maranger R. (2011) Anammox, denitrification and fixed-nitrogen removal in sediments of the Lower St. Lawrence Estuary. *Biogeosciences Discuss.* **8**, 9503-9534.
Dalsgaard T., Thamdrup B., and Canfield D. E. (2005) Anaerobic ammonium oxidation (anammox) in the marine environment. *Res. Microbiol.* **156**, 457-464.
Deutsch C., Sigman D. M., Thunell R. C., Meckler A. N., and Haug G. H. (2004) Isotopic constraints on glacial/interglacial changes in the oceanic nitrogen budget. *Global Biogeochem. Cycles* **18**, GB4012
Devol A. H. (1991) Direct measurement of nitrogen gas fluxes from continental shelf sediments. *Nature* **349**, 319-321.
Devol A. H. (2008) *Chapter 6: Denitrification including anammox*. In: Capone D., Carpenter E., Mullholland M., and Bronk D. (eds), Nitrogen in the marine environment. Elsevier, Amsterdam, pp. 263–302.
Duce R. A. *et al.* (2008) Impacts of atmospheric anthropogenic nitrogen on the open ocean. *Science* **320**, 893-897.
Eugster M. and Gruber N. (2012) A probalistic estimate of global marine N-fixation and denitrification. *Global Biogeochem. Cycles* **26**, GB4013.
Fennel K. *et al.* (2009) Modeling denitrification in aquatic sediments. *Biogeochemistry* **93**, 159-178.
Flach E. C. and Beukema J. J. (1994) Density-governing mechanisms in populations of the lugworm *Arenicola marina* on tidal flats. *Mar. Ecol. Prog. Ser.* **115**, 139-149.
Froelich P. N. *et al.* (1979) Early oxidation of organic matter in in pelagic sediments of the eastern equatorial Atlantic: suboxic diagenesis. *Geochim. Cosmochim. Acta* **43**, 1075-1090.
Furukawa Y., Bentley S. J., and Lavoie D. L. (2001) Bioirrigation modeling in experimental benthic mesocosms. *J. Mar. Res.* **59**, 417-452.
Galan A., Molina V., Belmar L., and Ulloa O. (2012) Temporal variability and phylogenetic characterization of planktonic bacteria in the coastal upwelling ecosystem off central Chile. *Prog. Oceanogr.* **92-95**, 110-120.
Galan A., Molina V., Thamdrup B., Woebken D., Lavik G., Kuypers M. M. M., and Ulloa O. (2009) Anammox bacteria and the anaerobic oxidation of ammonium in the oxygen minimum zone off northern Chile. *Deep-Sea Res. II* **56**, 272-275.
Galloway J. N. *et al.* (2004) Nitrogen cycles: past, present, future. *Biogeochemistry* **70**, 153-226.
Garcia H. E., Locarnini R. A., Boyer T. P., Antonov J. I., Baranova O. K., Zweng M. M., and Johnson D. R. (2010a) *World Ocean Atlas 2009, Volume 3: Dissolved Oxygen, Apparent Oxygen Utilization, and Oxygen Saturation.* S. Levitus, Ed. NOAA Atlas NESDIS 70, U.S. Government Printing Office, Washington, D.C., 344 pp.
Garcia H. E., Locarnini R. A., Boyer T. P., Antonov J. I., Baranova O. K., Zweng M. M., and Johnson D. R. (2010b) *World Ocean Atlas 2009, Volume 4: Nutrients (phosphate, nitrate, silicate).* S. Levitus, Ed. NOAA Atlas NESDIS 70, U.S. Government Printing Office, Washington, D.C., 398 pp.
Graaf A. van de, Mulder A., Slijkhuis H., Robertson L.A., Kuenen J.G. (1990) *Anoxic ammonium oxidation.* In: Christiansen C., Munck L., Villadsen (eds), Proceedings of the Fifth European Congress on Biotechnology, vol. I, Munksgaard, Copenhagen, 1990, pp. 388-391.
Glud R. N., Holby O., Hoffmann F., and Canfield D.E. (1998) Benthic mineralization and exchange in Arctic sediments (Svalbard, Norway). *Mar. Ecol. Prog. Ser.* **173**, 237-251.
Glud R. N., Thamdrup B., Stahl H., Wenzhoefer F., *et al.* (2009) Nitrogen cycling in a deep ocean margin sediment (Sagami Bay, Japan). *Limnol. Oceanogr.* **54**, 723-734.
Granger J., Prokopenko M. G., Sigman D. M., Mordy C. W., Morse Z. M., Morales L. V., Sambrotto R. N., and Plessen B. (2011) Coupled nitrification-denitrification in sediment of eastern Bering-Sea shelf leads to ^{15}N enrichment of fixed in N in shelf waters. *J. Geophys. Res.* **116**, C11006.

Großkopf T. *et al.* (2012) Doubling of marine dinitrogen-fixation rates based on direct measurements. *Nature* **488**, 361-364.
Gruber N. and Sarmiento J. L. (1997) Global patterns of marine nitrogen fixation and denitrification. *Global Biogeochem. Cycles* **11**, GB00077.
Gruber N. (2004) *The dynamics of the marine nitrogen cycle and atmospheric CO_2.* In: Orguz T. and Follows M. (eds), Carbon climate interactions, Kluwer, Dordrecht, pp. 97-148.
Gruber N. (2008) *Chapter 1: The marine nitrogen cycle: overview and challenges*. In: Capone D, Carpenter E., Mullholland M., and Bronk D. (eds), Nitrogen in the marine environment. Elsevier, Amsterdam, pp. 1–50.
Gruber N. and Galloway J. N. (2008) An earth-system perspective of the global nitrogen cycle. *Nature* **451**, 293-296.
Hagopian D. S. and Riley J. G. (1998) A closer look at the bacteriology of nitrification. *Aquacultural Eng.* **18**, 223-244.
Haldane J. B. S. (1930), *Enzymes,* 235 pp., Longmans, Green, London.
Herbert R. A. (1999). Nitrogen cycling in coastal marine ecosystems. *FEMS Microbiol. Rev*. **23**, 563-590.
Huettel M. (1990) Influence of the lugworm *Arenicola Marina* on porewater nutrient profiles of sand flat sediments. *Mar. Ecol. Prog. Ser.* **62**, 241-248.
Jensen H. M., Lomstein E., and Sorensen J. (1990) Benthic NH4 and NO3 flux following sedimentation of a spring phytoplankton bloom in Aarhus Bight, Denmark. *Mar. Ecol. Prog. Ser.* **61**, 87-96.
Jørgensen B. B. (2000) *Bacteria and Marine Biogeochemistry*. In: Marine Geochemistry, Springer, Berlin, pp. 173–207.
Kendall C. and Caldwell E. A. (1998) *Fundamentals of Isotope Geochemistry.* In: Kendall C. and McDonnell J. J. (eds), Isotope Tracers in Catchment Hydrology. Elsevier, Amsterdam, pp. 51-86.
Kristensen E., Hansen T., Delefosse M. Banta G. T. and Quintana C. O. (2011) Contrasting effects of the polychaetes Marenzelleria viridis and Nereis diversicolor on benthic metabolism in sandy coastal sediment. *Mar. Ecol. Prog. Ser.* **425**, 125-139.
Kuypers M. M. M. *et al.* (2003) Anaerobic ammonium oxidation by anammox bacteria in the Black Sea. *Nature* **422**, 608-611.
Laidler K. J. (1955) Theory of the transient phase in kinetics, with special reference to enzyme systems. *Can. J. Chem.* **33,** 1614-1624.
Le Bars, M. and Worster G. (2006) Interfacial conditions between a pure fluid and a porous medium: implications for binary alloy solidification. *J. Fluid Mech.* **550**, 149-173.
Lehmann M. F., Sigman D. M., and Berelson W. M. (2004) Coupling the $^{15}N/^{14}N$ of nitrate as a constraint on benthic nitrogen cycling. *Mar. Chem.* **88**, 1-20.
Lehmann M. F. *et al.* (2007) The distribution of nitrate $^{15}N/^{14}N$ in marine sediments and the impact of benthic nitrogen loss on the isotopic composition of oceanic nitrate. *Geochim. Cosmochim. Acta* **71**, 5384-5404.
Lohse L., Kloosterhuis H.T., van Raaphorst W., and Helder W. (1996) Denitrification rates as measured by the isotope pairing method and by the acetylene inhibition technique in continental shelf sediment of the North Sea. *Mar. Ecol. Prog. Ser.* **132**, 169-179.
Lonborg C. and Sondergaard M. (2009) Microbial availability and degradation of dissolved organic carbon and nitrogen in two coastal areas. *Estuar. Coast. Shelf Sci.***81**, 513-520.
Maggi F. and Riley W. J. (2009) Transient competitive complexation in biological kinetic isotope fractionation explains nonsteady isotope effects: Theory and application to denitrification in soils. *J. Geophys. Res.* **114**, G04012.
Mariotti A., Germon J. C., Hubert P., Kaiser P., Letolle R., Tardieux R., and Tardieux P. (1981) Experimental determination of nitrogen kinetic isotope fractionation: some principles; illustration for the denitrification and nitrification processes. *Plant Soil* **62**, 413–430.
Meile C., Berg P., Van Cappellen P., and Tuncay K. (2005) Solute-specific pore water irrigation: Implications for chemical cycling in early diagenesis. *J. Mar. Res.* **63**, 601-621.
Meile C., Tuncay K., and Van Cappelen P. (2003). Explicit representation of spatial heterogeneity in reactive transport models: application to bioirrigated sediments. *J. Geochem. Explor.* **78-79**, 231-234.

Meysman F. J. R., Galaktionov, O. S., Gribsholt, B., and Middelburg, J. J. (2006a). Bioirrigation in permeable sediments: Advective pore-water transport induced by burrow ventilation. *Limnol. Oceanogr.* **51**, 142-156.
Meysman F. J. R., Middelburg J. J., and Heip C. H. R. (2006b) Bioturbation: a fresh look at Darwin's last idea. *Trends Ecol. Evol.* **21**, 688-695.
Middelburg J. J., Soetaert K., Herman P. M. J., and Heip C. H. R. (1996). Denitrification in marine sediments: A model study. *Global Biogeochem. Cycles* **10**(4), 661–673.
Middelburg J. J., Soetaert K., and Herman P. M. J. (1997) Empirical relationships for use in global diagenetic models. *Deep-Sea Res. I* **44**, 327-344.
Mohr W., Großkopf T, Wallace D. W. R., and LaRoche J. (2010) Methodological underestimation of oceanic nitrogen fixation rates. *PLoS ONE* **5**, e12583.
Monod J. (1949) The growth of bacterial cultures. *Annu. Rev. Microbial* **3**, 371-394.
Na T., Gribsholt B., Galaktionov O. S., Lee T., and Meysman F. J. R. (2008) Influence of advective bio-irrigation on carbon and nitrogen cycling in sandy sediments. *J. Mar. Res.* **66**, 691-722.
Nedwell D. and Aziz S. (1980) Heterotrophic nitrogen fixation in an intertidal salt marsh sediment. *Est. Coast. Mar. Sci.* **10**, 699-702.
Nicholls J. C. and Trimmer M. (2009) Widespread occurrence of the anammox reaction in estuarine sediments. *Aquat. Microb. Ecol.* **36**, 293-304.
Norkko J. *et al*. (2012), A welcome can of worms? Hypoxia mitigation by an invasive species. *Glob. Change Biol.* **18**, 422-424.
Prokopenko M. G., Sigman D. M., Berelson W. M., Hammond D. E., Barnett B., Chong L., and Townsend-Small A. (2011) Denitrification in anoxic sediments supported by biological nitrate transport. *Geochim. Cosmochim. Acta* **75**, 7180-7199.
Redfield A. C., Ketchum B. H., and Richards F. A. (1963) *The influence of organisms on the composition of sea-water*. In: Hill M. N. (ed), The Sea. Wiley-Interscience, New York, pp. 26-77.
Reitze M. and Schöttler U. (1989) The time dependence of adaption to reduced salinity in the lugworm *Arenicola marina* L. (Annelida: Polychaeta). *Comp. Biochem. Physiol.* **93**, 549-559.
Riisgard H. U., Berntsen I., and Tarp B. (1996) The lugworm (*Arenicola marina*) pump: characteristics, modelling and energy cost. *Mar. Ecol. Prog. Ser.* **138**, 149-156.
Rysgaard S., Glud R. N., Risgaard-Petersen N., and Dalsgaard T. (2004) Denitrification and anammox activity in arctic marine sediments. *Limnol. Oceanogr.* **49**, 1493-1502.
Ryther J. K. and Dunstan W. M. (1971) Nitrogen, phosphorus and eutrophication in the coastal marine environment. *Science* **171**, 1008-1013.
Sarmiento J. L. and Gruber N. (2006) *Ocean Biogeochemical Dynamics.* Princeton University Press, Princeton.
Schmid M. C. *et al.* (2007) Anaerobic ammonium oxidizing bacteria in marine environments: widespread occurrence but low diversity. *Environ. Microbiol.* **9**, 1476-1484.
Sigman D. M. *et al.* (2009) The dual isotopes of deep nitrate as a constraint on the cycle and budget of oceanic fixed nitrogen. *Deep-Sea Res. 1* **56**, 1419-1439.
Sinninghe Damste J. S., Strous M., Rijpstra I. C., Hopmans E. C., Geenevasen J. A. J., Duin, A. C. T. van, Niftrik L. A. van, and Jetten M. S. M. (2002) Linearly concatenated cyclobutane lipids form a dense bacterial membrane. *Nature* **419**, 708-712.
Soetaert K., Herman P. M. J., and Middelburg J. J. (1996) A model of early diagenetic processes from the shelf to abyssal depths. *Geochim. Cosmochim. Acta* **60**, 1019-1040.
Strous M. *et al.* (1999) Missing lithotroph identified as new planctomycete. *Nature* **400**, 446-449.
Thullner M., Dale A. W., Regnier P. (2009) Global-scale quantification of mineralization pathways in marine sediments: A reaction-transport modeling approach. *Geochem. Geophys. Geosyst.* **10**, Q10012.
Thunell R. C., Sigman D. M., Muller-Karger F., Astor Y., and Varela R. (2004) Nitrogen isotope dynamics of the Cariaco Basin, Venezuela. *Global Biochem. Cycles* **18**, GB3001.
Van Cappellen P. and Wang Y. (1995) *Metal cycling in surface sediments: Modeling the interplay of transport and reaction.* In: Allen H. E. (ed), Metal Speciation and Contamination of Aquatic Sediments. Ann Arbor Press, Chelsea, Michigan, pp. 21-64.
Volkenborn N., Hedtkamp S. I. C., van Beusekom J. E. E. and Reise K. (2007) Effects of bioturbation and bioirrigation by lugworms (*Arenicola Marina*) on physical and chemical sediment properties and implications for intertidal habitat succession. *Estuar. Coast. Shelf Sci.* **74**, 331-343.

Volkenborn N., Polerecky L., Wethey D. S., and Woodin S. A. (2010) Oscillatory porewater bioadvection in marine sediments induced by hydraulic activities of *Arenicola marina*. *Limnol. Oceanogr.* **55**, 1231-1247.
Voss M., Dippner J. W., and Montoya J. P. (2001) Nitrogen isotope patterns in the oxygen-deficient waters of the Eastern Tropical North Pacific. *Ocean. Deep-Sea Res. 1* **48**(8), 1905–1921.
Wang Y. F. and Van Cappellen P. (1996) A multicomponent reactive transport model of early diagenesis: application to redox cycling in coastal marine sediment. *Geochim. Cosmochim. Acta* **60**, 2993-3014.
Ward B. B. (2008) *Chapter 5: Nitrification in Marine Systems.* In: Capone D., Carpenter E., Mullholland M., and Bronk D. (eds), Nitrogen in the marine environment. Elsevier, Amsterdam, pp. 199–262.
Woebken D. *et al.* (2008) A microdiversity study of anammox bacteria reveals a novel *Candidatus* Scalindua phylotype in marine oxygen minimum zones. *Environ. Microb.* **10**, 3106-3119.

A. Implementation model after Thullner *et al.* (2007)

```
library(marelac)
library(ReacTran)

################################################################################
## 1D solutes profiles for Hypsometric Analysis
## Calculates profiles based on Thullner, Dale, and Regnier (2009)
################################################################################

#===============================================================================
# Units used in the program:
#===============================================================================

# Time = year
# Mass = moles and grams
# Length = meters

#===============================================================================
# Assumptions
#===============================================================================

# (1) Porosity constant with depth

#===============================================================================
# Model domain and grid definition
#===============================================================================
L <- 30 / 100    # depth of sediment domain [m]
N <- 1000  # number of grid layers
grid <- setup.grid.1D(x.up = 0, L = L, N = N)

#===============================================================================
# Model parameters (Table 3, page 5):
#===============================================================================

# Model parameters
v_bur <- 3.98 * 10^-1#sedimentation rate [cm/yr]
Db <- 27.5 #mixing coefficient [cm^2/yr]
por <- 0.85 # porosity
alpha0 <- 283 #bioirrigation coefficient [yr-1]
TC <- 5 # temperature [deg C]
S <- 35 # salinity
dens <- 2.5 #density [gram cm-3]
#Upper boundary conditions
O20 <- 132 #O2 conc overlying water [uM]
NO30 <- 17.3 #NO3 conc overlying water [uM]
SO40 <- 28 #SO4 conc overlying water [mM]
J_MnO2 <- 1.35 #SWI flux manganese oxide [umol cm-2 yr-1]
J_FeOH3 <- 12.1 #SWI flux ironhydrite [umol cm-2 yr-1]
J_POM <- 510 #SWI flux particulate organic matter [umol C cm-2 yr-1]
pH <- 8.1 #pH seawater

#Other model parameters
DIC <- 2.1 #[mol/m3]
dens_sw <- 1.025 * 10^3 #density seawater [kg/m^3]

#===============================================================================
# Reaction rates  (Table A3, page 21):
#===============================================================================
convMyr <- 10^3
convuM <- 10^-3
convumol <- 10^-6

kc <- 0.221 #yr-1
k1 <- 1.5 * 1e7 * convMyr # dm3/mol/yr
k2 <- 2.0  * 1e9 * convMyr
k3 <- 2.0  * 1e9 * convMyr
k4 <- 2.46 * 1e8 * convMyr
```

```
k5 <- 6.0 * 1e8 * convMyr
k6 <- 1e4 * convMyr
k7 <- 1e4 * convMyr
k8 <- 2.2 * 1e7 * convMyr
k9p <- 1.15 * 1e-6
k9m <- 2.5 * 1e-1
k10p <- 1.15 * 1e-6
k10m <- 2.5 * 1e-1
k11p <- 5.97 * 1e-6
k11m <- 1e-3
KO2 <- 8 * convuM
KNO3 <- 10 * convuM
KMnO2 <- 2 * convumol
KFeOH3 <- 5 * convumol
KSO4 <- 1000 * convuM

#Variables that are independent of the SFD
Ka_HS <- 10^-6.9  #in 0.01 to 0.1 mol/L at 18 degrees C
Ka_HS = Ka_HS / 1000  # conversion dm^3/mol to m^3/mol
Kw <- 10^-14 #equilibrium water [mol^2/dm^6]
Kw <- Kw * 10^6 #conversion [mol^2/dm^6] to [mol^2/m^6]
Ka1_HCO3 <- 10^-6.37 #first acid constant [mol/dm3]
Ka2_HCO3 <- 10^-10.33 #first acid constant [mol/dm3]
Ka1_HCO3 <- Ka1_HCO3 * 1000 #[mol/m3]
Ka2_HCO3 <- Ka2_HCO3 * 1000 #[mol/m3]
H0 <- 10^-pH #mol/dm3
OH0 <- 10^-14/H0 #mol/dm3
H0 <- H0 * 1000 #mol/m3
OH0 <- OH0 * 1000 #mol/m3
K_MnCO3 <- 10^-10.39 * 10^6 #[mol^2/m^6] page 981 Aquatic Chemistry by Stumm & Morgan
K_FeCO3 <- 10^-10.45 * 10^6 #idem dito
K_FeS                <-                  10^-2.95                *                  10^3
#http://wwwbrr.cr.usgs.gov/projects/GWC_coupled/phreeqc/mail/msg00401.html

#Carbonate overlying water (Zeebe, pp 4-6)
K1star <- 10^-5.86
K2star <- 10^-8.92
Hplus <- 10^-pH
a <- 1 + K1star/Hplus + (K1star * K2star)/Hplus^2
b <- 1 + Hplus/K1star + K2star/Hplus
c <- 1 + Hplus /K2star + Hplus^2/(K1star * K2star)
#a,b and c are dimensionless
CO20 <- DIC / a
HCO30 <- DIC / b
CO30 <- DIC / c

#Unit conversions
u <- v_bur / 100  #sedimentation rate
Db = Db * 10^-4
O20  = O20 * 10^-3
NO30 = NO30 * 10^-3
#SO40 [mM = mol/m3]
J_MnO2 = J_MnO2 * 10^-2
J_FeOH3 = J_FeOH3 * 10^-2
J_POM = J_POM * 10^-2 #
sinyr <- 3600*24*365.25  #number of seconds in year

# Diffusion coefficients
# Uses routine 'diffcoeff' from 'marelac' package
P <- 1.013 # pressure [bar]
Dmol.O2 <- diffcoeff(S = S, t = TC, P = P, species = "O2")$O2 * sinyr
Dmol.NO3 <- diffcoeff(S = S, t = TC, P = P, species = "NO3")$NO3 * sinyr
Dmol.NH4 <- diffcoeff(S = S, t = TC, P = P, species = "NH4")$NH4 * sinyr
Dmol.SO4 <- 8.91e-10 * sinyr
Dmol.Mn <- diffcoeff(S = S, t = TC, P = P, species = "Mn")$Mn * sinyr
Dmol.Fe <- diffcoeff(S = S, t = TC, P = P, species = "Fe")$Fe* sinyr
Dmol.HS <- 1.49e-9* sinyr
Dmol.H2S <- diffcoeff(S = S, t = TC, P = P, species = "H2S")$H2S * sinyr
Dmol.CO3 <- diffcoeff(S = S, t = TC, P = P, species = "CO3")$CO3 * sinyr
Dmol.HCO3 <- diffcoeff(S = S, t = TC, P = P, species = "HCO3")$HCO3 * sinyr
Dmol.H <- diffcoeff(S = S, t = TC, P = P, species = "H")$H * sinyr
```

```
Dmol.OH <- diffcoeff(S = S, t = TC, P = P, species = "OH")$OH * sinyr
Dmol.CO2 <- diffcoeff(S = S, t = TC, P = P, species = "CO2")$CO2 * sinyr

tort <- 1 - 2*log(por) # tortuosity correction
Ds.O2 <- Dmol.O2/tort #Ds stands for diffusion coefficient
DO2 <- Db + Ds.O2
Ds.NO3 <- Dmol.NO3/tort
DNO3 <- Db + Ds.NO3
Ds.NH4 <- Dmol.NH4/tort
DNH4 <- Db + Ds.NH4
Ds.SO4 <- Dmol.SO4/tort
DSO4 <- Db + Ds.SO4
Ds.Mn <- Dmol.Mn/tort
DMn <- Db + Ds.Mn
Ds.Fe <- Dmol.Fe/tort
DFe <- Db + Ds.Fe
Ds.HS <- Dmol.HS/tort
DHS <- Db + Ds.HS
Ds.H2S <- Dmol.H2S/tort
DH2S <- Db + Ds.H2S
Ds.CO3 <- Dmol.CO3/tort
DCO3 <- Db + Ds.CO3
Ds.HCO3 <- Dmol.HCO3/tort
DHCO3 <- Db + Ds.HCO3
Ds.CO2 <- Dmol.CO2/tort
DCO2 <- Db + Ds.CO2
Ds.H <- Dmol.H/tort
DH <- Db + Ds.H
Ds.OH <- Dmol.OH/tort
DOH <- Db + Ds.OH

# Attachment of parameters to grid
por.grid <- setup.prop.1D(value = por, grid = grid)
u.grid <- setup.prop.1D(value = u, grid = grid)
svf <- 1-por
svf.grid <- setup.prop.1D(value = svf, grid = grid)

getDb <- function(x, y.0) { #Nie et al. 2001
  Db <- y.0
  erfc <- function(x2) 2 * pnorm(x2 * sqrt(2), lower = FALSE)

  xstar <- 10 / 100 #10 cm
  sigma <- 0.05 / 100 #0.05 cm

  (Db / 2) * erfc((x-xstar)/sigma)
}

#After 10 cm no bioturbation
Db.grid <- setup.prop.1D(func=getDb, grid = grid, y.0 = Db)

#smooth function for heaviside operator
getHOp <- function(SI) {
  SI <- -SI
  erfc <- function(x2) 2 * pnorm(x2 * sqrt(2), lower = FALSE)
  sigma <- 1#0.05 / 10
  #H <- erfc(seq(-1,1,len=1000/sigma)/2
  H <- erfc(SI/sigma)/2
  return(H)
}

alpha.grid <- setup.prop.1D(func = p.exp, grid = grid, y.0 = alpha0, y.inf=0,
                            x.L = 0, x.att=3.5/100) #see page 6 Thullner (15 cm deep)

DO2.grid <- setup.prop.1D(value = DO2, grid = grid)
DHCO3.grid <- setup.prop.1D(value = DHCO3, grid = grid)
DNO3.grid <- setup.prop.1D(value = DNO3, grid = grid)
DNH4.grid <- setup.prop.1D(value = DNH4, grid = grid)
DMn.grid <- setup.prop.1D(value = DMn, grid = grid)
DFe.grid <- setup.prop.1D(value = DFe, grid = grid)
DSO4.grid <- setup.prop.1D(value = DSO4, grid = grid)
DH2S.grid <- setup.prop.1D(value = DH2S, grid = grid)
```

```
DH.grid <- setup.prop.1D(value = DH, grid = grid)
DOH.grid <- setup.prop.1D(value = DOH, grid = grid)
DHS.grid <- setup.prop.1D(value = DHS, grid = grid)
DCO3.grid <- setup.prop.1D(value = DCO3, grid = grid)
DCO2.grid <- setup.prop.1D(value = DCO2, grid = grid)

#==========================================================================
# Rate constants carbonate system
#==========================================================================
acidbase <- function(TC, S, rho) {
  #TC = Temp. Celsius, S = salinity, rho = density seawater kg/m3

  # compute kinetic and equilibrium constants for DIC and Borate
  # based on Zeebe and Wolf-Gladrow's CO2 book, Table 2.3.1 and appendix C9
  # co2 + h2o = hco3 + h              k1. (p ->, m <-)
  # co2 + oh = hco3                   k4
  # co3 + h = hco3                    k5h
  # hco2 + oh - co3 + h2o             k5oh
  # h2o = h + oh                      k6
  # boh3 + oh = boh4                  k7
  # co3 + boh3 + h2o = boh4 + hco3    k8

  T   <- TC + 273.15  # temperature in K
  A4  <- 4.70e7       # kg/mol/s
  A7  <- 4.58e10      # kg/mol/s
  A8  <- 3.05e10      # kg/mol/s
  E4  <- 23.2e3       # J/mol
  E7  <- 20.8e3       # J/mol
  E8  <- E7
  R   <- 8.3144721345 # J*K/mol

  # Kw = [H+]*[OH-]
  lnKw <- 148.96502 - 13847.26/T - 23.6521 * log(T) +
    (118.67/T - 5.977 + 1.0495*log(T))*sqrt(S) - 0.01615*S
  Kw  <- exp(lnKw) # mol^2/kg^2

  # K1 = [H+] [HCO3-] / [CO2] (Roy, mol/kg)
  lnK1 <- 2.83655 - 2307.1266/T - 1.5529413 * log(T) -
    (0.20760841 + 4.0484/T)*sqrt(S) + 0.08468345 * S -
    0.00654208 * S * sqrt(S) + log(1 - 0.001005 * S)
  K1 <- exp(lnK1)

  # K2 = [H+] [CO3--] / [HCO3-] (Roy, mol/kg)
  lnK2 <- -9.226508 - 3351.6106 / T - 0.2005743 * log(T) +
    (-0.106901773 - 23.9722 / T) * sqrt(S) +
    0.1130822*S - 0.00846934 * S^1.5 + log(1 - 0.001005 * S)
  K2 <- exp(lnK2)

  # KB = [B(OH4)-]*[H+] / [B(OH)3] (Roy, mol/kg)
  lnKB <- (-8966.90 - 2890.53*sqrt(S) - 77.942*S + 1.728*S^(3/2) - 0.0996*S^2)/T +
    148.0248 + 137.1942*sqrt(S) + 1.62142*S -
    (24.4344 + 25.085*sqrt(S) + 0.2474*S)*log(T) +
    0.053105*sqrt(S)*T
  KB <- exp(lnKB)

  k1p <- exp(1246.98 - 6.19e4 / T - 183.0 * log(T)) # 1/s
  k1m <- k1p/K1                                     # kg/mol/s

  k4p <- A4*exp(-E4/(R*T))                    # kg/mol/s
  k4m <- k4p*Kw/K1                            # 1/s

  k5hp <- 5e10                                # kg/mol/s
  k5hm <- k5hp*K2                             # 1/s

  k5ohp <- 6e9                                # kg/mol/s
  k5ohm <- k5ohp*Kw/K2                        # 1/s

  k6p <- 1.4e-3                               # mol/kg/s
  k6m <- k6p/Kw                               # kg/mol/s

  k7p <- A7*exp(-E7/(R*T))                    # kg/mol/s
```

```
  k7m <- k7p*Kw/KB                            # 1/s

  k8p <- A8*exp(-E8/(R*T))                    # kg/mol/s
  k8m <- k8p*K2/KB                            # kg/mol/s

  # conversion from kg to L and pack into structure
  k.Kw   <- Kw * rho^2    # mol2/kg2 * (kg/m3)^2 = (mol/m3)^2
  k.K1   <- K1 * rho      # mol/kg * kg/m3 = mol/m3
  k.K2   <- K2 * rho      # mol/kg * kg/m3 = mol/m3
  k.KB   <- KB * rho      # mol/kg * kg/m3 = mol/m3
  k.k1p  <- k1p           # 1/s
  k.k1m  <- k1m/rho       # kg/mol/s /(kg/m3) = m3/mol/s
  k.k4p  <- k4p/rho       # kg/mol/s /(kg/m3) = m3/mol/s
  k.k4m  <- k4m           # 1/s
  k.k5hp <- k5hp/rho      # kg/mol/s /(kg/m3) = m3/mol/s
  k.k5hm <- k5hm          # 1/s
  k.k5ohp <- k5ohp/rho     # kg/mol/s /(kg/m3) = m3/mol/s
  k.k5ohm <- k5ohm         # 1/s
  k.k6p  <- k6p*rho       # mol/kg/s * kg/m3  = mol/m3/s
  k.k6m  <- k6m/rho       # kg/mol/s /(kg/m3) = m3/mol/s
  k.k7p  <- k7p/rho       # kg/mol/s /(kg/m3) = m3/mol/s
  k.k7m  <- k7m           # 1/s
  k.k8p  <- k8p/rho       # kg/mol/s /(kg/m3) = m3/mol/s
  k.k8m  <- k8m/rho       # kg/mol/s /(kg/m3) = m3/mol/s
  # k.Kh   = Kh*rho      # mol/kg/atm * kg/m3 = mol/m3/atm

  data.frame(Kw = k.Kw, K1 = k.K1, K2 = k.K2, KB = k.KB,
             k1p = k.k1p, k1m = k.k1m, k4p = k.k4p, k4m = k.k4m,
             k5hp = k.k5hp, k5hm = k.k5hm, k5ohp = k.k5ohp,
             k5ohm = k.k5ohm, k6p = k.k6p, k6m = k.k6m,
             k7p = k.k7p, k7m = k.k7m, k8p = k.k8p, k8m = k.k8m)
}
keq <- acidbase(TC, S, dens_sw)
#converting values
sinyr1 <- sinyr/1419.75
k1p <- keq$k1p * sinyr1
k1m <- keq$k1m * sinyr1
k4p <- keq$k4p * sinyr1
k4m <- keq$k1p * sinyr1
k5hp <- keq$k5hp * sinyr1
k5hm <- keq$k5hm * sinyr1
k5ohp <- keq$k5ohp * sinyr1
k5ohm <- keq$k5ohm * sinyr1
k6p <- keq$k6p * sinyr1
k6m <- keq$k6m * sinyr1

#==============================================================================
# Rate constants hydrogen sulfide
#==============================================================================
kHS_f <- 5.0 * 10^10 * dens_sw^-1 #[kg/mol/s]*[m3/kg]=[m3/mol/s]
KHS <- 10^-6.9 * 10^3 #[mol/dm3]*[dm3/m3]=mol/m3
kHS_b <- KHS * kHS_f#[mol/m3]*[m3/mol/s]=[1/s]

#==============================================================================
# Model formulation
#==============================================================================

model <- function(t, state, parms) {
  POM <- state[1:N]
  O2 <- state[(N+1):(2*N)]
  NO3 <- state[(2*N+1):(3*N)]
  MnO2 <- state[(3*N+1):(4*N)]
  FeOH3 <- state[(4*N+1):(5*N)]
  SO4 <- state[(5*N+1):(6*N)]
  NH4 <- state[(6*N+1):(7*N)]
  Mn <- state[(7*N+1):(8*N)]
  Fe <- state[(8*N+1):(9*N)]
  H2S <- state[(9*N+1):(10*N)]
  HS <- state[(10*N+1):(11*N)]
  FeS <- state[(11*N+1):(12*N)]
  MnCO3 <- state[(12*N+1):(13*N)]
```

```
FeCO3 <- state[(13*N+1):(14*N)]
H <- state[(14*N+1):(15*N)]
OH <- state[(15*N+1):(16*N)]
CO2 <- state[(16*N+1):(17*N)]
CO3 <- state[(17*N+1):(18*N)]
HCO3 <- state[(18*N+1):(19*N)]


#tran.1D calculates advection and diffusion
tranPOM <- tran.1D(C = POM, flux.up = J_POM, D = Db.grid,
                   v = u.grid, VF = svf.grid, dx = grid)
tranO2 <- tran.1D(C = O2, C.up = O20, D = DO2.grid,
                  v = u.grid, VF = por.grid, dx = grid)
tranNO3 <- tran.1D(C = NO3, C.up = NO30, D = DNO3.grid,
                  v = u.grid, VF = por.grid, dx = grid)
tranMnO2 <- tran.1D(C = MnO2, flux.up = J_MnO2, D = Db.grid,
                  v = u.grid, VF = svf.grid, dx = grid)
tranFeOH3 <- tran.1D(C = FeOH3, flux.up = J_FeOH3, D = Db.grid,
                   v = u.grid, VF = svf.grid, dx = grid)
tranSO4 <- tran.1D(C = SO4, C.up = SO40, D = DSO4.grid,
                  v = u.grid, VF = por.grid, dx = grid)
tranNH4 <- tran.1D(C = NH4, C.up = 0, D = DNH4.grid,
                   v = u.grid, VF = por.grid, dx = grid)
tranMn <- tran.1D(C = Mn, C.up = 0, D = DMn.grid,
                    v = u.grid, VF = por.grid, dx = grid)
tranFe <- tran.1D(C = Fe, C.up = 0, D = DFe.grid,
                     v = u.grid, VF = por.grid, dx = grid)
tranH2S <- tran.1D(C = H2S, C.up = 0, D = DH2S.grid,
                   v = u.grid, VF = por.grid, dx = grid)
tranHS <- tran.1D(C = HS, C.up = 0, D = DH2S.grid,
                  v = u.grid, VF = por.grid, dx = grid)
tranFeS <- tran.1D(C = FeS, flux.up = 0, D = Db.grid,
                   v = u.grid, VF = svf.grid, dx = grid)
tranMnCO3 <- tran.1D(C = MnCO3, flux.up = 0, D = Db.grid,
                     v = u.grid, VF = svf.grid, dx = grid)
tranFeCO3 <- tran.1D(C = FeCO3, flux.up = 0, D = Db.grid,
                     v = u.grid, VF = svf.grid, dx = grid)
tranH <- tran.1D(C = H, C.up = H0, D = DH.grid,
                 v = u.grid, VF = por.grid, dx = grid)
tranOH <- tran.1D(C = OH, C.up = OH0, D = DOH.grid,
                  v = u.grid, VF = por.grid, dx = grid)
tranCO2 <- tran.1D(C = CO2, C.up = CO20, D = DCO2.grid,
                   v = u.grid, VF = por.grid, dx = grid)
tranCO3 <- tran.1D(C = CO3, C.up = CO30, D = DCO3.grid,
                   v = u.grid, VF = por.grid, dx = grid)
tranHCO3 <- tran.1D(C = HCO3, C.up = HCO30, D = DHCO3.grid,
                    v = u.grid, VF = por.grid, dx = grid)

#transport and irrigation
dPOMdt <- tranPOM$dC
dO2dt <- tranO2$dC - alpha.grid$mid * (O2 - O20)
dNO3dt <- tranNO3$dC - alpha.grid$mid * (NO3 - NO30)
dMnO2dt <- tranMnO2$dC
dFeOH3dt <- tranFeOH3$dC
dSO4dt <- tranSO4$dC - alpha.grid$mid * (SO4 - SO40)

dNH4dt <- tranNH4$dC - alpha.grid$mid * NH4
dMndt <- tranMn$dC - alpha.grid$mid * Mn
dFedt <- tranFe$dC - alpha.grid$mid * Fe
dH2Sdt <- tranH2S$dC
dHSdt <- tranHS$dC

dFeSdt <- tranFeS$dC
dMnCO3dt <- tranMnCO3$dC
dFeCO3dt <- tranFeCO3$dC

dHdt <- tranH$dC - alpha.grid$mid * (H - H0)
dOHdt <- tranOH$dC - alpha.grid$mid * (OH - OH0)
dCO2dt <- tranCO2$dC - alpha.grid$mid * (CO2 - CO20)
dCO3dt <- tranCO3$dC - alpha.grid$mid * (CO30 - CO30)
dHCO3dt <- tranHCO3$dC - alpha.grid$mid * (HCO3 - HCO30)
```

```
  #Primary redox reactions
  #if ([X] > KX) then f_X = 1-somf, if ([X] < KX) then f_X = (1-somf) * X / K
  #concentrations are per volume water or solid, but rates are per total volume
  f_O2 <- (por.grid$mid * O2 < KO2) * por.grid$mid * O2 / KO2 + (por.grid$mid * O2 >=
KO2)
  somf <- f_O2
  f_NO3 <- (1-somf)*((por.grid$mid * NO3 >= KNO3) + (por.grid$mid * NO3 < KNO3) *
por.grid$mid * NO3 / KNO3)
  somf <- somf + f_NO3
  f_MnO2 <- (1-somf)*((svf.grid$mid * MnO2 >= KMnO2) + (svf.grid$mid * MnO2 < KMnO2) *
svf.grid$mid * MnO2 / KMnO2)
  somf <- somf + f_MnO2
  f_FeOH3 <- (1-somf)*((svf.grid$mid * FeOH3 >= KFeOH3) + (svf.grid$mid * FeOH3 < KFeOH3)
* svf.grid$mid * FeOH3 / KFeOH3)
  somf <- somf + f_FeOH3
  f_SO4 <- (1-somf)*((por.grid$mid * SO4 >= KSO4) + (por.grid$mid * SO4 < KSO4) *
por.grid$mid * SO4 / KSO4)
  somf <- somf + f_SO4

  RO2 <- kc * POM * f_O2
  RNO3 <- kc * POM * f_NO3
  RMnO2 <- kc * POM * f_MnO2
  RFeOH3 <- kc * POM * f_FeOH3
  RSO4 <- kc * POM * f_SO4
  #secondary reactions

  #Mass balances
  #Redfield ratio
  x <- 106/106
  y <- 12/106 #Thullner uses 12 instead of 16
  z <- 1/106

  fact <- svf.grid$mid / por.grid$mid #converts V_s^-1 to V_w^-1
  #Mass balances for primary redox reactions
  dPOMdt <- dPOMdt + (-RO2 - RNO3 - RMnO2 - RFeOH3 - RSO4)
  dO2dt <- dO2dt - fact * (x + 2*y) * RO2
  dNO3dt <- dNO3dt + fact * (y * RO2 - (4*x + 3*y)*RNO3/5)
  dMnO2dt <- dMnO2dt + (-2 * x * RMnO2)
  dFeOH3dt <- dFeOH3dt - (4 * x * RFeOH3)
  dSO4dt <- dSO4dt - fact * x* RSO4/2
  dNH4dt <- dNH4dt + fact * y * (RMnO2 + RFeOH3 + RSO4)
  dMndt <- dMndt + fact * 2 * x * RMnO2
  dFedt <- dFedt + fact * (4 * x * RFeOH3)
  dH2Sdt <- dH2Sdt + fact * x*RSO4/2

  dCO2dt <- dCO2dt + fact * ( (x+y+2*z)*RO2 + (x-3*y+10*z)*RNO3/5 - (3*x+y-2*z)*RMnO2 -
(7*x+y-2*x)*RFeOH3 -
    2*(y-2*z)*RSO4/2)
  dHCO3dt <- dHCO3dt + fact * ( -(y + 2*z)*RO2 + (4*x + 3*y - 10*z)*RNO3/5 + (4*x + y -
2*z)*RMnO2 +
    (8*x + y - 2*z)*RFeOH3 + 2*(x+y-2*z)*RSO4/2 )

  #secondary redox reactions
  R1 <- k1 * NH4 * O2
  R2 <- k2 * Mn * O2
  R3 <- k3 * Fe * O2
  R4 <- k4 * Fe * MnO2
  R5a <- k5 * O2 * HS
  R5b <- k5 * O2 * H2S
  R6a <- k6 * MnO2 * HS
  R6b <- k6 * MnO2 * H2S
  R7a <- k7 * FeOH3 * HS
  R7b <- k7 * FeOH3 * H2S

  #Mass balances for secondary redox reactions
  dO2dt <- dO2dt - 2 * R1 - 0.5 * R2 - 0.25 * R3 - 2 * (R5a + R5b)
  dNO3dt <- dNO3dt + R1
  dMnO2dt <- dMnO2dt + R2/fact - R4 - (R6a + R6b)
  dFeOH3dt <- dFeOH3dt +  R3/fact + 2 * R4 - 2 * (R7a + R7b)
  dSO4dt <- dSO4dt + (R5a + R5b)
```

```
dNH4dt <- dNH4dt + - R1
dMndt <- dMndt - R2 + fact * R4 + fact * (R6a + R6b)
dFedt <- dFedt - R3 - 2 * fact * R4 + 2 * (R7a + R7b) * fact
#==========================ACCOUNTING FOR TOTHS REACTIONS====================
dH2Sdt <- dH2Sdt - R5b - R6b * fact - R7b * fact # H2S --> ...
dHSdt <- dHSdt - R5a - R6a * fact - R7a * fact # HS + HCO3 -- > ... + CO3
dHCO3dt <- dHCO3dt - R5a - R6a * fact - R7a * fact
dCO3dt <- dCO3dt + R5a + R6a * fact + R7a * fact
#============================================================================
dCO2dt <- dCO2dt + 2 * R1 + 2 * R2 + 2 * R3 + 2 * fact * R4 + 2 * (R5a + R5b) -
  2 * fact * (R6a + R6b) - 4 * fact * (R7a + R7b)
dHCO3dt <- dHCO3dt - 2 * R1 - 2 * R2 - 2 * R3 - 2 * fact * R4 - 2 * (R5a + R5b) +
  2 * fact * (R6a + R6b) + 4 * fact * (R7a+R7b)

#equilibrium reactions
RHS_f <- kHS_f * H * HS
RHS_b <- kHS_b * H2S

R1p <- k1p * CO2
R1m <- k1m *  HCO3 * H
R4p <- k4p *  CO2 * OH
R4m <- k4m * HCO3
R5hp <- k5hp * CO3 * H
R5hm <- k5hm * HCO3
R5ohp <- k5ohp * HCO3 * OH
R5ohm <- k5ohm * CO3
R6p <- k6p
R6m <- k6m * H * OH

#mass balances for equilibrium reactions
dHSdt <- dHSdt -RHS_f + RHS_b
dH2Sdt <- dH2Sdt + RHS_f - RHS_b

dHdt <- dHdt + R1p - R1m - R5hp + R5hm + R6p - R6m - RHS_f + RHS_b
dOHdt <- dOHdt + -R4p + R4m - R5ohp + R5ohm + R6p - R6m
dCO2dt <- dCO2dt -R1p + R1m - R4p + R4m
dCO3dt <- dCO3dt -R5hp + R5hm + R5ohp - R5ohm
dHCO3dt <- dHCO3dt + R1p - R1m + R4p - R4m + R5hp - R5hm - R5ohp + R5ohm

#Mineral reactions
R8 <- k8 * FeS * O2

SI <- min(0, Mn * CO3 / K_MnCO3) - 1
R9f <- (SI > 0)  * (k9p/1) * SI #oversaturated: precipitation
R9b <- (1-(SI > 0)) * (k9m/1) * MnCO3 * SI #undersaturated: dissolution
SI2 <-  min(0, Fe * CO3 / K_FeCO3) - 1
R10f <- (SI2 > 0) * (k10p/1) * SI2 #oversaturated: precipitation
R10b <- (1-(SI2 > 0)) * (k10m/1) * FeCO3 * SI2 #undersaturated: dissolution
SI3 <-  Fe * HS / (H * K_FeS) - 1
R11f <- (SI3 > 0) * k11p * SI3 #oversaturated: precipitation
R11b <- (1-(SI3 > 0)) * k11m * FeS * SI3 #undersaturated: dissolution

dFeSdt <- dFeSdt - R8 + R11f - R11b
dO2dt <- dO2dt - fact * R8
dFedt <- dFedt + fact * R8 - fact * R10f + fact * R10b - fact * R11f + fact * R11b
dSO4dt <- dSO4dt + fact * R8
dMnCO3dt <- dMnCO3dt + R9f - R9b
dMndt <- dMndt - fact * R9f + fact * R9b
dHCO3dt <- dHCO3dt - 2 * fact * R9f + 2 * fact * R9b - 2 * fact * R10f +
  2 * fact * R10b - 2* fact * R11f + 2* fact * R11b
dCO2dt <- dCO2dt + 2 * fact * R9f - 2 * fact * R9b +
  fact * R10f - fact * R10b + 2 * fact * R11f - 2* fact * R11b
dFeCO3dt <- dFeCO3dt + R10f - R10b

results <- c(dPOMdt=dPOMdt, dO2dt = dO2dt, dNO3dt = dNO3dt,
             dMnO2dt = dMnO2dt, dFeOH3dt = dFeOH3dt, dSO4dt = dSO4dt,
             dNH4dt = dNH4dt, dMndt = dMndt, dFedt = dFedt,
             dH2Sdt = dH2Sdt, dHSdt = dHSdt, dFeSdt = dFeSdt,
              dMnCO3dt = dMnCO3dt, dFeCO3dt, dHdt = dHdt,
              dOHdt = dOHdt, dCO2dt = dCO2dt, dCO3dt = dCO3dt,
              dHCO3dt = dHCO3dt)
```

```
  return(list(results,
              RO2=RO2, RNO3=RNO3, RFeOH3=RFeOH3, RMnO2 = RMnO2, RSO4 = RSO4,
              FluxUpPOM = tranPOM$flux.up, FluxDownPOM =  tranPOM$flux.down,
              FluxUpO2 = tranO2$flux.up, FluxDownO2 =  tranO2$flux.down,
              FluxUpNO3= tranNO3$flux.up, FluxDownNO3 =  tranNO3$flux.down,
              FluxUpMnO2 = tranMnO2$flux.up, FluxDownMnO2 =  tranMnO2$flux.down,
              FluxUpFeOH3 = tranFeOH3$flux.up, FluxDownFeOH3 =  tranFeOH3$flux.down,
              FluxUpSO4 = tranSO4$flux.up, FluxDownSO4 =  tranSO4$flux.down))
}

#==============================================================================
# Model solution
#==============================================================================
names <- c("POM", "O2", "NO3", "MnO2", "FeOH3", "SO4",
           "NH4", "Mn", "Fe", "H2S", "HS", "FeS", "MnCO3", "FeCO3",
           "H", "OH", "CO2", "CO3", "HCO3")

load(file="/Users/jurjen/Documents/R/Hypsometry/100m.rda")

state <- c(POM, O2, NO3, FeOH3, MnO2, SO4, NH4, Mn, Fe, H2S, HS, FeS, MnCO3, FeCO3,
           H, OH, CO2, CO3, HCO3)

std <- steady.1D(y = state, func = model, parms = NULL,
                 names = names, nspec = 19, pos=TRUE)


steady.state.reached <- attributes(std)$steady

if (steady.state.reached) print("Hiep, hiep, hoi!")

#==============================================================================
# Writing results to data files in working directory
#==============================================================================
POM <- std$y[,1]
O2 <- std$y[,2]
NO3 <- std$y[,3]
MnO2 <- std$y[,4]
FeOH3 <- std$y[,5]
SO4 <- std$y[,6]
NH4 <- std$y[,7]
Mn <- std$y[,8]
Fe <- std$y[,9]
H2S <- std$y[,10]
HS <- std$y[,11]
FeS <- std$y[,12]
MnCO3 <- std$y[,13]
FeCO3 <- std$y[,14]
H <- std$y[,15]
OH <- std$y[,16]
CO2 <- std$y[,17]
CO3 <- std$y[,18]
HCO3 <- std$y[,19]

#save(file="/Users/jurjen/Documents/R/Hypsometry/100m.rda", POM,
#    O2, NO3, MnO2, FeOH3, SO4, NH4, Mn, Fe, H2S, HS, FeS, MnCO3, FeCO3, H, OH, CO2, CO3,
HCO3)

#making depth profiles
options(save.defaults=list(ascii=TRUE))
FeOH3tV <- FeOH3 * svf
save(file="/Users/jurjen/Documents/R/Thullner2009/FeOH3.txt", FeOH3tV)
z <- seq(0,0.3, length=1000)
save(file="/Users/jurjen/Documents/R/Thullner2009/depth.txt", z)

#==============================================================================
# Model validation: mass balances and analytical solution
#==============================================================================
Volume <- 1 * grid$dx
TotPOM.ox <- sum((std$RO2 + std$RNO3 + std$RNO3h + std$RSO4 + std$RMnO2 + std$RFeOH3) *
  svf.grid$mid * Volume)
mbPOM <- std$FluxUpPOM - std$FluxDownPOM - TotPOM.ox
```

```
print(paste("Mass balance POM: ", mbPOM))

NH4prod <- sum(y * (std$RMnO2 + std$RFeOH3 + std$RSO4) *
  svf.grid$mid * Volume)
NH4loss <- sum(por.grid$mid * Volume * (std$enhNH4 + std$R1))
mbNH4 <- NH4prod - NH4loss - std$FluxDownNH4 + std$FluxUpNH4
print(paste("Mass balance NH4: ", mbNH4))

NO3prod   <-   sum(y   *   std$RO2   *   svf.grid$mid*Volume   +   (std$R1-std$enhNO3)   *
por.grid$mid*Volume)
NO3loss <- sum((4*x+3*y)/5 * svf.grid$mid * std$RNO3 * Volume)
mbNO3 <- NO3prod - NO3loss - std$FluxDownNO3 + std$FluxUpNO3
print(paste("Mass balance NO3: ", mbNO3))

TotR2 <- sum(std$RNO3 * (4*x+3*y)/5 * svf.grid$mid * Volume * 1)
TotR2h <- sum(std$RNO3h * (4*x+3*y)/5 * svf.grid$mid * Volume * 1)
TotR1 <- sum(std$R1 * por.grid$mid *Volume)
TotR1h <- sum(std$R1h * por.grid$mid *Volume)

#Analytical solution
#unknowns A1, B1, A2
L <- 10 #Db depth
a <- (u - sqrt(u^2 + 4*kc*Db))/(2*Db)
b <- (u + sqrt(u^2 + 4*kc*Db))/(2*Db)

#Flux_SWI = A1 * a * Db - B * b * Db + u * A1 + u * B1
#A1 * exp(a*L) - B1 * exp(b*L) = A2 * exp(k * L / u)
#- A1 * a * Db * exp(a*L) - B1 * b * Db * exp(b*L) + u * A1 * exp(a*L) + u * B1 *
exp(b*L) = u * A2 * exp(-k*L/u)

AnalyticalSolution <- function(
  k=0.221, u=0.001,Db=0.1,
  L=10, flux=0.3, sed )
{
  a <- (u - sqrt(u^2 + 4*k*Db))/(2*Db)
  b <- (u + sqrt(u^2 + 4*k*Db))/(2*Db)

  A <- matrix(nrow=3,ncol=3,byrow=TRUE,data= c(
    -a*Db+u          , -b*Db+u          ,0              ,
    -a*Db*exp(a*L) + u*exp(a*L), -b*Db*exp(b*L) + u*exp(b*L),   -u*exp(-k*L/u),
    exp(a*L) , exp(b*L), -exp(-k*L/u) )
  )
  B  <- c(flux, 0, 0)
  X  <- solve(A,B)
  print(X)
  s1 <- which (sed<L)
  s2 <- which (sed>=L)
  conc <- vector(length=length(sed))
  conc[s1] <- X[1]* exp(a*sed[s1])+X[2]*exp(b*sed[s1])
  conc[s2] <- X[3]* exp(-(k/u)*sed[s2])
  return(conc)
}

depth       <- seq(0,0.30,len=1000)
anaPOM      <- AnalyticalSolution(sed=depth, k = kc, u = u, Db = Db, L=0.1, flux = J_POM)
#plot(Pb,depth,ylim=c(15,0),xlab="Pb, dpm/cm2/yr",
#     ylab="cm",type="l",lwd=2,main="75% injected")
plot(depth, POM*(1-por), type="l", col="blue")
lines(depth, anaPOM, col="red")
```

B. Model without bio-irrigation (1D)

```
######################################################################
# N cycling sediments without bioturbation
# N isotope fractionation
######################################################################
library(marelac)
library(ReacTran)

#=============================================================================
# Units used in the program:
#=============================================================================

# Mass =  mol
# Space = m
# Time = s

#=============================================================================
# Assumptions
#=============================================================================

# (1) Porosity constant with depth
# (2) Transport only through diffusion (no bioturbation or advection)

#=============================================================================
# Model domain and grid definition
#=============================================================================
L <- 0.2    # depth of sediment domain [m]
N <- 1000  # number of grid layers
grid <- setup.grid.1D(x.up = 0, L = L, N = N)

#=============================================================================
# Model parameters:
#=============================================================================

# Environmental parameters
por <- 0.85 # porosity
svf <- 1-por # solid volume fraction
Hplus <- 7.9433e-6 #activity H+ [mol/m^3]
stoich <- 12/106 #ratio N:C in organic matter
sed <- 0#
sedPOM <- 0.398 / 100 / (365*24*60^2)# #sedimentation rate m/s
JPOM <- 510*10^-6*100^2/(365*24*60^2)

# Biogeochemical parameters
k <- 2e-5 #rate constant DOM degradation [1/s]
KmO2 <- 0.008 #half-sat. constant oxic resp. [mol/m^3]
KmNO3 <- 0.01 #half-sat constant DNF [mol/m^3]
KmFeOH3 <- 12.5 #half-sat constant Fe(III)-reduction [mol/m^3]
KmSO4 <- 0.85 #half-sat constant SO4  reduction [mol/m^3]
kNit <- 1.9805e-4 #rate constant nitrification [m^3/mol/s]
kHS <- 0.022369 #rate constant HS oxidation [m^3/mol/s]
kFe <- 0.074564 #rate constant Fe(II) oxidation [m^3/mol/s]
kprecip <- 1.9e-9 #rate constant FeS precipitation [mol^2/m^6/s]
KFeS <- 1.1220 #equilibrium constant FeS [mol^2/m^6]
kPOM <- 7.0032e-9 #POM degradation rate [1/s]

#Isotope stuff
d15N_Org <- 1.5 #Isotopic composition of organic matter [per mil]
Rstd <- 0.366/99.634 #15N/14N in atmosphere
fracN15Org <- (d15N_Org/1000 + 1)*Rstd #15N/14N of organic matter
d15N_NO3 <- 5 #Isotopic composition of oceanic nitrate [per mil]
fracN15O3 <- (d15N_NO3/1000 + 1)*Rstd #15N/14N of nitrate
alpha_Nit <- 0.975 #fractionation factor nitrification
alpha_Den <- 1#0.980 #fractionation factor denitrification

# Diffusion coefficients [m^2 yr-1]
tort <- 1 - 2*log(por) # tortuosity correction
```

```
DO2 <- 1.349e-9/tort
DNO3 <- 1.079e-9/tort
DNH4 <- 1.091e-9/tort
DSO4 <- 8.91e-10/tort
DFe <- 3.83e-10/tort
DHS <- 1.49e-9/tort
DDOM <- 1e-9/tort

# Attachment of parameters to grid
tvf.grid <- setup.prop.1D(value = 1, grid = grid) #total volume fraction
u.grid <- setup.prop.1D(value = sed, grid = grid) #advection
sedPOM.grid <-  setup.prop.1D(value = sedPOM, grid = grid)
DO2.grid <- setup.prop.1D(value = DO2, grid = grid)
DNO3.grid <- setup.prop.1D(value = DNO3, grid = grid)
DNH4.grid <- setup.prop.1D(value = DNH4, grid = grid)
DSO4.grid <- setup.prop.1D(value = DSO4, grid = grid)
DFe.grid <- setup.prop.1D(value = DFe, grid = grid)
DHS.grid <- setup.prop.1D(value = DHS, grid = grid)
DDOM.grid <- setup.prop.1D(value = DDOM, grid = grid)
Db.grid <- setup.prop.1D(value = 0, grid = grid)

#==========================================================================
# Imposed concentration profiles POM and Fe(OH)3
#==========================================================================
POMfunc <- function(x) {
  A2 <- 271.81 #mol/m3
  #Db <- 8.7144e-11 #m2/s
  a <- -8.2701
  #u <- 0.5/100/(60^2*24*365) #0.5 cm /yr
  A2*exp(a*x)
  #
  #A <- JPOM / u
  #A

  #solution in DB constant
  #A2 <- 271.81
  #a <- -8.2701
  #A2*exp(a*x)

  #solution in DB first 10 cm
  #a <- -8.2701
  #b <- 9.7174
  #c <- 55.528
  #(x < 0.1) * (216.84*exp(a*x)+30.54*exp(b*x)) +
  #  (x >= 0.1) * (45283.05*exp(-c*x))
}

FeOH3func <- function(x) {
  (x > 0.002703 && x < 0.003295)*(3515.8*-x + 11.583) +
    (x <= 0.002703) * (289.28*-x + 2.9506)
}

FeOH3 <- FeOH3func(grid$x.mid)
POM <- POMfunc(grid$x.mid)

#==========================================================================
# Boundary conditions in overlying water
#==========================================================================
#concentrations in overlying water [mol/m^3]
NH40 <- 0
SO40 <- 28
Fe0 <- 0
HS0 <- 0
DOM0 <- 0.050
N15H40 <- 0
#High Latitudes
O20 <-0.340
NO30 <- 0.025
#Low latitudes
#O20 <-0.190
#NO30 <- 0.005
```

```
N15O30 <- fracN15O3 * NO30

#================================================================================
# Model formulation
#================================================================================
model <- function (t, state, parms) {
  # Initialisation of state variables
  O2 <- state[1:N]
  NO3 <- state[(N+1):(2*N)]
  NH4 <- state[(2*N+1):(3*N)]
  SO4 <- state[(3*N+1):(4*N)]
  Fe <- state[(4*N+1):(5*N)]
  HS <- state[(5*N+1):(6*N)]
  DOM <- state[(6*N+1):(7*N)]
  N15H4 <- state[(7*N+1):(8*N)]
  N15O3 <- state[(8*N+1):(9*N)]
  #POM <- state[(9*N+1):(10*N)]

  #transport terms
  #tran.1D calculates advection and diffusion
  tranO2 <- tran.1D(C = O2, C.up = O20, D = DO2.grid,
                    v = sedPOM.grid, VF = tvf.grid, dx = grid)
  tranNO3 <- tran.1D(C = NO3, C.up = NO30, D = DNO3.grid,
                   v = sedPOM.grid, VF = tvf.grid, dx = grid)
  tranNH4 <- tran.1D(C = NH4, C.up = NH40, D = DNH4.grid,
                    v = sedPOM.grid, VF = tvf.grid, dx = grid)
  tranSO4 <- tran.1D(C = SO4, C.up = SO40, D = DSO4.grid,
                     v = sedPOM.grid, VF = tvf.grid, dx = grid)
  tranFe <- tran.1D(C = Fe, C.up = Fe0, D = DFe.grid,
                      v = sedPOM.grid, VF = tvf.grid, dx = grid)
  tranHS <- tran.1D(C = HS, C.up = HS0, D = DHS.grid,
                    v = sedPOM.grid, VF = tvf.grid, dx = grid)
  tranDOM <- tran.1D(C = DOM, C.up = DOM0, D = DDOM.grid,
                    v = sedPOM.grid, VF = tvf.grid, dx = grid)
  tranN15H4 <- tran.1D(C = N15H4, C.up = N15H40, D = DNH4.grid,
                   v = sedPOM.grid, VF = tvf.grid, dx = grid)
  tranN15O3 <- tran.1D(C = N15O3, C.up = N15O30, D = DNO3.grid,
                    v = sedPOM.grid, VF = tvf.grid, dx = grid)
  #tranPOM <- tran.1D(C = POM, flux.up = JPOM, D = Db.grid,
  #                   v = sedPOM.grid, VF = tvf.grid, dx = grid)

  #reaction terms
  R1 <- k*DOM*O2/(O2+KmO2) #oxic respiration rate
  R2 <- (k*DOM-R1)*NO3/(NO3+KmNO3) #denitrification
  R2h <- alpha_Den*(k*DOM-R1)*N15O3/(NO3+KmNO3) #denitrification 15NO3
  R3 <- (k*DOM-R1-R2-R2h)*FeOH3/(FeOH3+KmFeOH3) #Fe(III) reduction
  R4 <- (k*DOM-R1-R2-R2h-R3)*SO4/(SO4+KmSO4) #SO4 reduction
  R5 <- kNit * NH4 * O2 #nitrification
  R5h <- alpha_Nit * kNit * N15H4 * O2 #nitrification 15NH4
  R6 <- kHS * HS * O2 #HS oxidation
  R7 <- kFe * Fe * O2
  R11 <- kprecip * (Fe * HS / (KFeS * Hplus) - 1)
  R12 <- kPOM * POM

  #mass balances
  dO2dt <- tranO2$dC - R1 - 2 * (R5 + R5h) - 2*R6 - 0.25*R7
  dNO3dt <- tranNO3$dC - 0.8*R2 + R5
  dN15O3dt <- tranN15O3$dC - 0.8*R2h + R5h
  dNH4dt <- tranNH4$dC + stoich*(R1+R2+R2h+R3+R4) - R5
  dN15H4dt <- tranN15H4$dC + fracN15Org*stoich*(R1+R2+R2h+R3+R4) - R5h
  dSO4dt <- tranSO4$dC - 0.5*R4 + R6
  dFedt <- tranFe$dC + 4*R3 - R7 - R11
  dHSdt <- tranHS$dC + 0.5*R4 - R6 - R11
  dDOMdt <- tranDOM$dC + R12 - R1 - (R2+R2h) - R3 - R4
  #dPOMdt <- tranPOM$dC - R12

  results <- c(dO2dt = dO2dt, dNO3dt = dNO3dt, dNH4dt = dNH4dt,
               dSO4dt = dSO4dt, dFedt = dFedt, dHSdt = dHSdt,
               dDOMdt = dDOMdt, dN15H4dt = dN15H4dt, dN15O3dt = dN15O3dt)
               #dPOMdt = dPOMd)
  return(list(results,
```

```
              R2 = R2, R2h = R2h, R5 = R5, R5h = R5h,
              R1 = R1, R3 = R3, R4 = R4,
              FUNO3 = tranNO3$flux.up, FUN15O3 = tranN15O3$flux.up,
              FUNH4 = tranNH4$flux.up, FUN15H4 = tranN15H4$flux.up,
              FDNO3 = tranNO3$flux.down, FDN15O3 = tranN15O3$flux.down,
              FDNH4 = tranNH4$flux.down, FDN15H4 = tranN15H4$flux.down))
}

#==============================================================================
# Steady state model solution
#==============================================================================

# State variables and initial conditions:
O2.in <- rep(0, length.out = N)
NO3.in <- rep(0, length.out = N)
NH4.in <- rep(0, length.out = N)
SO4.in <- rep(0, length.out = N)
Fe.in <- rep(0, length.out = N)
HS.in <- rep(0, length.out = N)
DOM.in <- rep(0, length.out = N)
N15H4.in <- rep(0, length.out = N)
N15O3.in <- rep(0, length.out = N)
POM.in <- rep(0, length.out = N)

state <- c(O2.in, NO3.in, NH4.in, SO4.in, Fe.in, HS.in,
           DOM.in, N15H4.in, N15O3.in)#, POM.in)
names <- c("O2", "NO3", "NH4", "SO4", "Fe", "HS", "DOM",
           "N15H4", "N15O3")#, "POM")

# Steady state calculation of concentration profiles
std <- steady.1D(y = state, func = model, parms = NULL,
                 names = names, nspec = 9, pos = TRUE)
steady.state.reached <- attributes(std)$steady

if (steady.state.reached) {
  print("Simulation complete")
  O2 <- std$y[,1]
  NO3 <- std$y[,2]
  NH4 <- std$y[,3]
  SO4 <- std$y[,4]
  Fe <- std$y[,5]
  HS <- std$y[,6]
  DOM <- std$y[,7]
  N15H4 <- std$y[,8]
  N15O3 <- std$y[,9]
  #POM <- std$y[,10]
} else stop


#already for the plots
depth <- grid$x.mid

#==============================================================================
# Model verification
#==============================================================================

#Mass balances
Volume <- 1 * grid$dx
mbNO3 <- std$FUNO3 - std$FDNO3 + sum((std$R5 - 0.8*std$R2) * Volume)
print(paste("Mass balance NO3: ", mbNO3))
mbN15O3 <- std$FUN15O3 - std$FDN15O3 + sum((std$R5h - 0.8*std$R2h) * Volume)
print(paste("Mass balance N15O3: ", mbN15O3))

plot(std)
depth <- grid$x.mid
plot(std$R2, depth, type="l")
plot(std$R2h, depth, type="l")
plot(std$R5, depth, type="l")
plot(std$R5h, depth, type="l")

#checking fractionation factors
```

```
plot(depth, std$R5h/std$R5/(N15H4/NH4)) #should be equal to alpha_Nit
plot(depth, std$R2h/std$R2/(N15O3/NO3)) #should be equal to alpha_Den

#==============================================================================
# Isotope fractionation
#==============================================================================
eps1 <- (sum(std$R2h)/sum(std$R2)/fracN15O3 - 1) * 1000
print(paste("Epsilon 1: ", eps1))

eps2 <- (sum(std$R2h)/sum(std$R2)/(sum(N15O3)/sum(NO3)) - 1) * 1000
print(paste("Epsilon 2: ", eps2))

Nitd15N <- (sum(std$R5h)/sum(std$R5)/(sum(N15O3)/sum(NO3)) - 1) * 1000

uc <- 60^2*1000*24 #mol/m^2/s -> mmol/m^2/d
DNFrate <- 0.8*sum(std$R2*Volume)*uc #mmol N m^-2 d^-1
print(paste("Integrated DNF rate: ", DNFrate, " mmol N m^-2 d^-1"))
Nit_rate <- sum(std$R5*Volume)*uc #mmol N m^-2 d^-1
print(paste(
  "Integrated nitrification rate: ", Nit_rate, " mmol N m^-2 d^-1"))

d15N <- function(N15, N14) {
  (N15/N14/Rstd -1)*1000
}
#because of no gradient b.c. and no advection there is no burial
#thus only fluxes at SWI are important
icFNH4 <- d15N(std$FUN15H4, std$FUNH4)
icFNO3 <- d15N(std$FUN15O3, std$FUNO3)
print(paste("Flux NH4: ", std$FUNH4*uc, "mmol/m^2/d, d15N of NH4 flux: ",
            icFNH4, "per mille"))
print(paste("Flux NO3: ", std$FUNO3*uc, "mmol/m^2/d, d15N of NO3 flux: ",
            icFNO3, "per mille"))
print(
  "NH4 is diffusing out of the sediment, while NO3 is entering the sediment"
  )

Rmin <- uc*(12/106)*sum(Volume*(std$R1 + std$R2 + std$R3 + std$R4))
print(paste("Mineralization rate: ", Rmin, "mmol/m^2/d"))

#plots of isotopic composition NH4 and NO3 over depth sediment
depth <- grid$x.mid
plot(depth, d15N(N15H4,NH4), type="l")
plot(depth, d15N(N15O3,NO3), type="l")
```

C. Code for O_2 and NO_3 bottom-water concentrations

```
%seafloor depth range
sfd=100;
sf_low_bnd = 0.9*sfd;
sf_upp_bnd = 1.1*sfd;

%% read in the WA09 data set
ncid = netcdf.open('/Users/jurjen/dissolved_oxygen_annual_1deg.nc')

%%read in the global nitrate file
ncno3 = netcdf.open('/Users/jurjen/nitrate_annual_1deg.nc');
%7 = nitrate annual
%water-depth, latitudes and longitudes are the same as in O2 file

%%read in the global AOU file
ncaou = netcdf.open('/Users/jurjen/apparent_oxygen_utilization_annual_1deg.nc');

[numdims,numvars,numglobalatts,unlimdimid] = netcdf.inq(ncid);
% see http://www.opendap.org/user/jimg/blog/matlab_2012a
[name,xtype,dimids,natts] = netcdf.inqVar(ncid,7); % content of 4th variable
name

%0 = longitude
%1 = latitude
%2 = depth
%3 = time
%4 = lat_bnds ??
%5 = lon_bnds
%6 = climatology bnds
%7 = oxygen annual
%8 = oxygen monthly
%9 = oxygen dd ??
%10 = o_ma ??
%11 = o_sd
%12 = o_se
%13 = o_gp
%14 = crs

%% assign it to variables
o2 = netcdf.getVar(ncid,7); % O2 conc in ml/L (longitude, latitude, layer)
zm = netcdf.getVar(ncid,2); % depth in m (1 x layer)
lo = netcdf.getVar(ncid,0); % longitude in degree
la = netcdf.getVar(ncid,1); % latitude in degree
no3 = netcdf.getVar(ncno3,7); %no3 conc umol/kg
aou = netcdf.getVar(ncaou,7); %aou ml/L

%% read in the global topography/bathimetry (1/12 x 1/12 degree)
bath = netcdf.open('/Users/jurjen/bath.cdf');
%0 = X
%1 = Y
%2 = elevation
elev = netcdf.getVar(bath, 2); % depth(X=long,Y=lat)
X = netcdf.getVar(bath, 0); %longitude 0 to 360
Y = netcdf.getVar(bath, 1); %latitude 90 to -90

% average depth for 1 x 1 grid
for y=1:size(la)
    area(y)=0;
    for x=1:length(lo)
        zz(x,y)=sum(sum(elev((x-1)*12+1:x*12,(y-1)*12+1:y*12)))/144;
        if((zz(x,y)>sf_low_bnd) && (zz(x,y)<sf_upp_bnd))
                area(y) = area(y)+1;
        end
    end
end
```

```
%% loop over lat and long, and select data that is near ocean bottom
count = 0;
no3_count = 0;
aou_count = 0;

cc=0;ck=0
for x = 1:length(lo)
   for y = 1:length(la)
      % if la(y) > -80 && la(y) < 80 && lo(x) > 200 && lo(x) < 250

       sf_depth =  - zz(x, y); %seafloor depth
       sample_depth_i = 0; %sample depth index of depth array
       if sf_depth > sf_low_bnd && sf_depth < sf_upp_bnd
           for d = 1:33  %select sample depth nearest to SWI
               if zm(d) > sf_depth
                   break;
               end
               sample_depth_i = d;
           end
           o2i = o2(x, y, sample_depth_i); %oxygen conc of site


           if (o2i > 0 && o2i < 100) % filter out wrong results
               no3i = no3(x, y, sample_depth_i);
               if (no3i > 0 && no3i < 100)
                   count = count + 1;
                   o2_res_100m(count) = o2i;
                   o2_lat_100m(count) = la(y);
                   o2_lon_100m(count) = lo(x);
                   dd(count)=sf_depth;

                   no3_count = no3_count + 1;
                   no3_res_100m(no3_count) = no3i;
                   no3_lat_100m(no3_count) = la(y);
                   no3_lon_100m(no3_count) = lo(x);
               end
           end
       end
   end
end

%% plot results
tit = sprintf('%d m', (sf_low_bnd+sf_upp_bnd)/2);

% globe & hist
figure,
subplot(1,3,1), imagesc(zz'), hold on, plot(o2_lon_100m,o2_lat_100m+90,'ko'), title(tit)
subplot(1,3,2), hist(o2_res_100m), title('O2 in ml/L')
subplot(1,3,3), hist(no3_res_100m), title('NO3 in umol/kg')


% lat
figure,
subplot(1,3,1), plot(o2_lat_100m,o2_res_100m,'o'), xlabel('lat'),ylabel('O2 in ml/L'),
title(tit)
subplot(1,3,2), plot(no3_lat_100m,no3_res_100m,'o'), xlabel('lat'),ylabel('NO3 in
umol/kg'), title(tit)
subplot(1,3,3), plot(o2_lon_100m,o2_res_100m,'o'), xlabel('lon'),ylabel('O2 in ml/L'),
title(tit)
```

D. Code for calculating global DNF rates

```
%specify range of seafloor depth to search
low_waterdepth = 2000
high_waterdepth = 5000

%in case of wrong values in database
%o2backup = 265 %uM
%no3backup = 15 %uM

sf_low_bnd = -high_waterdepth;
sf_upp_bnd = -low_waterdepth;

%% read in the WA09 data set
ncid = netcdf.open('/Users/jurjen/dissolved_oxygen_annual_1deg.nc');

%%read in the global nitrate file
ncno3 = netcdf.open('/Users/jurjen/nitrate_annual_1deg.nc');

%% read in the global topography/bathimetry (1/12 x 1/12 degree)
bath = netcdf.open('/Users/jurjen/bath.cdf');

elev = netcdf.getVar(bath, 2); % depth(X=long,Y=lat)
X = netcdf.getVar(bath, 0); %longitude 0 to 360
Y = netcdf.getVar(bath, 1); %latitude 90 to -90
%% assign it to variables
o2 = netcdf.getVar(ncid,7); % O2 conc in ml/L (longitude, latitude, layer)
zm = netcdf.getVar(ncid,2); % depth in m (1 x layer)
lo = netcdf.getVar(ncid,0); % longitude in degree
la = netcdf.getVar(ncid,1); % latitude in degree
no3 = netcdf.getVar(ncno3,7); %no3 conc umol/kg

LDIN = 0;
area = 0;
R = 6371; %radius earth (km)
for y=1:size(la)
    for x=1:length(lo)
        %calculate average seafloor depth
        zz(x,y)=sum(sum(elev((x-1)*12+1:x*12,(y-1)*12+1:y*12)))/144;
        if ((zz(x,y)>sf_low_bnd) && (zz(x,y)<sf_upp_bnd))
        %convert degrees into rad
            lo1 = (lo(x) - 0.5) * pi() / 180;
            lo2 = (lo(x) + 0.5) * pi() / 180;
            la1 = (la(y) - 0.5) * pi() / 180;
            la2 = (la(y) + 0.5) * pi() / 180;
            %calculate surface of grid cell:
            S = R*R*(lo2-lo1)*(sin(la2)-sin(la1));
            area = area + S;

            %retrieve O2 and NO3 concentrations
            global sfd;
            sfd = -zz(x,y);
            for d = 1:33  %select sample depth nearest to SWI
               if zm(d) > sfd
                   break;
               end
               sample_depth_i = d;
            end
            o2i = o2(x, y, sample_depth_i); %ml/L
            P = 1.013*10^5 / 133.32; %mm Hg
            T = 273; %K
            o2i = ((P/T)*0.5513*o2i)*1000/32; %uM

            no3i = no3(x, y, sample_depth_i); %uM
            if (o2i > 0 && o2i < 500 && no3i > 0 && no3i < 100)
                %calculate areal mineralization rate (Middelburg et al. 1997)
                global Cox;
                JPOM = 10^(-0.5086-0.000389*sfd)*1.8; %mmol C cm^-2 y^-1
                JPOM = JPOM * 10^4 / 365; %mmol C m^-2 d^-1
                Cox = JPOM;
                x0 = JPOM;
```

```
                %rrpom = JPOM + APOM (mmol C m^-2 d^-1)
                rrpom = fzero(@bohleneqn, x0, optimset('TolX', 1e-20));
                a = 0.060; b = 0.19; c = 0.99;
                %DEN1 = DNF (mmol N m^-2 d^-1
                DEN1 = (a+b*c^(o2i-no3i))*rrpom;
                %convert to Tg N y^-1
                DEN1 = DEN1 * S * 365 * 14.01 * 10^-9;
                LDIN = LDIN + DEN1;
            end
        end
    end
end

LDIN %Tg N y^-1
area * 10^-6 %km2 * 10^-6

%Place function below in separate file
%see bohlen et al. 2012: Simple transfer... biogeochemical models
function y = bohlenequation(rrpoc)
    global Cox
    global sfd
    if (sfd > 2000)
        y = rrpoc - Cox - 0.014*rrpoc^1.05;
    else
        y = rrpoc - Cox - 0.14*rrpoc^1.11;
    end
    [y rrpoc];
end
```